EFFECT OF ALUMINA ON REDUCTION SOFTENING AND MELTING BEHAVIOUR OF IRON ORE PELLETS

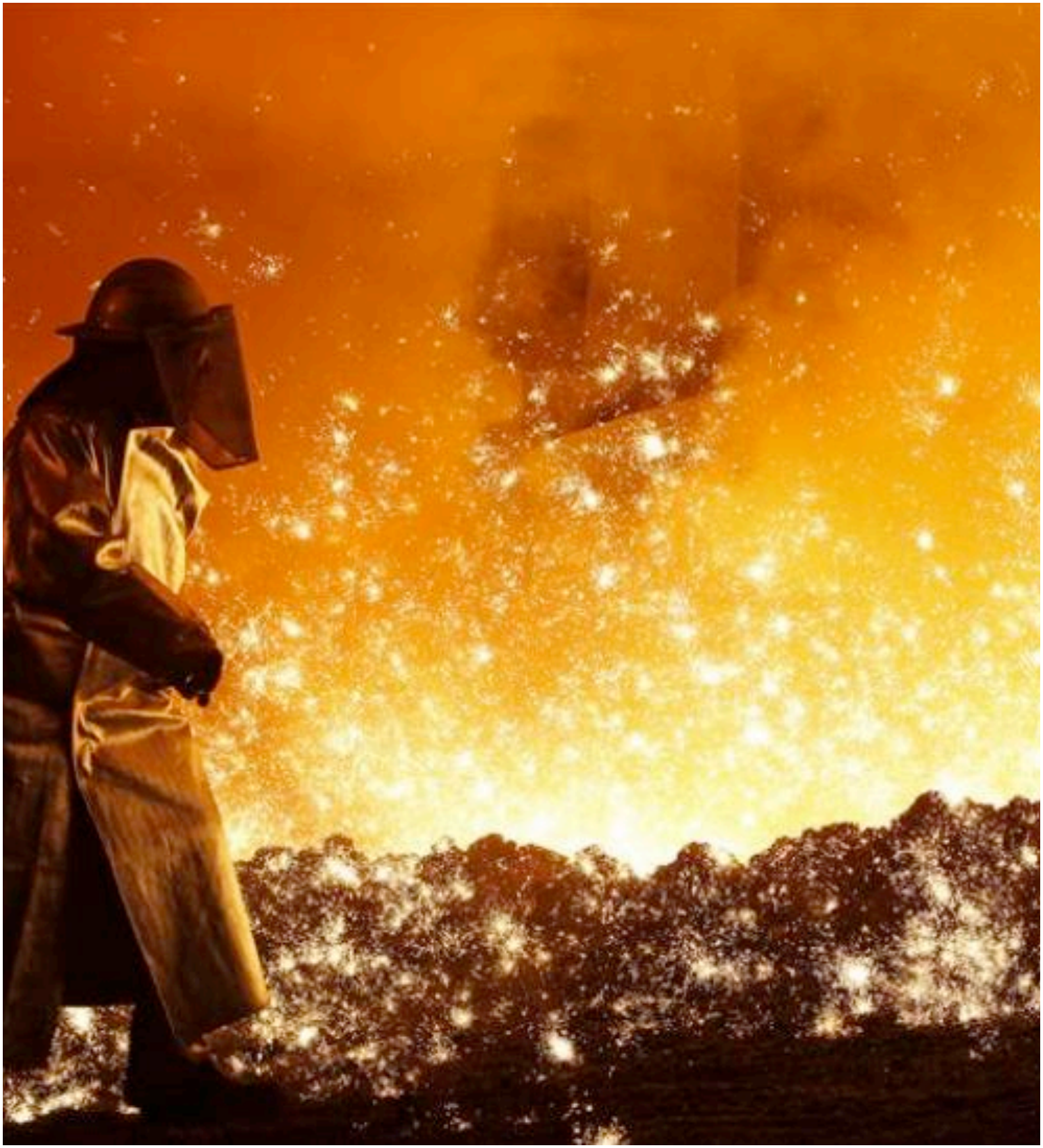

Devi Singh Chauhan

Effect of Alumina on Reduction Softening and Melting Behaviour of Iron Ore Pellets

Master thesis submitted to Delft University of Technology in partial fulfilment of the requirements for the degree of

Master of Science

in

Materials Science and Engineering

Specialization in

Metals Science and Technology

Supervisors

Dr. Yongxiang Yang	Delft University of Technology
Dr. Dharm Jeet Gavel	Delft University of Technology

Committee

Dr. Yongxiang Yang	Delft University of Technology
Dr. Dharm Jeet Gavel	Delft University of Technology
Dr. Timothy Kerry	Delft University of Technology
Dr. Jie Zhou	Delft University of Technology
Dr. Allert Adema	Tata Steel

Devi Singh Chauhan

4719492

Abstract

Aim of the blast furnace ironmaking process is the extraction of iron from iron ore, and prepare the raw iron (hot metal) for steel making. The iron oxides (ore) are charged into the furnace in the form of sinters and pellets containing the iron ore. Iron ore interacts with reducing gases and coke to form molten iron which in combination with slag are collected in the hearth of the blast furnace and tapped separately. Since blast furnace is a counter-current reactor, the permeability is of prime importance for its efficiency. When temperatures reach 1100 °C to 1200 °C the ore layers start to soften and gradually melt, and this region is called the cohesive zone. The cohesive zone consists of a series of approximate ring-shaped, doughnut-like masses of semi-molten, pasty ferruginous burden material. Here the loss of permeability is caused by melt onset and deformation of the solid phases due to the pressure of the burden. The shape and position of the cohesive zone affect the efficiency of the process and it is advantageous to have the cohesive zone located at as high temperatures as possible and its thickness as small as possible. This is governed by the properties of the pellets and sinter which in turn depends on the nature of ore or concentrate, associated gangue, type and amount of fluxes added, and their subsequent treatment. With the depletion of high-quality iron ore resources, the consumption of iron ores with high alumina (Al_2O_3) content is increasing. Therefore, it is important to investigate the influence of alumina on the reduction, softening, and melting behaviour of iron-bearing materials like sinters and pellets, hence its effect on the cohesive zone.

This thesis explores the effect of alumina on the pellet's behaviour in the cohesive zone, for which Reduction, Softening, and Melting apparatus (RSM) is used as a blast furnace simulator. With RSM, the pellet samples with similar basicity but varying alumina content are subjected to conditions similar to the blast furnace, and their reduction, softening, and melting behaviour are compared. It is observed that with an increase in alumina content the cohesive zone shifts to a lower temperature and its thickness increases, therefore the resistance offered to the gas flow increases. The alumina plays a multifaceted role, where it affects reduction degree, degree of carburization, the viscosity of primary slag, and finally wettability of slags with coke and iron. Alumina causes reduction retardation in heterogeneous conditions, due to the formation of low melting interfaces. This on one hand does not influence the total reduction degree but on the other increases the rate of homogenization of the pellet microstructure. Alumina induces reduction retardation in homogenous condition, by increasing the rate of melt formation due to an increase in the fraction of low melting phases. This causes an increase in the rate of softening and early melting. Degree of reduction is not the only factor that influences softening and melting behaviour, as a pellet sample with lower reduction degree and lower alumina showcase better softening melting properties than the pellet sample with a higher reduction degree and higher alumina content. Alumina acts as network former in the chemistries considered, increasing the viscosity of primary slag, hence increasing the resistance to gas flow. Alumina increases the proportion of high melting phases in the FeO lean slag. The possible effects of alumina on carburization and wettability are explored with the help of literature, one possibility is that alumina decreases the wettability of slag with iron shell, hence increases the degree of carburization causing early melting of iron shells. Simultaneously, the possible effects of basicity are also explored using literature; it seems with an increase in basicity the negative effects of alumina lessen.

Table of Contents

1. Introduction

1.1. Background

The steel industry played a central role in the industrial revolution and now is playing a crucial role in the development of a sustainable society. The blast furnace is known as the heart of an integrated steel plant. The significance of both is underlined below in section 1.1.1. Section 1.1.2 briefly introduces the process of the ironmaking blast furnace, wherein 1.1.3, one of the main ingredients for making iron, namely pellets, is introduced. Section 1.1.4 highlights the rise of alumina content in iron ores and also briefly underlines its deleterious effects. Overall section 1.1 provides the under footing on which topic of research will be introduced in section 1.2.

1.1.1. Steel Industry

Steel is one of the largest produced, consumed, and traded commodities of the world [1]. It is indispensable to the modern way of life because of its versatility, more than 3500 grades. Steel is fundamental to achieving a circular economy as it ensures the maximum value from resources through recovery, reuse, remanufacturing, and recycling. Since it is an alloy, primarily made up of iron, which is the fourth most common element found in the earth's crust, steel becomes an obvious choice wherever possible.

In 2019 the world crude steel production reached 1.869 billion tonnes [2]. Figure 1.1 depicts the steel production around the world by region. Europe is the second-largest producer of steel after Asia.

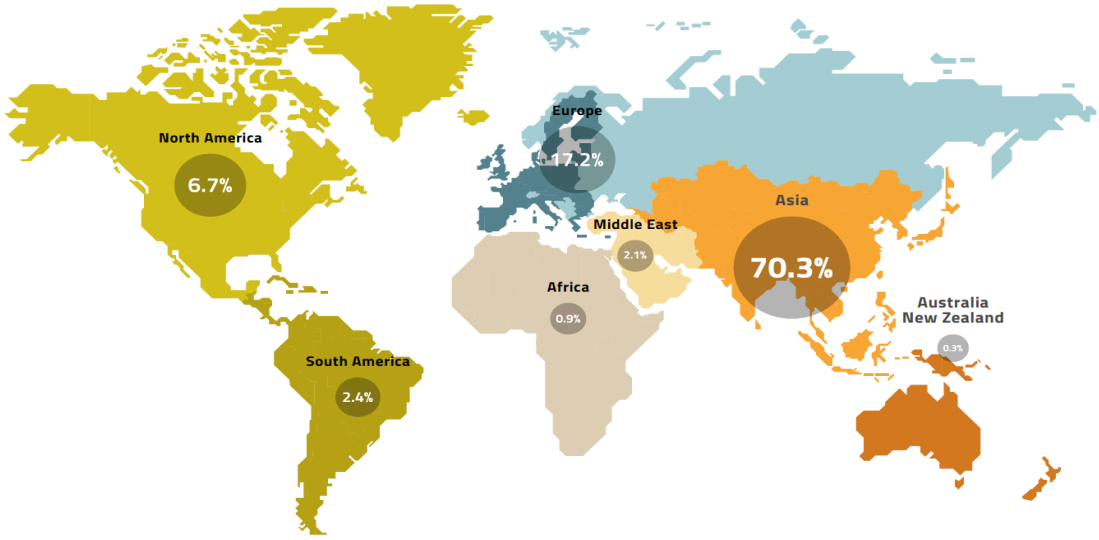

Figure 1.1. Map of steel production by region [2].

The four-major steel production route, classified on the basis of raw materials and source of energy input, are:

a) Blast Furnace (BF) – Basic Oxygen Furnace (BOF) route: Raw materials like iron ore, coal, limestone, and dolomite are used in the blast furnace to produce liquid iron also called hot

metal. Hot metal is then converted into primary steel in the BOF converter by using oxygen. The BOF process is autogenous, no external source of energy is required. In addition to hot metal, recycled steel is also used as a raw material in the BOF.

b) Smelting Reduction (SR): It is similar to the route 1, as here again the liquid hot metal is converted to primary steel in the BOF. The major difference here is that the blast furnace is replaced with processes where there is no longer a need for coke. SR is aimed at using a wide range of coals and iron fines. Here the entire blast furnace process is divided into two stages, where first iron ore is heated and pre-reduced using gas generated from stage 2. In the second stage, in the smelter, further iron reduction takes place in the liquid state with coal and oxygen. The Finex which is an improved version of the Corex process is the main SR technology. Additionally, the HISARNA technology is another SR process developed under the Ultra-Low Carbon Dioxide Steelmaking (ULCOS) program at Tata Steel Ijmuiden.

c) Electric arc furnace (EAF) route: Uses primarily; recycled steels/scrap, the direct reduced iron (DRI), and even sometimes the hot metal. For the source of energy, electricity is required in order to produce steel. Direct reduced iron can be produced in numerous ways. Direct reduction is a solid-state process as iron oxide reduces at temperatures lower than its melting temperature. The reduction takes place by reducing gas or elemental carbon produced from natural gas or coal. The reduction can take place in a shaft furnace technology like MIDREX and HYL, Rotary kiln technology such as Fastmet/Fastmelt and ITmk3, and fluidized bed technology such as Circored and Circofer.

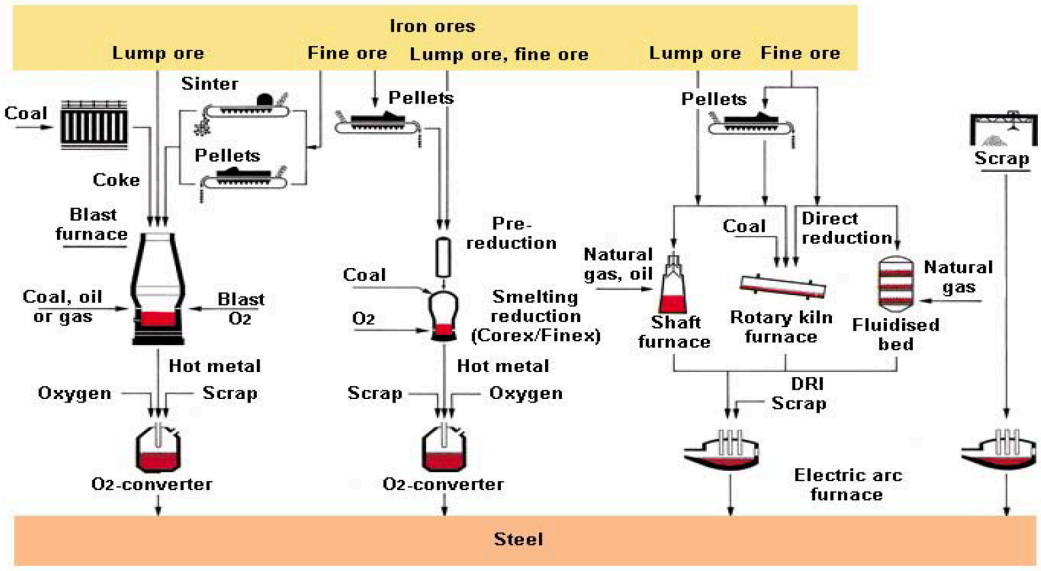

Figure 1.2. Steel making route (a) BF – BOF (b) Smelting Reduction (c) EAF route [3].

All three routes are summarized in Figure 1.2. Though the share of the EAF and smelting reduction route has been consistently increasing, still the BF-BOF route accounts for 72% of the steel that is produced today [1]. In Europe, the contribution of EAF route is above the world average (Figure 1.3) but still below BF-BOF route; in 2018, 167.6 million tons of crude steel were produced in Europe, 98.1

million tons of which via the Blast Furnace (BF)—Basic Oxygen Furnace (BOF) route and 69.5 million tons via the scrap-based Electric Arc Furnace (EAF) route [13]

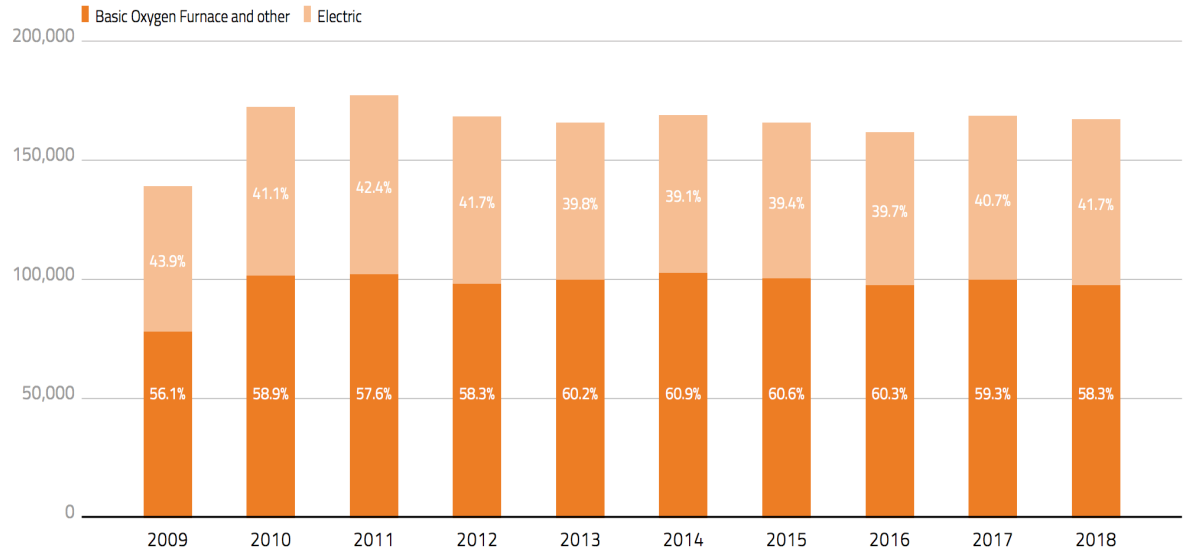

Figure 1.3. EU crude steel output by production route [2].

1.1.2. Ironmaking Blast Furnace

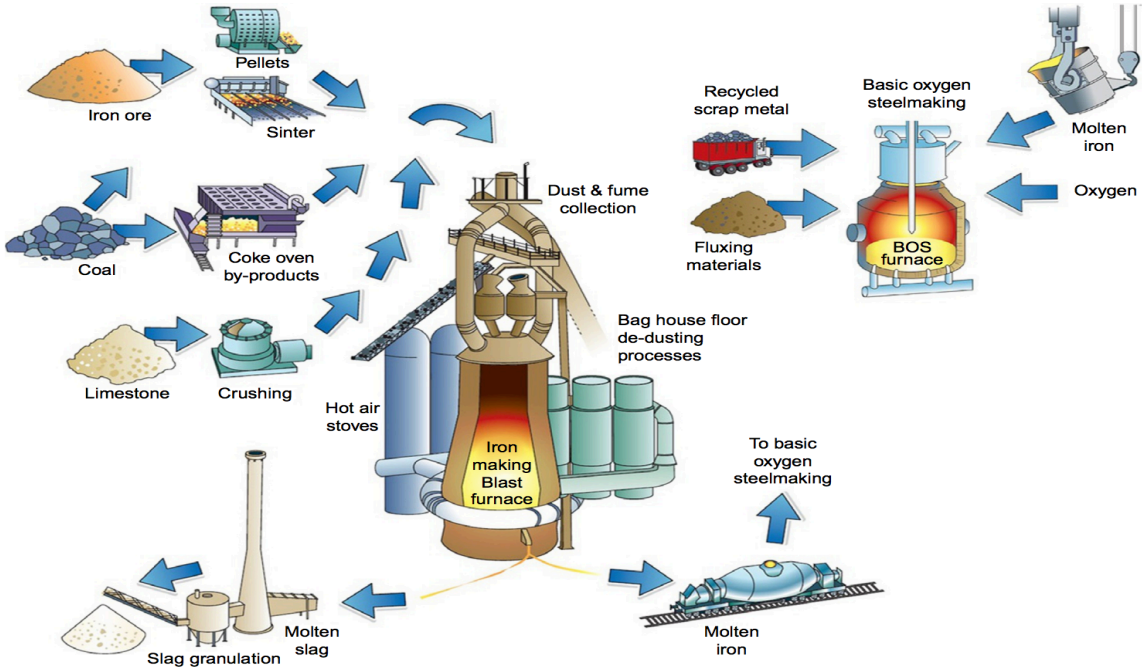

Figure 1.4. BF – BOF route of steel making [12]

The discussion in 1.1.1, highlights the importance that blast furnace holds for steel making industry. Blast furnace process has been around for quite some time, the earliest extant of the blast furnace was found in China dating back to 5th century AD [5]. But the modern blast furnace, with its accessories like the stove, the gas cleaning system, the raw material storage facilities, charging system, etc. had been developed by the beginning of the 20th century [6]. Figure 1.4 shows the BF-BOF route of steel making, where the blast furnace is the most resource-intensive, energy-consuming, and difficult operation. Figure 1.5 depicts schematically a blast furnace process,

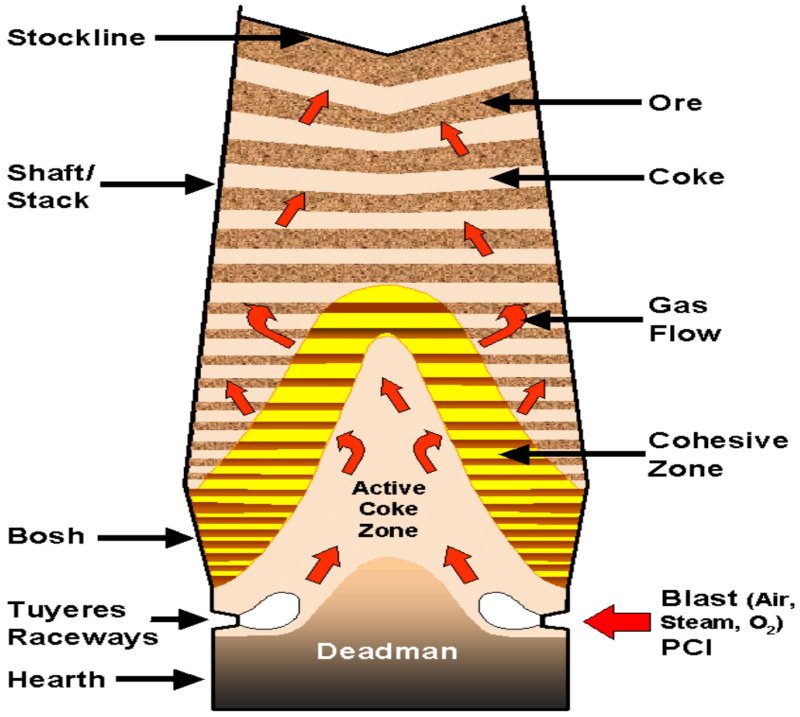

Figure 1.5. Schematic of a blast furnace [4].

The aim of the ironmaking blast furnace is to extract iron from iron ores. Iron is present in different forms mainly associated with oxides like Fe_2O_3 (hematite, 69.94% Fe), Fe_3O_4 (magnetite, 72.36% Fe), $FeCO_3$ (siderite, 48.2% Fe) [17]. It is also accompanied by impurities like SiO_2, Al_2O_3, P_2O_5, and small amounts of alkalis collectively called gangue. Iron ore fines are agglomerated into a particulate form called sinter and pellets, which is then fed to the blast furnace. It is imperative to make sure impurities do not accompany the extracted iron. Coke is the most expensive raw material in the blast furnace [15]. It is obtained from the destructive distillation of metallurgical coal in coke ovens. The uses of coke are manifold:

- It acts as a reducing agent by not just directly reacting with iron oxide but also by producing CO which again reduces the iron oxide. For this reason, a hot blast of air is introduced from the bottom of furnace, tuyeres, which when reacting with coke, produces CO. CO on its way up gives its heat and takes away oxygen from the burden. Coke also regenerates CO from CO_2, formed after reduction.
- Coke acts as a fuel inside the furnace, this is important because both thermodynamically and kinetically, reduction of iron oxide becomes feasible at higher temperatures. Also, the physical separation of iron from gangue, called slag in the liquid state, becomes easier in the molten

state as the density of liquid iron is greater than slag. Additionally, the fluidity of slag increases with temperature. Heat is also required for other endothermic processes like calcination and evaporation of volatiles.

- Coke provides an open permeable bed through which slag and metal pass down to the hearth and hot reducing gases ascends upward. This becomes highly important in the cohesive zone, where the burden behaves as pseudo-solid and become a pasty mass before melting completely. The permeability of the gases would reduce to zero if not for the presence of coke, which provides slits through which gases move up.
- Since coke doesn't melt, it supports overlying burden at high temperature regions.
- Coke carburizes the freshly produced iron, lowering its melting point and consequently reducing the working temperature of the blast furnace.

To improve the iron-slag separation, fluxes like limestone and dolomite are used with burden. These are basic in nature as oppose to major gangue constituents which are acidic in nature, hence they increase the ease of separation of gangue and metal. Therefore, the blast furnace is a counter-current reactor, where coke and iron-bearing burden loaded with fluxes are charged from the top which when descends, interacts with reducing gases produced by the reaction of coke and hot blast. The interaction between gases and burden is twofold, one heat transfer, and another mass transfer, so as the burden moves down not only its temperature increase but also its oxidation state decreases.

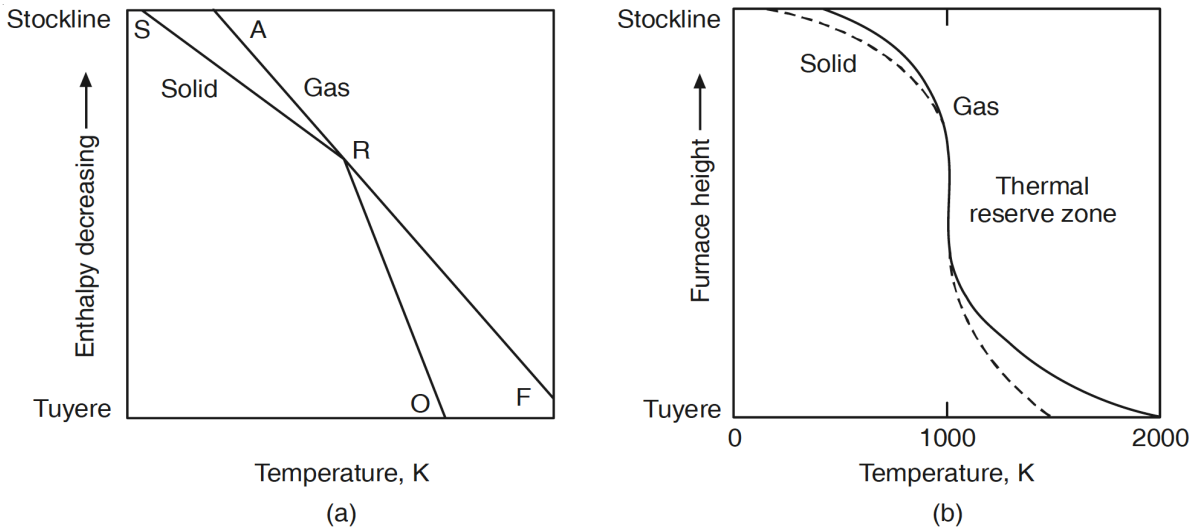

Figure 1.6. Simplified sketch of (a) Reichardt's diagram, and (b) Thermal reserve zone [16].

Thermal capacity is a temperature-dependent property, for solids the thermal capacity is smaller than gases at lower temperatures, which is in the upper part of the furnace [6]. Therefore, for the solids, temperature increases more than it falls for gases. Hence gases are discharged at relatively higher temperatures from the top of the furnace. In contrast, in the bottom part of the furnace, the solid burden requires large quantities of heat to be supplied owing to the highly endothermic Boudouard reaction as well as the other endothermic reactions involved in the fusion of solids. The situation can be idealized by 'lumping' all these endothermic heats together, and considering that the solid has a hypothetically large heat capacity [16]. This can be better understood by Reichardt's diagram, Figure 1.6 (a), where the ARF is the variation in enthalpy with temperature for gas and SRO is the same for solid. As the gas moves up, its enthalpy (heat content) decreases and as solids move down, its enthalpy (heat content) increases. Interestingly at "R" both become equal, this is where thermal reserve zone for an ideal blast furnace occurs (1.6(b)). Before "R" the heat capacity of solids is lower than the gases, which can be seen by comparing the slope, and after "R" the heat capacity of solids is greater than

gases. The enthalpy on the other hand always stays below that of gases. The oxides remain in this zone for sufficient length of time, that chemical equilibrium between wüstite and gas is reached, this zone is called chemical reserve zone or inactive zone (Figure1.7).

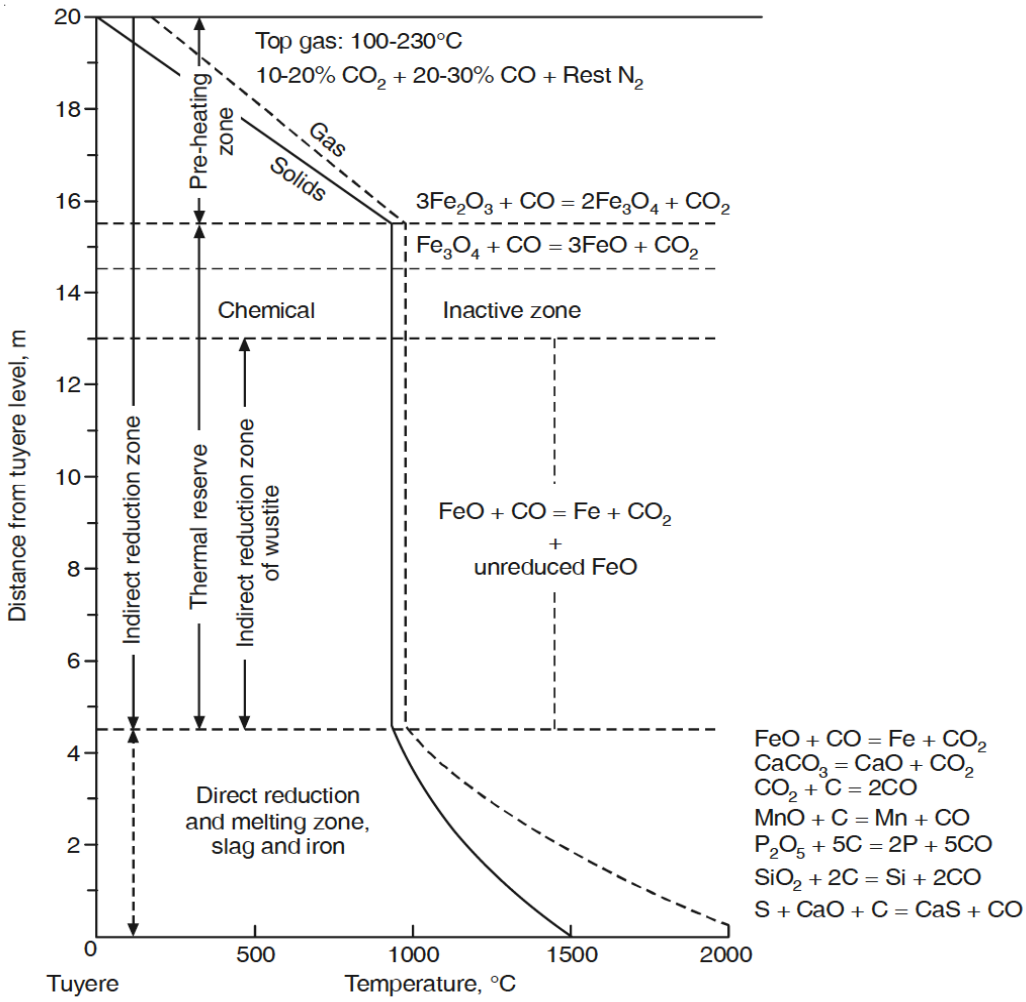

Figure 1.7. An idealized scheme of temperature distribution of gas and solids along the height of a blast furnace showing the chemical reactions occurring in the three main temperature zones [16].

Above and during reserve zone (Figure 1.7), that is at lower temperature regions, from 400 to 900°C, where the burden is solid, the main source of reduction potential comes from reducing gases. The solid-solid reaction between iron oxide and coke is kinetically very sluggish, because the area of contact between ore and coke is small. The sequence of reaction occurring here can be written as:

$$3Fe_2O_{3(s)} + CO_{(g)} \rightarrow 2Fe_3O_{4(s)} + CO_{2(g)} \quad (1.1)$$

$$Fe_3O_{4(s)} + CO_{(g)} \rightarrow 3Fe_{(s)} \quad (1.2)$$

$$Fe_3O_{4(s)} + CO_{(g)} \rightarrow 3FeO_{(s)} \quad (1.3)$$

$$FeO_{(s)} + CO_{(g)} \rightarrow Fe_{(s)} + CO_{2(g)} \quad (1.4)$$

The reaction (1.3) is only possible below 570°C. In addition to carbon monoxide, H_2 is another reducing agent that can cause a reduction of oxides. This is achieved by humidification of the blast, where water

reacts with carbon of the coke to produce hydrogen (1.5). Hydrogen reacts with the burden in a similar manner shown above for CO.

$$H_2O_{(g)} + C_{(s)} \rightarrow CO_{(g)} + H_{2(g)} \quad (1.5)$$

Below 800°C, the CO content of the gas is higher than that in the equilibrium with carbon, the conditions are therefore prone to deposition of carbon by *Nauman reversion reaction* (1.6). Fortunately, this reaction is sluggish, otherwise it may cause choking due to carbon soot deposition.

$$2CO_{(g)} \rightarrow C_{(s)} + CO_{2(g)} \quad (1.6)$$

At higher temperatures, the reaction (1.6) reverses, now called solution loss reaction. And the equilibrium as a whole is called Boudouard equilibrium. It is the solution loss reaction which recuperates the reduction potential of gas.

Once the burden leaves the reserve zone, it gradually enters the cohesive zone. In cohesive zone the gangue, fluxes, and FeO, forms highly oxidizing and low melting slag. This slag trickles through the coke bed present below, bringing FeO of the slag in the intimate contact with the coke. The carbon of the coke directly reduces iron oxide to iron, as seen from (1.7).

$$FeO_{(liq)} + C_{(s)} \rightarrow Fe_{(s)} + CO_{(g)} \quad (1.7)$$

Initially the iron produced will be in solid-state, but as it picks up carbon, it melts and trickles down. In addition to the reduction of FeO from slag, slag also picks up ash from coke, decreasing its basicity and changing its nature from primary (FeO rich), through bosh (FeO less) to hearth slag (ash from coke). The tuyere is the region where oxygen from the hot blast reacts with coke as shown in reaction (1.8).

$$C_{(s)} + O_{2(g)} \rightarrow CO_{2(g)} \quad (1.8)$$

And because of high stability of CO at these temperatures, immediately reverse of reaction (1.6) take place, the solution loss reaction.

$$CO_{2(g)} + C_{(s)} \rightarrow 2CO_{(g)} \quad (1.9)$$

Finally, the hearth is that part of the furnace where molten products of the blast furnace accumulate and stay there until tapped out. The two immiscible products, one being highly carburized liquid iron with all those elements which are reduced and collected by it, and the other being the slag containing oxides like silica, alumina, magnesia, manganese oxide, alkali oxide, sulphur, calcium oxide, etc. These two are tapped out of furnace separately. Slag is tapped every 2-3 hours and metal is tapped every 5-6 hours.

The above was only a very brief discussion of the blast furnace process; it is out of scope for this work to discuss the process in detail.

1.1.3. Pellets and Sinters as Iron Feed for Blast furnace

As mentioned in the previous section, the blast furnace is a counter-current reactor, for the smooth operation of which permeability is of prime importance. That means only lumpy ores can be directly charged into the blast furnace and the fine ore concentrates require agglomeration before charging it to the furnace. Generally, 10 - 40 mm natural lump can be fed directly to the blast furnace, +100 mesh

to -10 mm are sintered at blast furnace site, and all the -100-mesh are pelletized, thereby ensuring maximum utilization of iron ore [6]. The process of sintering and pelletizing is briefly explained below.

Sintering: The process of sintering involves mixing the iron ore, return fines, recycled products of the steel plant industry, slag forming elements, fluxes, and coke fines and conveying them to a sintering machine. The mix is then fed on to the grate of sintering machine, the surface is ignited in the ignition hood and the air is sucked from the bottom. This causes coke in the mix to ignite as the air, carrying heat with it, travels down. Due to the combustion of the coke the temperature rises up to 1400°C [17]. This produces a semi-molten mass which solidifies into a porous cake of sinter. Sinter cake is then crushed into the size range of 15 to 25 mm before feeding them into the blast furnace. The sintering process provides the feed material whose reducibility, strength, size, softening, and melting properties can be optimized, which are all very important for the blast furnace process. Since the sintering process, itself requires permeability, only a certain size range of ore fines (0.15 – 8 mm) can be used. In order to utilize smaller sizes, they are subjected to pelletization.

Pelletization: It is a process which involves finely ground particles of iron ore, having a size which is less than 100 mesh (0.149 mm). These are mixed with additives like bentonite and then shaping them into near oval/spherical balls having the size in the range of 8 mm to 16 mm in diameter. This is achieved in a pelletizer. The hardening of the balls is done by firing with a fuel in a process called induration. Hence pelletization is an agglomerating process of converting iron ore fines into uniformed sized iron ore pellets which can be charged directly into the blast furnace (BF). Similar to sinter, pellet properties like strength, reducibility, softening and melting, and especially swelling are very important for the blast furnace process.

1.1.4. Alumina in Iron Feed

The consumption and high global demand for high-quality raw materials have significantly increased the costs associated with ironmaking. This is forcing the steel producers to increase their utilization of low-cost, low-grade raw materials. As a result, cheaper iron ores with high Al_2O_3 from Australia and India have become an alternative choice [7]. For example, the alumina content of iron ores from the Newman and Hamersley mines in Australia and the Carlo Degas and Goa mines in India is greater than 2 wt.%[26]. In second quarter of 2018, the price of iron ore decreased by $8.5 per dry metric ton, for every 1% increase of alumina in the ores [21]. Recent process changes in the blast furnace process, including the increased use of pulverized coal injection (PCI), have also increased the Al_2O_3 concentration in the slag.

As an example, high alumina iron ores used in some of the Indian steel plants are shown in Table 1.1. Sweden by far is the biggest producer of iron ore in Europe and iron ore has traditionally been sourced from two principal regions, the Kiruna-Malmberget province in northern Sweden and the Bergslagen region in central Sweden [19], the chemistry of iron ores from some of the mines in Kiruna district is shown in Table 1.2. The chemistry of iron ore pellets produced from ores from Kryvyi Rih deposits (Ukraine) is shown in Table 1.3. When compared with Table 1.1 it is easy to see the difference in alumina content. Therefore, the amount of alumina in the blast furnace feed depends on the source of the iron ores and can vary a lot accordingly.

Plant	Fe (wt.%)	SiO_2 (wt.%)	Al_2O_3 (wt.%)
Durgapur Steel Plant	60 – 62	2.5 – 3.5	5.5 – 6.0
IISCO Steel Plant	60 – 62	2.5 – 3.0	4.6 or more
Rourkela Steel Plant	60 – 62	2.5 – 3.0	4 – 4.5
Bhilai Steel Plant	63 – 64	3.0 – 3.5	3.25 – 3.75
Bokaro Steel Plant	62 – 64	1.4 – 3.0	4 – 4.5

Table 1.1. Chemistry of iron ores used in some of the Indian Steel Plants [6].

Mine	Fe (wt.%)	SiO_2 (wt.%)	Al_2O_3 (wt.%)
Haukivaara	51.3	1.8	0.9
Lappmalmen	61.6	2.4	0.8
Kiriunavaara	63.1	1.1	0.2
Kiriunavaara	61.2	2.1	0.2
Nukutus	50.6	6.4	1.1

Table 1.2. Chemical analysis of iron ores from Kiruna district of Sweden [18].

Plant	Fe (wt.%)	SiO_2 (wt.%)	Al_2O_3 (wt.%)
Northern Iron Ore Dressing Works (SevGOK)	65	5.8	0.26
Northern Iron Ore Dressing Works (SevGOK)	62.5	8.9	0.3
Central Iron Ore Enrichment works (CGOK)	65.5	5.2	0.23

Table 1.3. Chemical analysis of iron ore pellets from Ukraine [20].

Iron ores invariably contains alumina and silica as main gangue constituents. Some of the deleterious effects of alumina are:

- In the upper part of the blast furnace shaft, the permeability of the burden is influenced by the breakdown of sinter upon reduction. Sinter degradation during reduction at low temperature is usually determined by the RDI static test, which is carried out at 550 °C. Low values are desirable for this index. Alumina is known to worsen the sinter RDI. Industrial experience with the blast furnace shows that within a 10 – 10.5% CaO content range an increase of 0.1% in the alumina content raises the RDI by 2 points [23]. According to authors of reference [22], the effect of alumina on RDI depends on the type of alumina present in the ores. When alumina is present in the form of gibbsite ($Al(OH)_3$), it adversely affects the RDI. Whereas, alumina is less detrimental when present as kaolinite ($Al_2O_3.2SiO_2.2H_2O$). Alumina also adversely affects the process of sintering. Due to poor reactivity of alumina and high

viscosity of the melt, high alumina type iron ores are expected to demand a high sintering temperature and a longer sintering time to promote melt formation. As a result, fuel rate increases and sintering productivity decreases with an increase in alumina.

- Similar to sinters, pellets also require liquid slag formation during pelletization, which acts as a bonding phase. Pellets with higher alumina require higher firing temperatures to melt and fuse [24], hence decreasing productivity. In reference [25] authors observed that pellets with a high Al_2O_3/SiO_2 ratio exhibited poor RDI behaviour, also the cold crushing strength was found to decrease. In reference [26], authors observed that with an increase in alumina from 1 wt.% to 3.5 wt.%, the compressive strength of the pellets decreases. All of which are detrimental to blast furnace permeability.
- The final slag produced in the blast furnace hearth should be very fluid for its clean separation from the metal phase. Fluxes like CaO are used to modify the properties of slag, like viscosity and liquidus temperature. But in order to achieve desired slag properties the original ratio Al_2O_3/SiO_2 has to be within a certain limit (0.5 – 1.5) [6]. If the ratio is outside this limit, the addition of fluxes will not result in slag with desired properties. The slag, in that case, will have to be produced by operating at higher temperatures causing an increase in coke rate.
- Studies on quenched and dissected blast furnaces in Japan and Germany have revealed the importance of softening and melting behaviour for stable blast furnace operation. This determines the position and shape of the blast furnace cohesive zone. A low, narrow inverted "V" shaped cohesive zone is generally desirable to improve blast furnace performance. Historically blast furnace operators have focused more on iron feed size, cold strength, reduction degradation, and final slag properties, as far as the effect of alumina is concerned. The information on the influence of alumina on the cohesive zone is very limited [22], this is where the current topic comes into the picture as will be discussed in section 1.2.

1.2. Topic of Research

The cohesive zone is the region where softening and melting of burden takes place. The softening of the iron burden should occur at as high a temperature as possible to provide sufficient time for gaseous reduction to occur, as indirect reductions are not only kinetically faster but also exothermic in nature. Whereas the direct reduction reactions, which occur once the burden melts and drips, is endothermic in nature. Therefore, a lower share of direct reduction causes the coke charge to decrease. Coke is the most expensive raw material in the blast furnace, lowering of coke rate, improves the efficiency of the blast furnace operation. In addition to the position, the thickness of the cohesive zone is also important, as it governs resistance to gas flow. The greater the resistance, the lower is the amount of gas that can be introduced inside the furnace, hence decreasing the productivity of the furnace. Both the thickness and position of the cohesive zone are governed by the softening melting temperatures, which in turn is dependent on the nature of ore or concentrate, type and amount of fluxes added, and associated gangue and their distribution in the microstructure. Since alumina is a gangue constituent, it can have a significant effect on cohesive zone properties.

This research aims to understand the effect of alumina on reduction, softening, and melting behaviour of pellets. To simulate the blast furnace conditions on a lab-scale, a reduction softening and melting (RSM) apparatus has been used for this study. RSM apparatus helps in understanding the formation of the cohesive zone in the lower portion of the blast furnace. To mimic the blast furnace conditions, the temperature and gas inlet composition is varied with time. The gas and thermal profile are obtained from vertical probing of blast furnace [27], also a constant load is applied to the samples, which simulates the presence of burden on top. It is not common for a blast furnace to utilize just pellets as iron feed. Pellets are mostly used in combination with sinters. The reason for studying the effect of alumina only on pellets is to exclude the effect of sinter on softening melting behaviour. This

provides a basis for conducting similar studies later on sinters and then finally on the mixed burden. Interestingly very few studies have been conducted where the impact of alumina on reduction, softening, and melting behaviour of pellet and sinter is investigated. Higuchi et.al [28] subjected pellets with constant basicity (B2 = 1.1) and varying alumina content (0.85%, 1.70%, and 2.29%) to reduction tests under load and found that cohesive zone shifts to lower temperature with increase in alumina, also, the rate of reduction increased with decrease in alumina. Meng et al [10] conducted a similar study on sinters, where they found a clear effect of alumina on sinters. It was observed that the cohesive zone shifts to lower temperatures and its thickness increase with increasing alumina from 1.58% to 3.08% in sinters. Hence based on existing studies it is expected that with an increase in alumina, the softening and melting zone will shift to lower temperatures.

Three Commercial pellets are selected for the current study with alumina content of 0.81, 1.37, and 1.85 %. Ideally, it is desired that just alumina content should vary with pellets, and other factors like basicity, micropore structure, and minor gangue elements, like alkalis, are kept constant. This is difficult to achieve with commercial pellets and the case in hand is no different. Additionally, the amount of variation in alumina content is limited for commercial pellets. Hence, the effect of alumina when present in very low and very high quantities cannot be investigated. This is important for understanding the fundamental behaviour. On the bright side, commercial pellets paints a better picture as alumina is generally associated with gangue and not present as free Al_2O_3 particles, as is the case with custom made pellets.

To serve this end, Chapter 2 is dedicated to understanding various factors that can affect the cohesive zone. Chapter 2 lays the foundation for chapter 5 where the case in hand will be discussed. Here, additionally, the possible effects of alumina on the factors discussed in chapter 2 and in turn on the cohesive zone are presented. In chapter 3, the RSM experimental setup and procedure is showcased, additionally, the characterization techniques utilized will be introduced. Chapter 4 first explains the nature of RSM results and then exhibits its reproducibility, and finally presents the difference in results for tested samples. Chapter 6 concludes the discussion and further provides the scope for future research.

1.3. References

[1] World Steel Association. (2019). Fact Sheet: Steel and Raw materials. *15*(4), 710–739. https://www.worldsteel.org/en/dam/jcr:16ad9bcd-dbf5-449f-b42c-b220952767bf/fact_raw%2520materials_2019.pdf

[2] The European Steel Association (EUROFER). (2019). *European Steel in Figures 2019*. 74. http://www.eurofer.org/News%26Events/PublicationsLinksList/201907-SteelFigures.pdf

[3] Remus, R., Roudier, S., Aguado Monsonet, M. a., & Sancho, L. D. (2013). Best Available Techniques (BAT) Reference Document for Iron and Steel Production. In *Industrial Emissions Directive 2010/75/EU: Vol. BREF-IS*.

[4] Wright, B., Zulli, P., Bierbrauer, F., & Panjkovic, V. (2003). Assessment of Refractory Condition in a Blast Furnace Hearth Using Computational Fluid Dynamics. *Third International Conference on CFD in the Minerals and Process* Industries, CSIRO, Melbourne, Australia, April 2015, 645–650.

[5] Peter J. Golas (25 February 1999). Science and Civilisation in China: Volume 5, Chemistry and Chemical Technology, Part 13, Mining. *Cambridge University Press. p. 152.* [6] Tupkary R.H (2010),

An Introduction to Modern Iron Making. Physical-thermal- chemical processes in a blast furnace, Khanna Publishers

[7] Yan, Z., Lv, X., Zhang, J., Qin, Y., & Bai, C. (2016). Influence of MgO, Al2O3 and CaO/SiO2 on the viscosity of blast furnace type slag with high Al2O3 and 5 wt-% TiO2. *Canadian Metallurgical Quarterly*, *55*(2), 186–194.

[8] Sohn, I., & Min, D. J. (2012). A review of the relationship between viscosity and the structure of calcium-silicate-based slags in ironmaking. *Steel Research International*, *83*(7), 611–630.

[9] Dwarapudi, S., Ghosh, T. K., Shankar, A., Tathavadkar, V., Bhattacharjee, D., & Venugopal, R. (2011). Effect of pellet basicity and MgO content on the quality and microstructure of hematite pellets. *International Journal of Mineral Processing*, *99*(1–4), 43–53.

[10] Meng, F. Y., Wang, Z., Zhang, J. L., & Wang, R. B. (2015). Fundamental study of high Al2O3 sinter softening and melting behaviour. 6th International Symposium on High-Temperature Metallurgical Processing. *TMS (The Minerals, Metals and Materials Society) Annual Meeting*, *2015-March*, 643–650.

[11] Pan, Y. Z., Zhang, A. J., Lin, L., Wang, J. S., Feng, H. X., & Lin, Q. S. (2019). Correlation Between Reduction Degree and Softening and Melting Properties of Pellets. Minerals, Metals and Materials Series, 523–530.

[12] Ghanbari, H. (2018). Polygeneration systems in iron and steelmaking. In *Polygeneration with Polystorage: For Chemical and Energy Hubs*. Elsevier Inc.

[13] Rieger, J., & Schenk, J. (2020). State-of-the-art Processing Solutions of Steelmaking ResidualsStand der Technik bei der Behandlung von Stahlwerksreststoffen. *BHM Berg- Und Hüttenmännische Monatshefte*.

[14] Spirin, N., Onorin, O., Gurin, I., Lavrov, V., & Shchipanov, K. (2018). Structure of the Optimal Management System for Raw Materials, Fuel and Energy Resources in Blast-furnace Production. *KnE Engineering*, *3*(5), 118.

[15] Osborne, D. G., & Gupta, S. K. (2013). Industrial uses of coal. In *The Coal Handbook: Towards Cleaner Production* (Vol. 1). Woodhead Publishing Limited.

[16] Ghosh, A., & Chatterjee, A. (2008). Ironmaking and Steelmaking Theory and Practice*: PHI Learning Private Limited* (Vol. 20).

[17] Yang, Y., Raipala, K., & Holappa, L. (2014). Ironmaking. In Treatise on Process Metallurgy (Vol. 3). Elsevier Ltd.

[18] Loberg, B. E. H., & Horndahl, A. K. (1983). Ferride geochemistry of Swedish precambrian iron ores. *Mineralium Deposita*, *18*(3), 487–504.

[19] Jonsson, E., Troll, V. R., Högdahl, K., Harris, C., Weis, F., Nilsson, K. P., & Skelton, A. (2013). Magmatic origin of giant "Kiruna-type" apatite-iron-oxide ores in Central Sweden. *Scientific Reports*, *3*, 1–8.

[20] Iron Ore, Metinvest semi-finished products, Retrieved from https://metinvestholding.com/en/products/semi-finished-products-chemical-and-by-products/iron-ore-concentrate

[21] Roe, C. and Lu, J. (2018). Has an Australia-to-Europe iron ore arbitrage opened?, S&P Global Platts, Retrieved from https://blogs.platts.com/2018/07/12/australia-europe-iron-ore-arbitrage/

[22] Lu, L., Holmes, R. J., & Manuel, J. R. (2007). Effects of alumina on sintering performance of hematite iron ores. *ISIJ International*, *47*(3), 349–358.

[23] MOCHÓN, J., CORES, A., RUIZ-BUSTINZA, Í., VERDEJA, L. F., ROBLA, J. I., & GARCIA-CARCEDO, F. (2014). Iron Ore Sintering Part 2. Quality Indices and Productivity. *Dyna*, *81*(183), 168–177.

[24] Kadhe, Dhiraj & Kumar, Abhishek & Umadevi, T & Kaza, M & Sah, Roshan & Sampath, K. (2016). Optimization of pelletization process for iron ore with high alumina by use of high silica fluxes*, International Seminar on Mineral Processing Technology, retrievd from*

[25] Dwarapudi, S., & Ranjan, M. (2010). Influence of oxide and silicate melt phases on the RDI of iron ore pellets suitable for shaft furnace of direct reduction process. *ISIJ International*, *50*(11), 1581–1589.

[26] Zhang, J. L., Wang, Z. Y., Xing, X. D., & Liu, Z. J. (2014). Effect of aluminum oxide on the compressive strength of pellets. *International Journal of Minerals, Metallurgy and Materials*, *21*(4), 339–344.

[27] Chaigneau, Renard & Sportel, Heiko & Trouw, J. & Vos, R. & Droog, J.. (1997). Blast furnace burden quality: Laboratory simulation. Ironmaking & Steelmaking. 24. 461-467.

[28] Higuchi, K., Naito, M., Nakano, M., & Takamoto, Y. (2004). Optimization of chemical composition and microstructure of iron ore sinter for low-temperature drip of molten iron with high permeability. *ISIJ International*, *44*(12), 2057–2066.

2. Factors Affecting Cohesive Zone: A Literature Review

The Softening, Melting, and Dripping phenomena, which characterizes the cohesive zone inside the blast furnace is a result of not one but multiple factors associated with the properties of burden and imposed conditions. For a given condition a complex interplay between various properties manifests into a distinctive behaviour of the cohesive zone. In order to understand how Al_2O_3 has an influence on the cohesive zone, it is first imperative to look into the fundamentals of these properties and their possible effect on the cohesive zone. Then finally the effect of Al_2O_3 on these properties, in turn on the cohesive zone, will be the topic of discussion of chapter 5.

It is the softening and melting of the burden that constitutes a cohesive zone, the general behaviour is discussed in section 2.1. Section 2.2 onwards explores the various factors that affect the softening and melting phenomena. Where section 2.2 deals with the influence of reduction degree on softening and melting characteristics. Section 2.3 discusses the degree of carburization and its mechanisms. Section 2.4 spreads light on fundamentals of the viscosity of slag and section 2.5 does the same for surface tension and wettability of slags.

2.1. General Cohesive Zone Behaviour

To understand the general sequence of the phenomena taking place in cohesive zone, the reduction softening and melting experiments provides a good starting point, result of a typical softening melting experiment is shown schematically in Figure 2.1

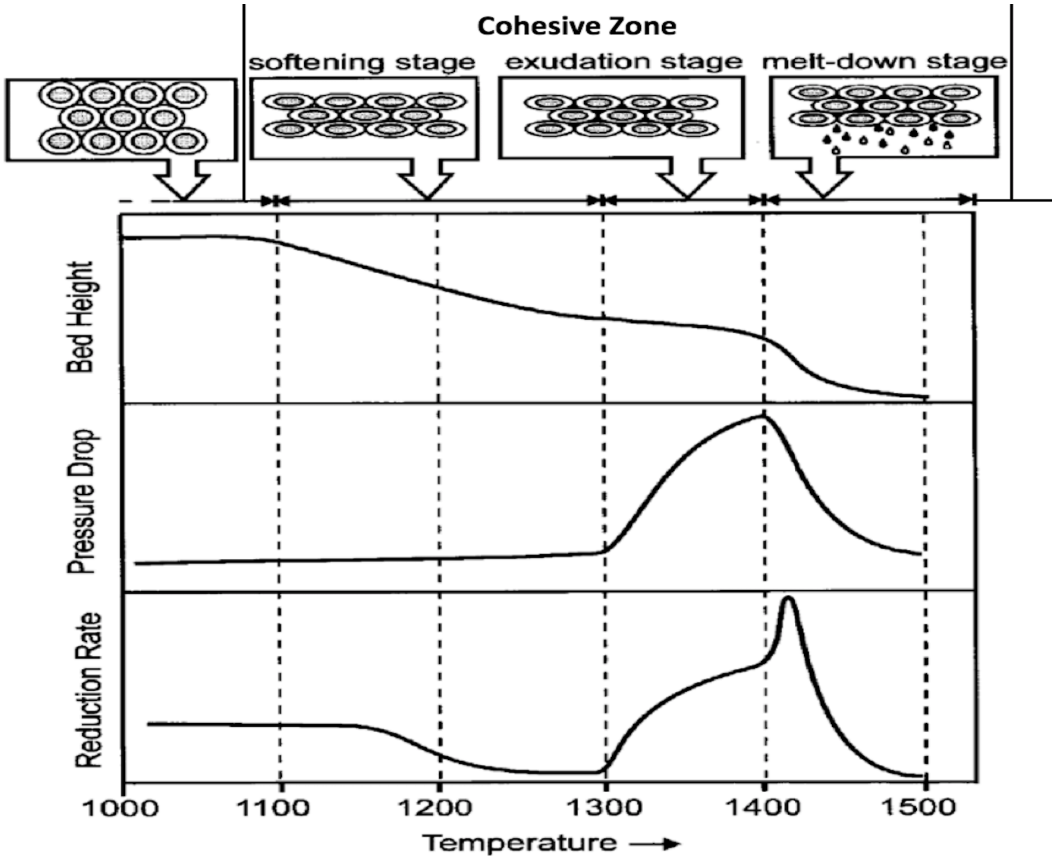

Figure 2.1. Typical phenomena observed during a reduction softening and melting experiment [17].

Before the cohesive zone, the burden undergoes indirect reduction, thermal expansion, compression under load and solid-state sintering. Additionally, pellets also experience swelling in 900 to 1000°C temperature range [24]. As shown in Figure 2.1, the cohesive zone can be classified into three stages. These are discerned on the basis of changes in four properties, i.e. bed height, pressure drop over the bed, reduction rate and material dripping from the bed;

Softening Stage: It is the stage where a gradual decrease in the height of the bed is observed without any marked increase in the pressure drop over the bed. Typically, the softening stage commences at a temperature around 1100°C [17], interestingly this is the temperature at which softening has been observed in the current research for all three tested samples. The temperature at which softening commences is termed as Softening Start Temperature (Ts or T1). In the softening stage the deformation of the bed takes place at a more or less constant deformation rate and dripping of melt from the bed is not observed. The reduction rate drops markedly during the softening stage; this phenomenon is usually referred to as reduction retardation and is attributed to the formation of melt within the iron-bearing material. The melt hampers further reduction because it is thought to close pores, shield off reduction surfaces, and cause longer overall diffusion paths. Reduction retardation is usually observed to commence at 1150-1200°C, i.e. slightly after the onset of the softening stage. The reduction degree governs the iron shell thickness and the amount of liquid present in the core. The burden chemistry and its distribution control the temperature at which liquid starts appearing in the core. Therefore, it is not hard to see that both reduction degree and distribution of gangue and fluxes in the pellet decides the softening start temperature and the rate of softening. The softening starts when liquid appears in the core while shell thickness and amount of liquid in the core governs the rate of the softening.

Melt Exudation Stage: At 1300°C the softening stage changes over to the melt exudation stage. In the temperature range from 1100°C to 1300°C, typically, a bed height decrease of 50% is attained. The temperature at which this stage begins is called Melting Temperature (Tm). A general phenomenon appears to be that upon approaching 1300°C, the deformation rate slows down. It seems as if some sort of maximum deformation level is reached, possibly related to the disappearance of all voidage initially present in the bed. The transition from the softening to the exudation stage is characterized by a very marked increase in pressure drop over the bed. Gas flow through the bed becomes virtually entirely restricted in this stage. The clogging of the bed is caused by the exudation of ferrous melt, initially present within the pieces of burden material, into the voidage of the bed. As the exuded FeO rich primary slag comes in direct contact of coke a sudden rise in the reduction rate is observed due to direct reduction. After the instantaneous exudation of melt, a very high rate of deformation of the bed is observed due to the collapse of the pellets, leading to a further narrowing of the available passageways for the gas. One can see how shell thickness (reduction degree), degree of carburization, and properties of slag present in the core (wettability) can have an influence on the temperature at which this stage begins. That is, the greater the shell thickness, which also means lower the amount of liquid slag in the core, the better is the integrity of the shell hence higher the temperature required for melt exudation. On the other hand, higher wettability of slag with iron-shell means the lower tendency of slag to exude out. Finally, the greater the degree of carburization, the lower is the temperature at which exudation is observed.

Complete Meltdown Stage: The final stage of the softening and melting sequence is the melt-down of the bed. Melting in this specific case refers to the dripping of melt from the bed, creating empty spaces in the bed, causing the pressure drop to decrease. The end of this stage

is called Dripping Temperature (Td) whereas the beginning of this stage is Flooding Temperature (Tf) as adopted from the work of Gavel et al [36]. In most cases, significant dripping of melt starts at around 1400°C [17]. Since the melting temperature of pure iron is 1536°C, dripping at 1400°C indicates that the iron absorbs significant levels of carbon, in the order of 1-2 weight percentage. In addition to the degree of carburization this stage is also governed by slag properties, namely viscosity, and wettability. Higher the viscosity, the higher would be the dripping temperature. Similarly, with the rise in the wettability of the slag with iron and coke, the dripping temperature should also rise. Reduction degree plays an indirect role here as lower the degree of reduction, greater is the amount of slag that exudes out of the pellet. This causes higher resistance to the ascending gases, resulting in an increase of the area under the pressure drop curve. The reduction rates remain high in this stage due to direct contact between FeO rich slag and coke.

2.2. Reduction Degree

As the burden gradually descends inside the blast furnace, the conditions become more suitable for reduction as both the temperature and the reduction potential (CO/CO_2 & H_2/H_2O) increases. Therefore, after leaving the reserve zone, the thermodynamic conditions in the furnace favour the formation of a metallic iron layer on the exterior of iron bearing burden material. From that point onward, an individual iron ore pellet in essence consists of an inwardly growing, porous metallic iron shell on a shrinking oxide core. It is widely believed that minimum reduction degree of the metallic burden reaching the cohesive zone is 50% [5]. In a microscopic sense, this shell region consists of a skeleton of more or less interconnected porous iron, throughout which the non-ferrous slag phases resulting after reduction of the iron are dispersed [13] [15] [17]. As an example, the morphology of an iron shell of a partially reduced pellet is shown in Figure 2.2.

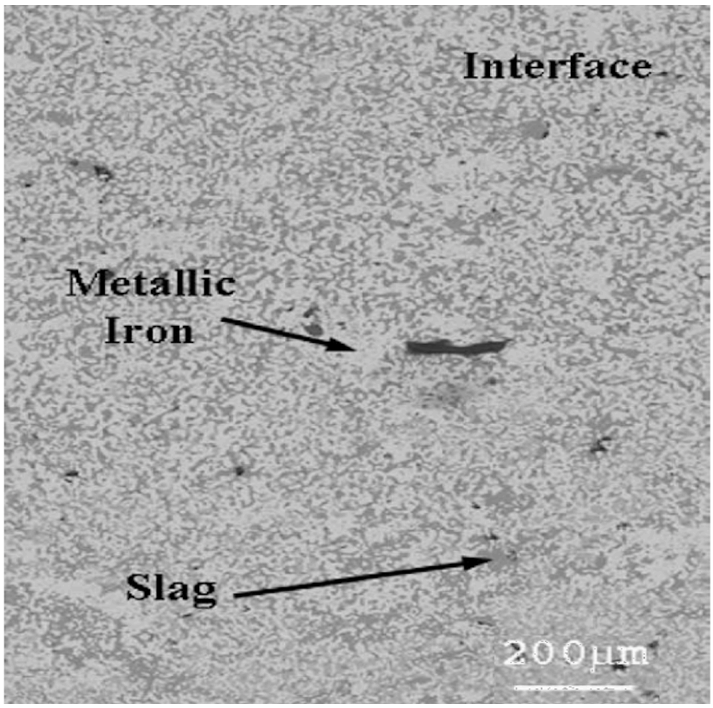

Figure 2.2. Iron shell of a pellet reduced to 60% and cooled from 1150°C [14].

Below temperatures at which melt develops within the core, both the core and the shell region offers resistance to deformation under load. However, a relatively small quantity of melt within the core

greatly affects its deformation properties. The core is rendered inactive in a mechanical sense and the shell becomes essentially as if it were hollow as far as mechanical load carrying capacity is concerned. Because of its limited mechanical strength and the lack of internal support, the iron shell gradually collapses under the combined action of load and temperature (Creep) encountered in the blast furnace. The rate at which this collapse proceeds, the rate of softening, depends on the thickness of the shell. The shell thickness also governs the temperature at which shell breaks and liquid is exuded out (Tm). Thus, both softening and melting temperatures are a function of the attained degree of reduction at the time of first melt development within the core region and thereafter. Another effect of the reduction degree is that it regulates the amount of FeO rich slag in the core, which in turn influences the resistance to gas flow and dripping temperature (Td). [13].

It was observed in reference [6] that metallic iron acts to strengthen the sample and minimise the total level of contraction. In reference [10], authors are convinced that softening of the pellets is caused by the softening of the pellet core where wüstite is the dominant phase of iron, and the reduction degrees of 50–70% has no significant effect on the softening behaviour. That is the iron shell is mainly irrelevant as far as softening is concerned.

The authors in reference [5] studied the effect of Reduction Degree (RD) on the softening behaviour of individual acid and olivine fluxed iron ore pellets under the inert conditions, experimentally. They noticed that the reduction degrees of 50–70% for acid, and 50–65% for olivine fluxed pellet has no significant effect on softening behaviour. Reaching the conclusion that softening of pellets is caused by the softening of the pellet core which happens due to the formation of liquid in the core. They found that acid pellets show early softening due to the formation of low melting fayalitic slag, which also has a high solubility for wüstite. Whereas, in the case of olivine pellets the presence of higher fluxes and lower SiO_2, increases the temperature at which liquid appears, therefore, delaying the softening. Lower SiO_2 means a lower amount of slag in which wüstite readily dissolves. Though there was no difference in softening start temperature with varying pre-reduction degrees for both olivine and acidic pellets, an interesting observation was that the rate of softening for pellets, with a higher reduction degree, was slightly lower than the ones with lower reduction degrees. The rate of softening of acid pellets was greater when compared with olivine, for the same pre-reduction degree. Hence it is not the reduction degree but chemistry that determines the softening start temperature, on the other hand, the rate of softening is dependent on shell thickness (reduction degree) and/or on the rate at which liquid phase proportion increase in the pellets.

Similar to reference [5], the author in reference [12] also observed that olivine pellets possess better-softening properties than acidic pellets. Olivine pellets have higher MgO content, which increases the melting temperature of the slag and the wüstite. Lime fluxed pellets showed behaviour similar to olivine fluxed pellets due to the lower presence of SiO_2 which is known for forming low melting phases. But unlike authors of reference [5], the author of reference [12] suggests that there is a relation between reduction degree and softening start temperature, which increases with an increase in reduction degree.

According to reference [2] there is a direct correlation between the melting temperature and the degree of reduction, especially for lower basicity. They observed that melting temperature for acid pellets increase with increasing reduction degree, on the other hand no effect was seen on the softening temperatures, hence increasing the width of the softening melting zone. In reference [4] as cited in [3] a clear dependence of softening and melting temperature and reduction degree was seen, but only for acid pellets, whereas for basic pellets no effect of reduction degree was observed on the melting behaviour. Similarly, in reference [6], authors found no correlation between pre-reduction degree and softening temperature, on the other hand they observed that for acid pellets, the

temperature at which pressure drop rises, increased with pre-reduction degree.

According to Yi. S.H [7], softening temperature decreases and melting temperature increase with an increase in reduction degree. The decrease in softening temperature is due to the collapse of micropores due to reduction. As far as melting is concerned author of reference [8] suggested that degree of reduction alone does not affect the start of rapid contraction, that is melting because it was observed that the temperature for the start of rapid contraction was found to be the same for both strong and weak reducing gases. Therefore, the melting start temperature must be also governed by the degree of carburization. Hence it must be the combined effect of carburization and the amount of liquid slag phase present in the core causing melting phenomena.

The authors in reference [5] are of the opinion that the rise in pressure drop is caused by deformation of pellets and not by exudation of melt from the pellets. In reference [11], to understand the effect of reduction degree on pellets, authors subjected the samples with same chemistry to different reduction degrees and then subjected them to high temperatures of cohesive zone in nitrogen atmosphere. The results showed that with the increase of the reduction degree, the softening start temperature (T1) of pellets did not change significantly whereas the melting start temperature (Tm) increased. The dripping temperature (Td) of the pellets slightly increased with the reduction degree of the pellets. Also, the permeability of the pellets was improved as the reduction degree increased. Therefore, as the reduction degree of the pellets increased, the range of the cohesive zone of the pellets expanded. The softening stage of the cohesive zone was increased and the extent of melting zone reduced, the gas permeability of the pellets layer improved. In literature [16] as cited in [13], author found that the melting temperature decreases with increase in reduction degree, while the dripping temperature increases.

A common shortcoming for the above-mentioned studies with pre-reduced samples is that the softening melting is not carried out simultaneously with the reduction, as happens in the actual blast furnace. It is also important to note here that reduction degree also plays a role during contraction which is not exactly softening, that is more the amount of removal of oxygen greater is the contraction in the pellets apart from actual softening. Also, the effect of thermal expansion of the pellets is needed to be taken into account.

2.3. Degree of Carburization

The carburization of reduced iron is quite important, as with carbon the melting temperature of the iron-carbon alloy decreases, resulting in the lowering of the energy consumption in the blast furnace. On the other hand, for the cohesive zone, a higher degree of carburization results in the early melting of iron shell causing early melt exudation and dripping, hence shifting the cohesive zone to lower temperatures. The aim of this section is to highlight the hypothesis that the layer of slag is present between the iron shell and coke even before melt exudation (Tm), and this layer influences the transport of carbon to the iron affecting the degree of carburization. In addition, it is also necessary to discuss briefly the possible mechanisms of carburization. Murakami et. al [18] summarised the two main mechanisms which include carburization by CO and solid carbon as discussed in sections 2.3.1 and 2.3.2 respectively. The topic of interest is the carburization through slag, which will be explored in section 2.3.3.

2.3.1. Carburization by CO Gas

The proposed carburization reactions on the iron surface are:

$$CO(g) \rightarrow C_{ad} + O_{ad} \quad (2.1)$$

$$CO\ (g) + O_{ad} \rightarrow CO_2(g) \quad (2.2)$$

Where "ad" denotes adsorption of the respective species on the iron surface, the adsorbed carbon molecule diffuses in the iron leading to carburization. The combined reaction, (2.1) and (2.2), is the Boudouard reaction. According to literature [18] the rate of reaction (2.1) is faster than (2.2), hence (2.2) is the rate-determining step. According to citation [14], in the blast furnace, the carbon potential of the gas in equilibrium with iron and FeO is insufficient to saturate the metal in the burden which is away from the coke layer in the thermal reserve and cohesive zone. On the other hand, in reference [3] pellet samples were put on the coke substrate simulating the contact between pellets and cokes in cohesive zone. Each CO and argon was used separately to verify the effect of solid carbon and CO on the carburization reaction. The result of the experiment can be seen in the Figure 2.3.

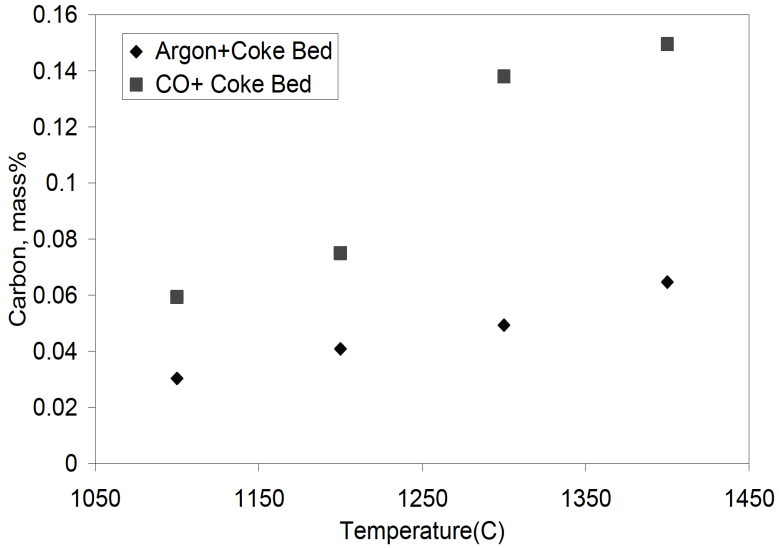

Figure 2.3. Carbon content of reduced pellet with different reaction condition [3].

From the above result, it seems in the cohesive zone, CO plays a significant role in carburization, especially in the early stages when reduced iron is yet to melt and the contact between solid iron and coke is only on the surface.

2.3.2. Carburization by Solid Carbon

The density of carbon in gas phase, which is present as CO, is much smaller than in the solid carbon, so, even after assuming CO activity of gas phase as unity the rate of carburization and iron melting by CO gas should be much smaller than that by solid carbon [18]. For direct carburization, it has been observed that iron melting starts immediately, though locally, as soon as iron comes in contact with a source of solid carbon like graphite or coke [18]. The melting happens at temperatures much lower than the melting point of pure iron, as the liquidus temperature of iron decreases with increase in

carbon content as can be seen from iron-carbon diagram in Figure 2.4. Therefore, it is the mass transfer in this liquid phase that controls the rate of carburization for rest of the bulk iron.

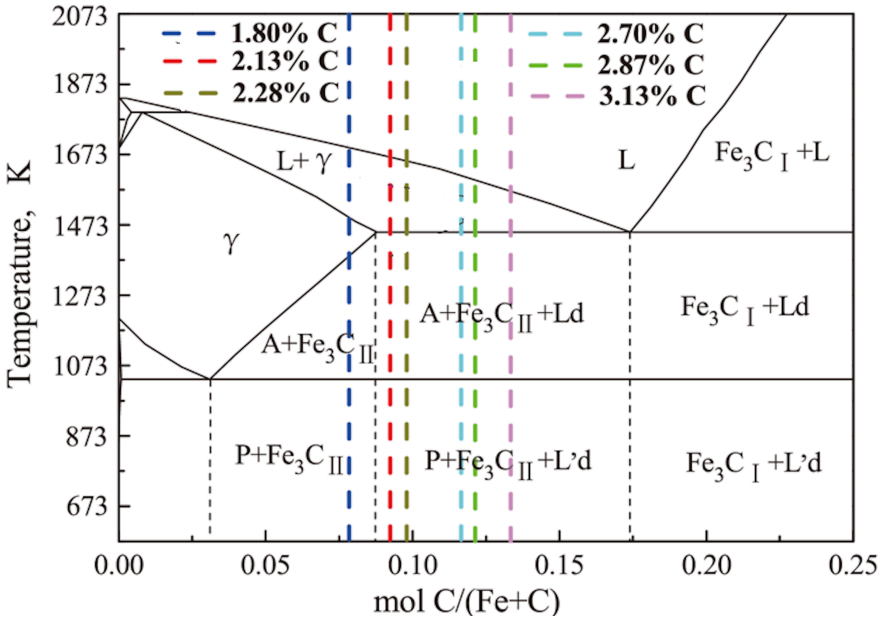

Figure 2.4. Iron-carbon Diagram [19].

Coming to the macroscopic view of the phenomena that leads to meltdown and dripping; at temperatures above 1400°C the carburisation of the metallic iron is fast, and due to the increasing temperature, the metal in contact with carbon will eventually melt.

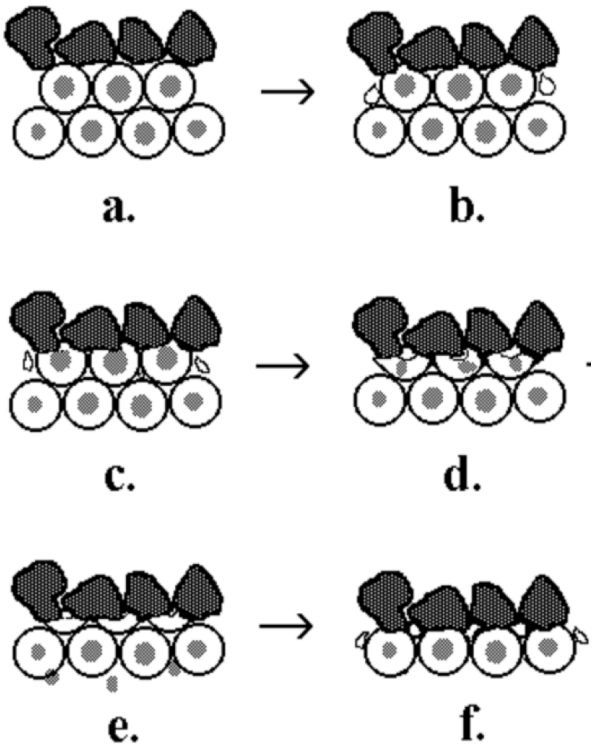

Figure 2.5. Schematic of continuous process of carburization and melt down [8].

The step wise process of carburisation and melt-down during rapid contraction is schematically shown in Figure 2.5, each stage can be understood as;

a) & b) At the start of the melting, only a small part of the pellets is in contact with solid carbon and the melting rate is low.

c) The melting rate accelerates due to an increase in contact surfaces between the iron and the carbon as the melted parts drip away from the interface. Possibly also the carburized liquid metal penetrating down through the sample bed helps in accelerating the process by carburizing the metal not in direct contact with carbon.

d) Finally, the outer metallic shell of the particle becomes very thin and breaks. The core of liquid slag retained inside the shell is released and penetrates down through the sample bed.

e) In the coke layer below the sample, the iron oxide of the slag phase will be quickly reduced due to the high temperature and the favourable kinetics of the liquid/solid phase reaction.

f) This process of carburisation, melting and collapsing will repeat for the next layer of particles now exposed to the carbon surfaces of the coke layers.

2.3.3. Carburization Through Slag

Carburization through slag can be classified into carburization through slag containing FeO (primary slag) and slag without FeO (bosh slag), which are discussed in sections 2.3.3.1 and 2.3.3.2 respectively.

2.3.3.1. Carburization Through FeO Rich Slag

According to Ohno et al [20], in the cohesive zone, where FeO rich primary slag is formed, there is a possibility of iron carburization through the slag phase during smelting reduction as shown in Figure 2.6. Here three phases namely; carbon from coke, slag, and the reduced iron shell comes in contact with each other. It has been observed by the authors of reference [14] that at temperatures as low as 1150°C, large pockets of slags amid the metallic iron network, probably filling pre-existing pores, appearing to be exuded from the core of the sample. These can cause reduction retardation and also take part in carburization. The proposed mechanism of carburization by authors of literature [21] is shown in Figure 2.7.

Briefly the mechanism entails that; when iron oxide rich slag comes in contact with the carbon of coke, the iron oxide in the slag is reduced. The Fe particles are formed accompanied by CO gas bubbling at the slag-carbon interface, the carburization and melting of the Fe particles takes place (2.7 a). Due to the Marangoni effect, the molten Fe-C particles are carried from slag-carbon interface to slag-iron interface (2.7 b). Once reaching the slag-iron interface, the Fe and the CO is again generated due to the reduction of FeO of slag by carbon from Fe-C particles. More importantly Fe-C particle wet the surface of Fe causing carburization of Fe surface, carbon then diffuses into the bulk (2.7 c). Hence reduced iron is carburized via molten metal particles carburized by carbonaceous materials through the slag phase. To better understand the role of slag in the mechanism of carburization, the whole process can be divided into three main parts:

1) Smelting reduction reaction
2) Slag Flow
3) Diffusion of Carbon in Iron

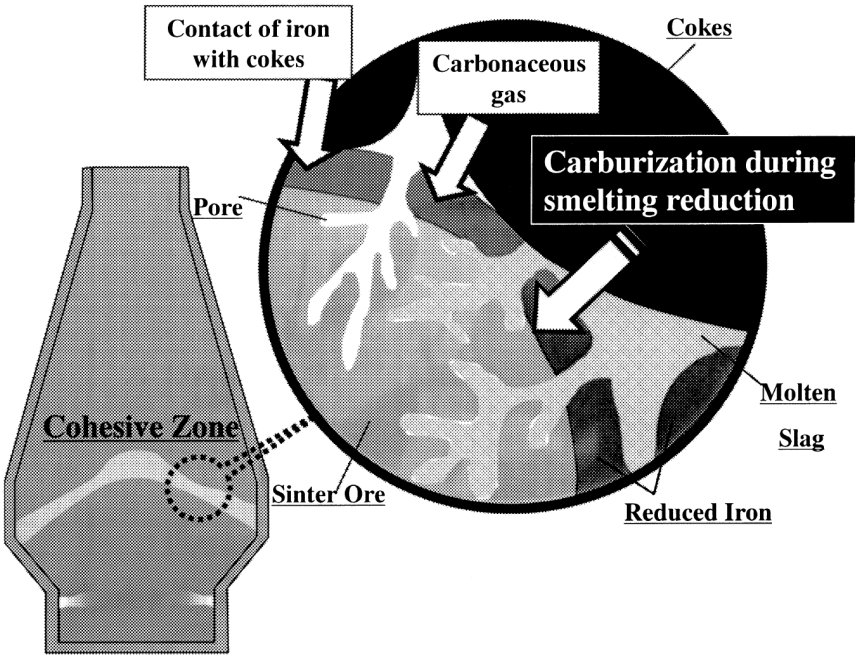

Figure 2.6. Illustration of carburization phenomena through slag at the cohesive zone [20].

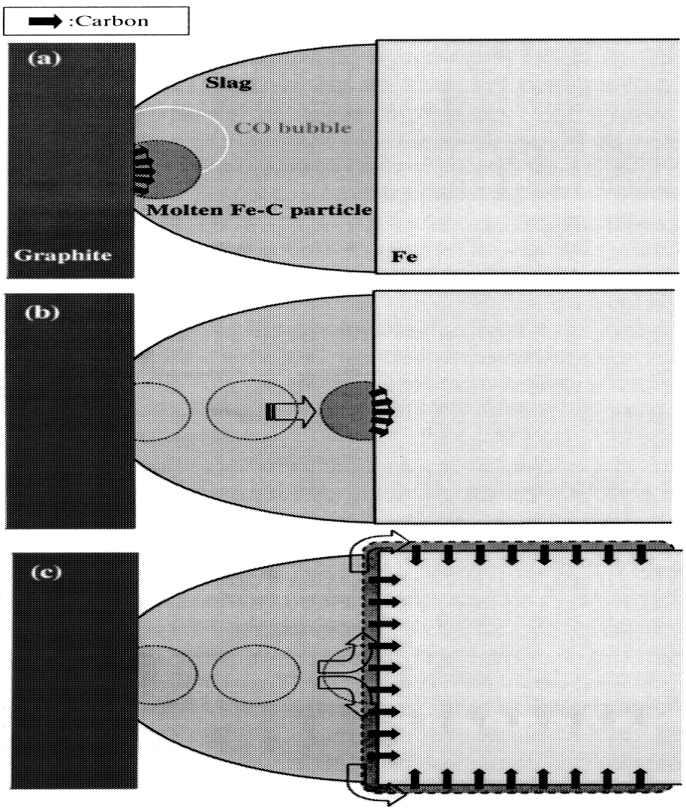

Figure 2.7. Illustration of carburization mechanism during smelting Reduction [21].

Smelting Reduction Reaction

The reaction in a nut shell is the removal of oxygen from the slag, hence the rate of reaction can be written as:

$$Rate = -\frac{dW_0/dt}{A} \quad \text{[Kg of Oxygen/ m}^2\text{ s]} \qquad (2.3)$$

Where, W_0 is the amount of oxygen removed by smelting reduction, t is reaction time, and A is interfacial area of reaction. Equation (2.3) can be modified for the change in weight of FeO of the slag due to reduction as follows:

$$Rate = -\frac{M_0}{M_{FeO}}.\frac{dW_{FeO}}{dt}.\frac{1}{A} \quad \text{[Kg of Oxygen/ m}^2\text{ s]} \qquad (2.4)$$

Where, M_0 [kg] is atomic weight of oxygen and M_{FeO} [kg] is molecular weight of wüstitel. According to literature review done by Nagasaka et al [22] this is a second order reaction; hence rate can also be written as:

$$Rate = K^{2nd}.mass\%FeO^2 \quad \text{[Kg of Oxygen/ m}^2\text{ s]} \qquad (2.5)$$

Where K^{2nd} is the rate constant for second order reaction. Further, it is convenient to bring weight of slags into calculations, this can be done by using equation (2.6).

$$dW_{FeO} = W_{slag}.\frac{d(mass\%FeO)}{100-mass\%FeO} \quad \text{[Kg - iron oxide]} \qquad (2.6)$$

Where, W_{slag} [kg] is initial amount of slag. Substituting equation (2.6) in equation (2.4) and then equating modified equation (2.4) and equation (2.5) and then integrating leads to equation (2.7):

$$\left[\frac{1}{(mass\%FeO)} + \frac{1}{100}\ln\left(\frac{100}{(mass\%FeO)} - 1\right)\right]_{mass\%FeO_{initial}}^{mass\%FeO_{time}} = 100.A.\frac{M_0}{M_{FeO}}.\frac{k^{2nd}}{W_{slag}}.[t]_0^{time} \qquad (2.7)$$

Ohno et al compared the theoretical values for removed FeO using equation (2.7) with actual experimental values and found a good agreement between the two.

Slag Flow

Marangoni flow is caused by gradient in surface tension where a liquid with high surface tension pulls a liquid having low surface tension. The gradient in surface tension in slag is caused by gradient in concentration of FeO, which in turn is caused by the smelting reduction reaction at the carbon slag interface. Therefore, this flow of slag takes Fe-C particles, produced at slag carbon interface, with it to Fe surface. This can be expressed by the equation below:

$$V = \frac{\partial f}{\partial C}\frac{\Delta C}{\mu} \tag{2.8}$$

Where V is velocity [m/sec] of the slag which would be the same for the Fe-C particle flowing with it, ƒ is the surface tension [N/m], μ is the viscosity [Pa.sec], ΔC is the difference in FeO content at slag-Fe and slag-carbon interface.

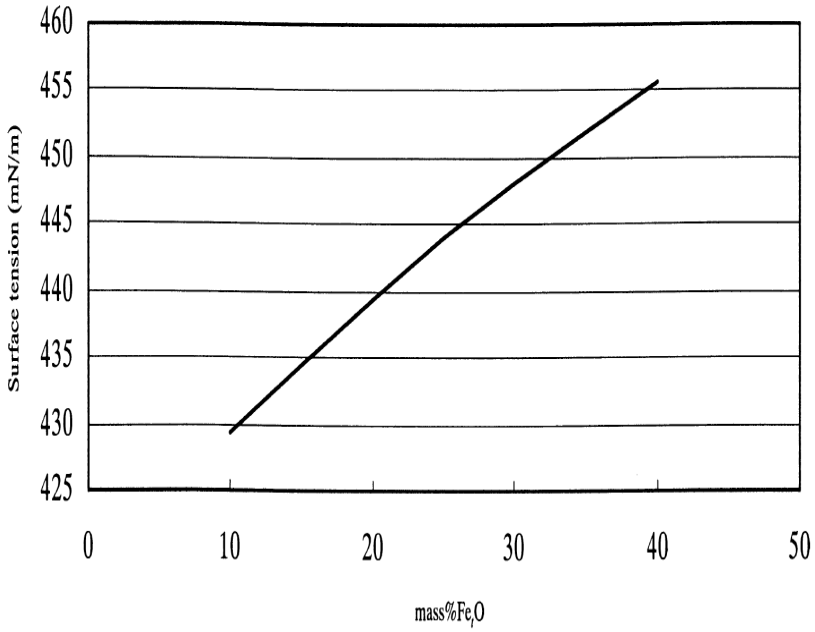

Figure 2.8. Effect of FeO Content on surface tension with rest of the components of slag being constant [20].

Figure 2.8 shows that surface tension of a slag increases with FeO content, which explains why slag flows from carbon-slag interface to iron-slag interface. Authors of reference [20] observed that even slight difference of FeO create slag flow sufficient to carry Fe-C particles with it.

Diffusion of Carbon in Iron

The last step is the diffusion of carbon in iron, for this authors of reference [20] assumed semi-infinite diffusion in longitudinal-direction from the slag–Fe interface, the fundamental equation for this is given by Fick's second law:

$$\frac{\partial C}{\partial t} = D \cdot \frac{\partial^2 C}{\partial x^2} \tag{2.9}$$

Where, t is the reaction time, C is the carbon content in iron, D is the diffusion coefficient, x is the distance in Fe, the solution of differential equation (2.9) is:

$$\frac{C-C_s}{C_0-C_s} = erf\,\frac{x}{2\sqrt{Dt}} \qquad (2.10)$$

C_0 is the initial's carbon content in iron matrix and Cs is the carbon content on solidus in Fe–C system at the fixed experimental temperature. The curve fitting between calculated and experimental carbon profile showed a good match.

2.3.3.2. Carburization Through Slag Containing No FeO

In the previous discussion, the mechanism of carburization via slag containing FeO was discussed, where FeO played the central role in transferring Fe-C particles from slag-carbon to slag-iron interface. This is true for the primary slag, but the slag gradually losses its FeO due to reduction. Hence, it is of interest to see the mechanism of carburization on other extreme, that is in the FeO less slag. The mechanism proposed by Ono et al [23] is presented here. In the absence of FeO, the dissolution of carbon in the slag phase is given by:

$$C(s) + \frac{1}{2}O^{2-}(slag) \rightarrow C^{-}(\text{slag}) + \frac{1}{4}O_2\,(g) \qquad (2.11)$$

$$CO_2 + O^{2-}(in\ slag) \rightarrow CO_3^{2-}\,(in\ slag) \qquad (2.12)$$

That is, the carbon can dissolve in slag as both carbide and carbonate ion, these reactions take place at the carbon/slag interface and reverse reaction will take place at the slag/Fe interface where carburization of Fe surface will occur. The carbon concentration profile for carburization reaction through the successive phases of carbon, slag, and iron is shown in Fig 2.9. This discussion will be continued in section 5.2, where the effect of alumina and basicity on the degree of carburization will be discussed.

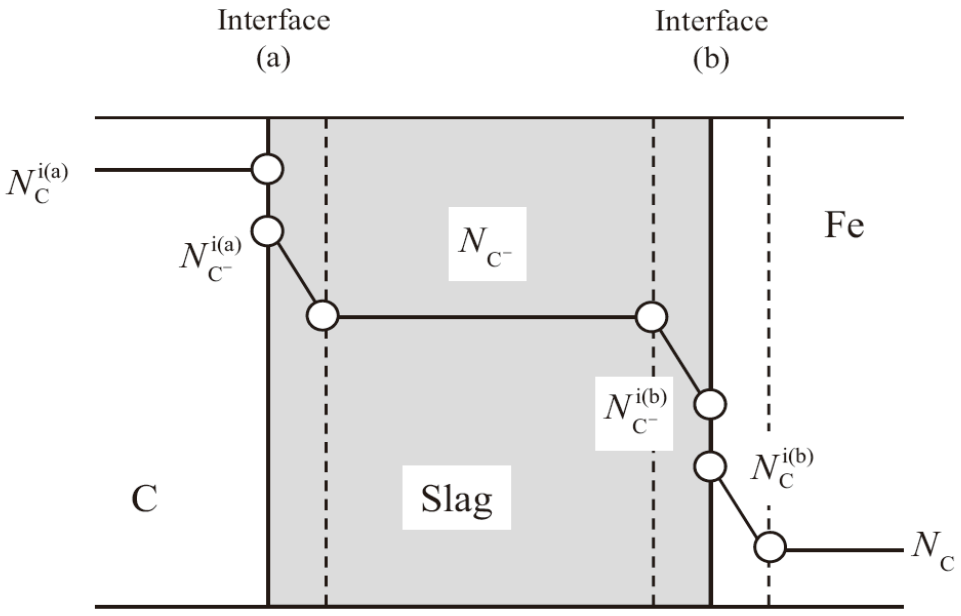

Figure 2.9. Profile of carbon contents through successive phases of carbon, slag, and iron [23].

This section highlights the possible role slag play during carburization. Since Al_2O_3 is one of the constituents of slag, the change in its proportion changes the properties of slag hence affecting

decarburization. Unfortunately, this topic hasn't been given due attention yet, therefore a theoretical attempt will be made in section 5 towards understanding possible effects of Al_2O_3.

2.4. Viscosity of Slags

Another property that has a huge influence on the cohesive zone is the viscosity of the slag. In particular, viscosity has a direct impact on the metal/slag separation efficiency, the metal/slag reaction kinetics, and more importantly on the permeability of the intermediate gases used for reduction and heat transfer.

In the later stage of the cohesive zone, coke is the only solid material present and is responsible for providing a passageway for the tuyere gas to flow up. The liquid from the melting burden fills the interstices of the coke grid impeding the gas flow. The resistance to gas flow ultimately results in liquid hold-up (loading) in the coke voids causing a steep rise in pressure drop. The gas has to bubble through a mass of liquids, which in extreme cases is carried upwards mechanically leading to the so-called flooding. The tendency of flooding is proportional to the viscosity of the liquid [24]. Since iron is much heavier it drips easily, hence it is the slag, and its viscosity which becomes an important for permeability and in turn productivity of the blast furnace. A viscous slag severely deteriorates the permeability, forcing the blast furnace operator to reduce the blast volume, the blast volume determines the coke burning rate, the reduction rate of iron ores, hence productivity.

Viscosity is a measure of the ability of slag to flow when the shear stress is applied. It is commonly assumed that a fully liquid slag is a Newtonian fluid, which means its viscosity is independent of the applied force (shear stress) [26]. As a result, viscosity is defined by the Newton's equation:

$$\tau_{xy} = \eta . \frac{dV_x}{dy} \qquad (2.13)$$

where;

η - dynamic viscosity coefficient, Pa.s

τ_{xy} - shear stress, Pa,

$\frac{dV_x}{dy}$ - the gradient of normal velocity to the shear stress, so called shear rate.

Since viscous flow takes place by movement of particles past other particles, one can better understand viscosity by considering the mobility of an individual particle. Einstein equation shows that the mobility of a particle under the influence of an external force is related to the diffusion coefficient which is given by the relationship shown in equation (2.14) [25]:

$$D = Bk_bT \qquad (2.14)$$

where,

D – diffusion coefficient

B – mean velocity divided by force acting on the particle

K_b – Boltzmann constant

T – Temperature

Diffusion is an activated process, that is a minimum activation energy has to be supplied for the particle to move from one stable position to another, since viscosity is opposite to fluidity, viscosity can be expressed as in equation (2.15) [25]:

$$\eta = A\, exp^{\frac{\Delta Gvis}{RT}} \quad (2.15)$$

A – Arrhenius constant

ΔG_{Vis}– activation energy for viscous flow

It is important to note that the viscosity is an exponential function of operating temperature, that is viscosity is very sensitive with changes in temperature. One important parameter arising from this is Critical Temperature (CT), it is defined as the temperature below which the slag viscosity rises steeply, and a low critical temperature represents a wide thermostable operation region, which is advantageous to actual production. It has been reported that the slag with more content of high-melting-point substances shows stronger crystallization capacity, hence higher critical temperature, therefore CT is very much dependent on phases present in the slags [31].

Since transport process of liquid is all about flow of particles from one stable position to another, it is the structure of slag that governs the viscosity. Much less is known about the structure of liquids than about the structures of solids or gases. However, there is more similarity between liquids and solids than between liquids and gases. This similarity is based on the small increase in volume on melting, and the fact that the heat of fusion is quite less than the heat of vaporization. In addition, X-ray analysis, have shown that at a short distance from a central atom, the arrangement of nearest neighbours is reasonably predictable [25]. However, as the distance increases, the predictability of atom positions decreases rapidly, hence in order to understand the structure of liquid slag, the structure in solid state serves a good starting point. Blast Furnace slags are homogeneous melts, mainly consisting of oxides of silicon in addition to other elements. Crystal analysis of solid silica shows that silicon occupies the centre of a tetrahedron surrounded by 4 oxygen atoms, one at each of the four corners [25]. Each oxygen atom is bonded to two silicon atoms and the network is continuous in three dimensions. These tetrahedra can share only corners. On one hand where the solids show a long-range order, on the other hand in molten state, the structure becomes distorted but most of the corners remains shared [25]. Figure 2.10 shows schematically the comparison of silica structure in solid and liquid state. When SiO_2 is melted, the arrangement presumably continues, but the long-range order is destroyed, however, the same Si-O bonds are present and these strong high energy bonds need to be broken so that viscous flow can take place.

Blast furnace slag also consists of cations and other anions resulting from ionization of basic and acidic constituents in molten oxide solution. It is considered that an acidic component is an oxide which consumes free oxygen ions (O^{2-}) to produce bridged oxygen (O^0) and polymerize the slag producing complex structures. While a basic oxide provides free oxygen ion (O^{2-}) which reacts with the bridged oxygen (O^0) in the silicate melts to produce non-bridged oxygen (O^-) and depolymerize the network structure of the slags [27]. The complexity (polymerization) of the silicate, and the degree of polymerization (DOP) is correlated with the non-bridged oxygen per tetrahedrally coordinated cation (NBO/T). For silicate structures, NBO/T can be defined as NBO/Si.

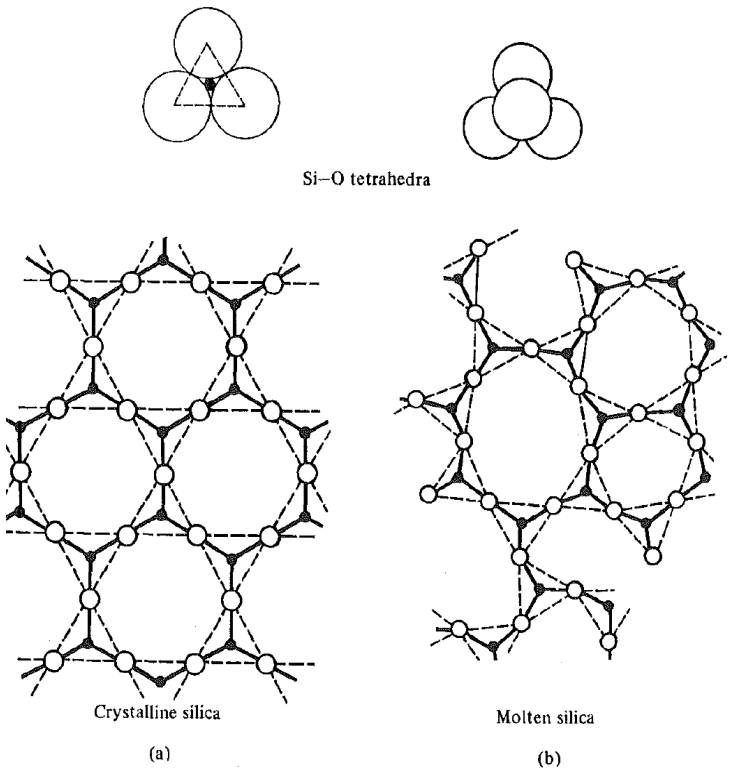

Figure 2.10. Structure of Silica in solid and molten state [24].

Ca and Mg have a tendency for losing electrons easily in order to complete their electronic configuration, unlike Si which has a tendency of forming strong covalent bonds. So, calcium and magnesium lose oxygen ion easily and dissociates into its cation (M^{x+}) and anion (O^{2-}) and reacts with the bridged oxygen of the silicate to form non-bridged oxygen. As the three-dimensional network breaks down due to addition of basic oxides the number of Si-O bonds that needs to be broken during the viscous flow decreases hence activation energy falls off continuously as the basic oxides are added.

On first look it might seem that only purpose of basic oxide is to provide O^{2-} ions for depolymerisation, but the cationic part also plays a role in modifying the structure, hence viscosity. When considering the effect of cations on the melt structure, both the electrical charge and the cation size are required to be considered [27]. This can be done by using the parameter Z/r^2 (ionization potential) where Z is the valence of ion and r is the ionic radius. Higher the Z, stronger the tendency of cation to form ionic bond. The smaller r, results in higher bond strengths and makes it easier for the cation to position itself in the network to provide charge balancing and to connect the non-bridged oxygen of the various structural units like Q^0 (NBO/T = 4), Q^1 (NBO/T = 3), Q^2 (NBO/T = 2), and Q^3 (NBO/T = 1). An example of Cation modifying the structure of slag is shown in Figure 2.11, where cation is placed in an octahedral void formed by non-bridged oxygens. The above discussion provides a good under footing to discuss the effect of alumina on structure hence viscosity of slag, which will be done in the chapter 5.

Before moving ahead, it is important to remind that in the above discussion, slag is considered to be a Newtonian fluid, which is true only when it is in the complete liquid state. In the blast furnace, the burden softens and melts gradually and there is a very real possibility that primary slag which forms in the cohesive zone might already start dripping in a semisolid state. Even if it does not drip in a semi-solid state, the solid particles can still precipitate from liquid slag, due to changes in the chemical composition as a result of elements entering the slag from the outside (e.g. coal dust, carbides, nitrides

insoluble in slag) [26]. Also, locally the temperatures might fall, causing partial re-solidification, as the condition in the blast furnace is not uniform. As soon as any of this happens the viscous behaviour becomes non-Newtonian.

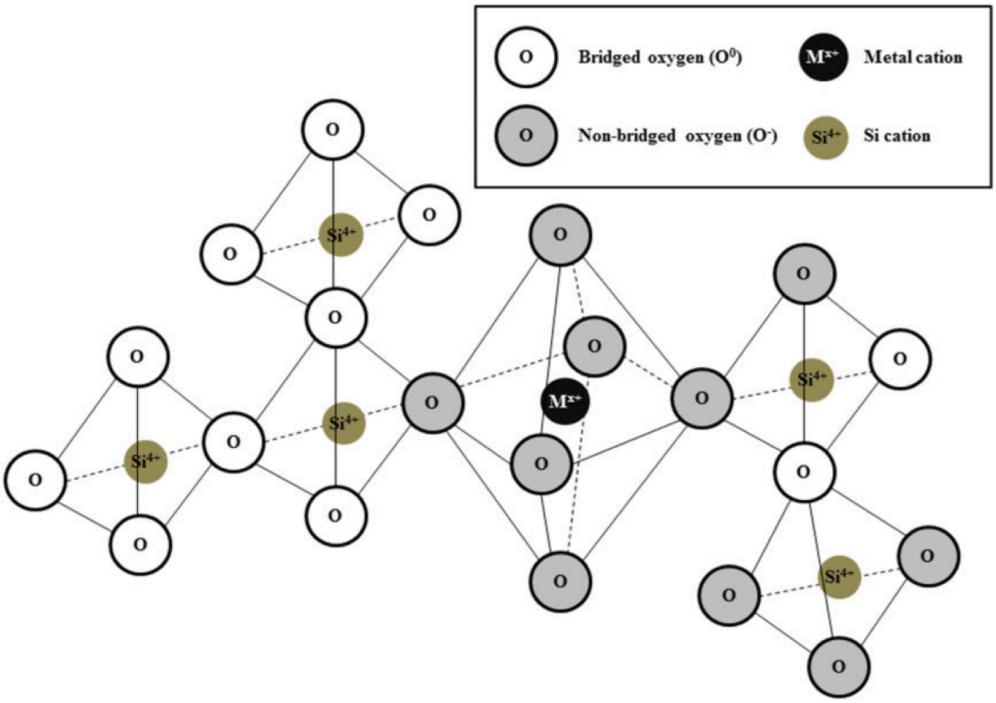

Figure 2.11. Schematic illustration of the charge balancing and structural relationship of cation (M^{x+}), bridged oxygen (O^0) and non-bridged oxygen (O^-) in silicate melts [27].

According to refernces [26] [28] [30], the viscosity of the primary slag with solid particles can be estimated using Einstein–Roscoe equation:

$$\eta = \eta_0(1 - \alpha f)^{-n} \qquad (2.16)$$

where,

η – viscosity of the solid-containing slag

η_0– viscosity of the solid-free slag

f – volume fraction of solid particles in melt

α and n – constants

Roscoe suggested α and n to be 1.35 and 2.5, respectively [29].

Einstien Roscoe is one of many models which are used for finding the viscosity of fluids with solids suspended in them, some others being Ostwald de Waele'a power law model, Bingham model, Krieger-Dougherty and Carreau-Yasuda mode [26].

2.5. Surface Tension and Wettability

Just like viscosity, the wettability of the slags also play an important role in permeability of cohesive zone, as it is seen that tendency for flooding increases with decrease in surface tension of wetting slags [24]. Therefore, hydraulic resistance to gas flow is likely to increase with decreasing surface tension of the wetting slag. Taking a step back, wettability also governs the ease with which exudation of slag takes place from the pellets. It has been observed that it is actually the difference in surface energy between slag and metallic shell that causes flow of slag from core to the surface [17]. According to author of reference [17], once melt has formed within the core, matter is transferred from this region into the porosity of the metallic iron shell. This transfer is surface-energy driven, and does not require some kind of mechanical driving force. Melt is not pushed, but pulled into the shell. A remarkable observation during the experimental work in reference [17] was that, melt did not spontaneously exude from the samples, unless a large crack was present within the iron shell. Even at temperatures significantly above the liquidus temperature of the iron oxides/slag combinations, melt remained within the porosity of the metallic iron shell. Similarly, in reference [14], when authors observed a slag layer surrounding the metallic shell at temperatures as low as 1150°C, difference in surface tension between the slag and the metallic iron was considered as the most plausible driving force.

In order to understand surface tension, a very simple thermodynamic model based on Butler equation [34] as presented in reference [32] is shown here, which lays the foundation for further discussion. Starting from a pure system, in a standard state condition, the total energy of a system can be written as:

$$Total\ Energy = Energy\ Bulk + Energy\ Surface \tag{2.17}$$

$$\frac{Energy\ Bulk}{mole} = \mu_i^{0,b} \tag{2.18}$$

$$\frac{Energy\ Surface}{mole} = \mu_i^{0,s} \tag{2.19}$$

Where, $\mu^{0,b}$ and $\mu^{0,s}$ are the chemical potential in the bulk and the surface of the species. Since the energy on the surface is greater than that in the bulk, it can be written that:

$$\mu_i^{0,s} = \mu_i^{0,b} + A_i.\sigma_i^{pure} \tag{2.20}$$

where, A_i is the molar surface area, and σ_i is the surface tension of the pure species *i*.

The cohesive force between molecules down into a liquid is shared with all the neighboring atoms. Those on the surface have no neighboring atoms above, therefore, they exhibit a stronger attractive force upon their nearest neighbors on the surface. This is why force on the surface is stronger, leading to surface tension. Now, the same argument of equation 2.17 can be applied for calculating the total energy of a liquid alloy consisting of various components;

$$\mu_i^b = \mu_i^{0,b} + RTln^{a_i^b} \tag{2.21}$$

$$\mu_i^s = \mu_i^{0,b} + A_i.\sigma_i^{pure} + RTln^{a_i^s} \tag{2.22}$$

Where, μ_i^b and μ_i^s are the chemical potential of the i[th] species in the bulk and the surface, in an alloy and a_i^b and a_i^s are their activities in bulk and surface respectively. The difference in the chemical potential is the net surface energy of the system

$$\mu_i^s - \mu_i^b = A_i.\sigma_{net} \quad (2.23)$$

Where, σ_{net} is the surface tension for the alloy here. Expanding and rearranging the equation (2.23), results in the equation (2.24)

$$\sigma_{net} = \sigma_i^{pure} + \frac{RT}{A_i} ln^{a_i^s}/a_i^b \quad (2.24)$$

Equation (2.24) was first derived by Butler [34]. Based on Butler equation, Tanaka et al [35] derived a semi-empirical equation which better represents the surface tension of slags,

$$\sigma_{net} = \sigma_i^{pure} + \frac{RT}{A_i} ln^{M_i^{Surf}}/M_i^{Bulk} \quad (2.25)$$

where

$$M_i^p = \frac{\left(\frac{Rc_i}{Ra_i}\right).N_i^p}{\sum_i\left(\frac{Rc_i}{Ra_i}\right).N_i^p} \quad (2.26)$$

Superscripts "*Bulk*" and "*Surf*" refer to the bulk and surface respectively (p = Bulk or surface). Rc_i and Ra_i are the radius of cation and anion of a given species respectively. N_i^p is the mole fraction of given species on bulk when "*p"* is bulk, and surface when "*p"* is surface. The reason for complicating a simple Butler equation can be understood by looking into the principal parameters which influence the surface tension of liquid slags, these are.

1) Melt Temperature
2) Melt Composition
3) Ionic Structure

The butler equation takes care of only the Temperature (RT) and composition part (activity), whereas it is well known that for ionic systems structure also depends upon the ratio of the radius of cation to that of anion hence these were empirically inserted by Tanaka et al [33]. It is known that the structure and molecular distribution (composition) of the molten slag at the surface is quite different from that present in the bulk, which happens in order to minimize the total energy of the system. Also, it is important to note that the proportion of a component present on the surface is not completely independent from the bulk composition.

Now, surface tension is just a material property, on the other hand wetting is a behaviour arising from solid-liquid couple. This is traditionally quantified as contact angle, as seen from famous Young's equation:

$$\gamma_{LV}.cos\theta = \gamma_{SV} - \gamma_{SL} \quad (2.27)$$

Where γ_{LV} is surface tension of a liquid-vapor system, γ_{SV} is surface tension of a solid-vapor system, γ_{SL} is the interfacial tension of the actual liquid–solid contact. The lower the value of θ the greater the wettability. It is visible from Young's equation that surface tension of slag is only one part of the equation. The effect of surface tension, on wettability, depends on γ_{SV} and γ_{SL}. That is, when surface

tension of solid is greater than the solid-liquid interfacial tension, then with increase in surface tension of liquid, the contact angle increases that is wettability decreases. On the other hand, if the surface tension of solid is smaller than the solid-liquid interfacial tension, then with increase in surface tension of liquid, the contact angle decreases that is wettability actually increase. Hence in section 5.4 first the effect of alumina on surface tension of slags will be seen and then wettability.

2.6. Summary

The characteristic feature of the cohesive zone is the softening and melting of the ferrous burden. This includes a decrease in the rate of reduction called reduction retardation, then melt exudation leads to a rise in pressure drop over the bed, and finally dripping of the liquid through the bed results in direct reduction. The degree of reduction governs the iron shell thickness, hence the ability of the pellet to resist the combined effect of load and temperature. A Large shell thickness requires a high temperature for melt exudation. Also, with the reduction degree the amount of slag in the core of the pellets reduces. Lower slag means lower resistance to dripping.

In addition to the reduction degree, the degree of carburization also influences the melt exudation temperature. With an increase in carbon content, the melting point of iron shell decreases, causing early melting and dripping. The mechanisms for carburization of the iron shell include; via CO gas, directly through solid coke and through a slag layer sandwiched between iron shell and coke. Carburization through slag involves three major steps namely; smelting reduction at the coke-slag interface, transport of the Fe-C particles from the coke-slag interface to the slag-Fe interface, carburization of the iron shell, and diffusion of carbon to the bulk.

Once the melt exudes, the ease of dripping is governed by the viscosity and wettability of the slag with iron and coke. The viscous flow is an activated process, therefore, it is expressed with the Arrhenius type equation. In addition to temperature, viscosity is highly dependent on the chemistry of slag. There are mainly two types of oxides, acidic and basic. Acidic oxides are network formers, causing polymerization of the melt and increasing its viscosity. Basic oxides are network modifiers, causing de-polymerization and reduction in viscosity. The third kind of oxides is the amphoteric oxides which will be discussed later in chapter 5 with example of alumina.

Due to a lack of bonds on the surface, molecules exhibit stronger cohesive forces with their nearest neighbors resulting in the surface tension. The surface tension can be understood with a simple thermodynamic model. The difference in the energy of atoms/molecules on the surface and bulk is used to derive the surface tension of the system. The Butler equation developed from this simple approach only considers the effect of composition and temperature. The ionic structure is another important aspect. The effect of the ionic structure was incorporated by Tanaka et al [35] using the cation to anion radius ratios of the relevant species. The wettability is dependent on solid-liquid couple and is usually quantified by the contact angle. The Young's equation is commonly used for calculating contact angles.

2.7. References

[1] Shatokha, V., & Velychko, O. (2012). Study of softening and melting behaviour of iron ore sinter and pellets. *High Temperature Materials and Processes*, *31*(3), 215–220.

[2] Ritz, V.J., Kortmann, H.A and Koch, K.: "Reduction, softening and melting properties of pellets, sinters, Lumpy ore and mixed furnace burden", 1998 ICSTI/Ironmaking Conference Proceedings, ISS, Warrendale, PA, USA, pp.1635-1654

[3] Lee, S. H. (2009). Reduction and Softening/Melting Behaviour of Olivine Pellet in the Experimental Blast Furnace Certificate of Originality. September.

[4] Barnaba, P.: "Influence of chemical characteristics on softening and melt-down properties of iron ore sinter", Ironmaking and Steelmaking, v.12(2), 1985, pp.53-63

[5] Kemppainen, A., Ohno, K. I., Iljana, M., Mattila, O., Paananen, T., Heikkinen, E. P., Maeda, T., Kunitomo, K., & Fabritius, T. (2015). Softening behaviour s of acid and olivine fluxed iron ore pellets in the cohesive zone of a blast furnace. *ISIJ International*, *55*(10), 2039–2046.

[6] Clixby, G. (1981). *The softening and melting of blast furnace burden materials.*

[7] Yi, S-H.: "Softening and melting properties of pellets for a high level of pulverized coal injected blast furnace operation", Scandinavian J. of Metallurgy 28, 1999, pp. 260-265

[8] J. Sterneland: "Some aspects on the reduction of olivine pellets in laboratory scale and in an experimental blast furnace", Doctoral thesis

[9] Lee, S. H., Khanna, R., Lindblom, B., Hallin, M., & Sahajwalla, V. (2009). Reduction behaviour of olivine iron ore pellets in the experimental blast furnace. *Steel Research International*, *80*(10), 702–708.

[10] Iljana, M., Kemppainen, A., Paananen, T., Mattila, O., Heikkinen, E. P., & Fabritius, T. (2016). Evaluating the reduction-softening behaviour of blast furnace burden with an advanced test. *ISIJ International*, *56*(10), 1705–1714.

[11] Pan, Y. Z., Zhang, A. J., Lin, L., Wang, J. S., Feng, H. X., & Lin, Q. S. (2019). Correlation Between Reduction Degree and Softening and Melting Properties of Pellets. *Minerals, Metals and Materials Series*, 523–530.

[12] Borinder, T.: "High temperature behaviour of some blast furnace pellets. Part II", Scandinavian J. of Metallurgy 16, 1987, pp. 129-133

[13] Nogueira, P. F., & Fruehan, R. J. (2004). Blast furnace burden softening and melting phenomena: Part I. Pellet bulk interaction Observation. *Metallurgical and Materials Transactions B: Process Metallurgy and Materials Processing Science*, *35*(5), 829–838.

[14] Nogueira, P. F., & Fruehan, R. J. (2005). Blast furnace burden softening and melting phenomena: Part II. Evolution of the structure of the pellets. Metallurgical and Materials Transactions B: Process Metallurgy and Materials Processing Science, 36(5), 583–590.

[15] Nogueira, P. F., & Fruehan, R. J. (2006). Blast furnace burden softening and melting phenomena: Part III. Melt onset and initial microstructural transformations in pellets. *Metallurgical and Materials Transactions B: Process Metallurgy and Materials Processing Science*, *37*(4), 551–558.

[16] Khaki, J.V.: "High temperature behaviour of fluxed pellets during heating up reduction", Ironmaking and Steelmaking, v.21(1), 1980, pp.56-63

[17] Bakker, T.: "Softening in the Blast Furnace Process" PhD Thesis, Delft University of Technology, Netherlands, 1999

[18] Murakami, T., & Nagata, K. (2003). New ironmaking process from the viewpoint of carburization and iron melting at low temperature. *Mineral Processing and Extractive Metallurgy Review*, *24*(3–4), 253–267.

[19] Fan, X., Jiao, K., Zhang, J., Wang, K., & Chang, Z. (2018). Phase transformation of cohesive zone in a water-quenched blast furnace. *ISIJ International*, *58*(10), 1775–1780.

[20] Ohno, K. I., Miki, T., & Hino, M. (2004). Kinetic analysis of iron carburizaiton during smelting reduciton. *ISIJ International*, *44*(12), 2033–2039.

[21] Ohno, K. I., Nagasaka, T., & Hino, M. (2003). "In situ" observation of smelting reduction and carburization of iron ore with carbonaceous materials by laser scanning microscope. *Steel Research*, *74*(1), 5–8.

[22] Nagasaka, T., Hino, M. & Ban-Ya, S. Interfacial kinetics of hydrogen with liquid slag containing iron oxide. *Metall and Materi Trans B* **31,** 945–955 (2000).

[23] Ono, H., Tanizawa, K., & Usui, T. (2011). Rate of iron carburization by carbon in slags through carbon/slag and slag/metal reactions at 1 723 K. *ISIJ International*, *51*(8), 1274–1278.

[24] Biswas, A. K. (Anil K. (1981). *Principles of blast furnace ironmaking : theory and practice / Anil K. Biswas*. Cootha Publishing House.

[25] Poirier, D. R., & Geiger, G. H. (2016). *Viscous Properties of Fluids BT - Transport Phenomena in Materials Processing* (D. R. Poirier & G. H. Geiger (eds.); pp. 3–37). Springer International Publishing.

[26] Migas, P., & Korolczuk-Hejnak, M. (2014). Semi-solid state of blast furnace slag admixtures of Al2O3. *Archives of Metallurgy and Materials*, *59*(1), 173–182.

[27] Sohn, I., & Min, D. J. (2012). A review of the relationship between viscosity and the structure of calcium-silicate-based slags in ironmaking. *Steel Research International*, *83*(7), 611–630.

[28] Wu, S., Huang, W., Kou, M., Liu, X., Du, K., & Zhang, K. (2015). Influence of Al2O3 content on liquid phase proportion and fluidity of primary slag and final slag in blast furnace. *Steel Research International*, *86*(5), 550–556.

[29] R. Roscoe, Br. J. Appl. Phys. 3, 1952, 267.

[30] Vetere, F., Behrens, H., Holtz, F., Vilardo, G., & Ventura, G. (2010). Viscosity of crystal-bearing melts and its implication for magma ascent. *Journal of Mineralogical and Petrological Sciences*, *105*(3), 151–163.

[31] li, Tingle & Sun, Changyu & Song, Sunny & Wang, Qi. (2019). Influences of Al2O3 and TiO2Content on Viscosity and Structure of CaO–8%MgO–Al2O3–SiO2–TiO2–5%FeO Blast Furnace Primary Slag. Metals. 9. 743. 10.3390/met9070743

[32] Liu, Y., Lv, X., Bai, C., & Yu, B. (2014). Surface tension of the molten blast furnace slag bearing TiO2: Measurement and evaluation. *ISIJ International*, *54*(10), 2154–2161.

[33] Tanaka, T. (2013). Surface Tension Models. In *Treatise on Process Metallurgy* (Vol. 2). Elsevier Ltd.

[34] J.A.V. Butler, Proc. R. Soc. A. 135 (1932) 348.

[35] Hanao, M., Tanaka, T., Kawamoto, M., & Takatani, K. (2007). Evaluation of surface tension of molten slag in multi-component systems. *ISIJ International*, *47*(7), 935–939.

[36] Gavel, D. J., Adema, A., Stel, J. Van Der, Sietsma, J., Boom, R., & Yang, Y. (2019). Effect of nut coke addition on physicochemical behaviour of pellet bed in ironmaking blast furnace. *ISIJ International*, *59*(5), 778–786.

3. Experiment and Characterization

Section 3.1 introduces the Reduction, Softening, and Melting (RSM) apparatus, where various systems important for its working are explained. Section 3.2 deals with the niceties of procedural aspects of the experiment. Section 3.3 presents the iron ore pellets used in the RSM experiments which were characterized using the tools mentioned in section 3.4.

3.1. Reduction, Softening and Melting (RSM) apparatus

The aim of the experiment is to mimic the blast furnace conditions, till the end of the cohesive zone, and observe the behaviour of the pellets. To do this a blast furnace simulator is required which subject the pellets to similar conditions as they would experience under the blast furnace process. The process includes; 1) gradual increase of temperature and increase in reduction potential of gases with it, simulating the descend of burden in the actual blast furnace, 2) layer of pellets sandwiched between layers of coke replicating blast furnace burden distribution 3) presence of mechanical load on the top of samples, as blast furnace is a continuous process and there is always burden present above, exerting load.

The Reduction, Softening and Melting (RSM) apparatus is used here as a blast furnace simulator, it was developed by Song [1] at Delft University of Technology with financial support from Materials innovation institute (M2i) in the Netherlands and technical support from Tata Steel Europe (IJmuiden) and was further modified by Gavel [2]. The schematic of the setup is shown in Figure 3.1

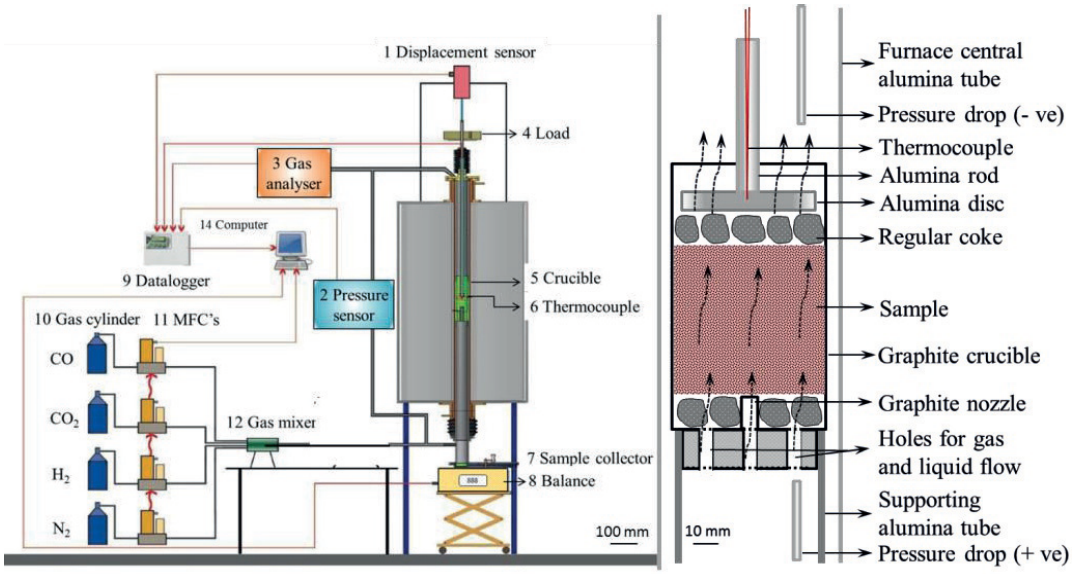

Figure 3.1. Schematic of Reduction Softening and Melting apparatus [2].

In an actual blast furnace, as material gradually moves down, it experiences a change in conditions like temperature and oxygen potential of the gas. Inside the RSM, since the sample bed is stationary inside a crucible, the conditions are made to change around it with time, and the response of the material is recorded. This is established with the help of the following systems:

Heating system: The Carbolite furnace consists of six heating elements which are located such that they symmetrically surround the sample, resulting in homogenous heating. The sample is placed in a

graphite crucible, which is then inserted in the hot zone of the furnace. The temperature of the sample bed is monitored with a thermocouple present inside the crucible, placed on top of the sample.

Mass flow controller: The gas inlet composition and rate are controlled by the Brooks mass flow controller, with which flow of CO, CO_2, H_2, and N_2 gases are controlled. The individual gases are mixed in a gas mixer before it enters the furnace.
The heating rate and gas profile that the sample is subjected to had been derived from the vertical probing of real blast furnace [5], and the thermal and gas profile is shown in Table 3.1.

Step	Temperature Range (°C)	Heating rate(°C/min)	CO (%)	CO_2 (%)	H_2 (%)	N_2 (%)	Gas flow rate (litre/min)
Step 1	20 - 400	7.0	0	0	0	100	5
Step 2	400 - 600	5.0	25	20.5	4.5	50	15
Step 3	600 - 950	5.0	30	15.5	4.5	50	15
Step 4	950 - 1050	1.2	33	12.0	5.0	50	15
Step 5	1050 - 1550	5.0	42	0	8.0	50	15
Step 6	1550 - 20	-5.0	0	0	0	100	5

Table 3.1. Thermal and gas profiles followed during the experiments [2].

Gas analyser: The off-gas is analysed using a gas analyser. The gas is first filtered and then analysed for CO, CO_2, H_2, and H_2O, and the balance is assumed to be N_2. Gas analyser records data once every ten seconds.

Using the data obtained from the gas analyser, degree of reduction (DOR) of the samples is calculated, using the equation below:

$$DOR = \frac{m_O^{Rem}}{m_O^{Raw}} \tag{3.1}$$

Where,

m_O^{Rem} is the total mass of oxygen removed (g) from the sample at any instant during the experiment.

m_O^{Raw} is mass of oxygen present in ferrous raw materials (g) before the start of the experiment.

The mass of removed oxygen at any instant during the experiments is given as:

$$\dot{m}_O^{Rem} = \dot{m}_O^{Outlet} - \dot{m}_O^{inlet} \tag{3.2}$$

The above equation can be written as

$$\dot{m}_O^{Rem} = \{ \left(\frac{[CO]^{outlet} + 2[CO_2]^{outlet} + [H_2O]^{outlet}}{[N_2]^{outlet}} \right) - \left(\frac{[CO]^{inlet} + 2[CO_2]^{inlet} + [H_2O]^{inlet}}{[N_2]^{inlet}} \right) \} \frac{M_O . \theta_{N_2}}{V_o} \tag{3.3}$$

where

$[x]$: Volume fraction of species *x*
θ_{N_2}: Volume flow rate of N_2 gas, dm^3/min
M_o : Molar mass of oxygen, 16 g/mol
V_o : standard volume of an ideal gas at room temperature, 24 dm^3/mol

The mass of the oxygen removed can be estimated by summing the oxygen removal rate over time

$$m_O^{Rem} = \sum(\dot{m}_O^{Rem}) \quad (3.4)$$

Displacement Sensor: Displacement transducer (RDP, ACT2000C) measures the change in sample bed height. The values are recorded once in every 5 seconds, where the sample swelling is recorded as a positive change in bed height, and sample shrinkage, softening and melting are recorded as a negative change in bed height.

Pressure drop sensor: The advent of melting causes an increase in pressure drop across the sample bed, due to the decrease in permeability. The differential pressure transducer (Honeywell, KZ) measures this pressure difference across the bed once in every 5 seconds.

Data Logger: Atal, ATM-05 data logger records the data from the gas analyser, pressure transducer, and displacement transducer which is then recorded and displayed on a computer.

Load: A constant weight of 25 kg is applied to the top of the sample with the help of an alumina tube. This weight corresponds to a load of 96 kPa, which is commonly used for tests under simulated blast furnace conditions [1]. In actual blast furnace condition, the load on the sample is also dynamic, it increases as the material travels down. However, the effect of stress in low temperature is limited, hence a constant load is taken.

Sample collector: In the bottom of RSM furnace a sample collector, fitted with 12 rotatable metal cups is used, and it collects the liquid droplets over time separately.

An important aspect to take into account here is that both gases and solids are heated externally through the reactor tube in the test, whereas heat transfer and oxygen transfer reactions in the blast furnace are interrelated. Consequently, heat transfer in the furnace and its possible effect on the kinetics of the reduction of iron oxides cannot be accurately simulated.

3.2. Procedure

Commercially supplied iron ore pellets (10-15mm) are used as representative of blast furnace burden, but due to crucible size restrictions (height 270mm; internal diameter 64mm), as shown in Figure 3.2 (a), the smaller sized coke samples (20 – 25 mm) are used. Similar to blast furnace burden distribution, iron ore pellets are sandwiched between the two coke layers (Figure 3.2 (b))

Taking a coke rate of 300kg/t of hot metal for an actual blast furnace [1] and assuming on average iron pellets with approximately 65% iron content (Fe(total)), for the pellet sample size of 500 gm the amount of coke used in the experiment comes out to be 100 gm. This proportion is maintained for all the experiments. The coke is equally distributed in the top and bottom layers (Figure 3.2 (b)). The graphite crucible containing the sample bed is placed inside the RSM furnace. The lower flange is then connected with the rest of the furnace where the connection is sealed with graphite rings in order to avoid leakage. The gas and water inlet – outlet pipes are connected, as well as displacement and

pressure drop sensors are attached. The assembly is completed by applying the load on top of the sample bed. Leak tests are conducted using CO_2 gas and CO_2 detectors. Once ensured of no leakage, the gas analyser and furnace is switched on, the furnace is purged using nitrogen gas (5 litre/min) for an hour before starting the experiment.

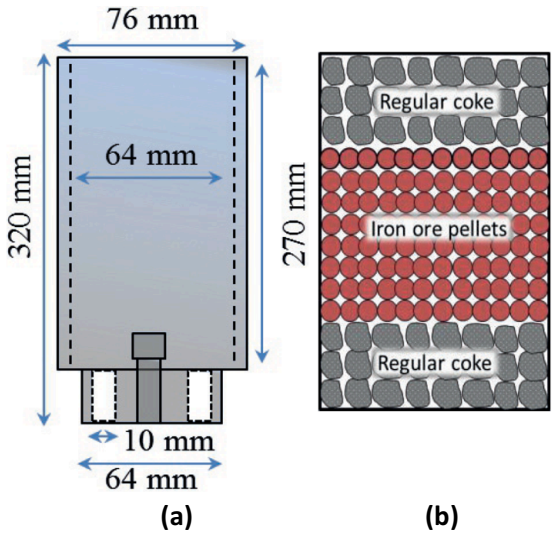

Figure 3.2. (a) Graphite crucible (b) sample arrangement in the crucible [2].

Gases (N_2, CO, CO_2, and H_2) flow through mass flow controllers (MFC) to a gas mixing chamber. The MFC are computer-controlled, hence they regulate the composition and amount of reducing gas. From the mixing chamber, the gas flows into RSM furnace through an inlet present in the bottom flange and to the graphite crucible, via holes and nozzle present at the bottom of the crucible. In the crucible, the gas interacts with the sample bed. The gas leaves the furnace through the off-gas pipe. The off-gas pipe is connected to a gas analyser which is used to analyse the composition of the mixing gas and the data is continuously logged by the computer.

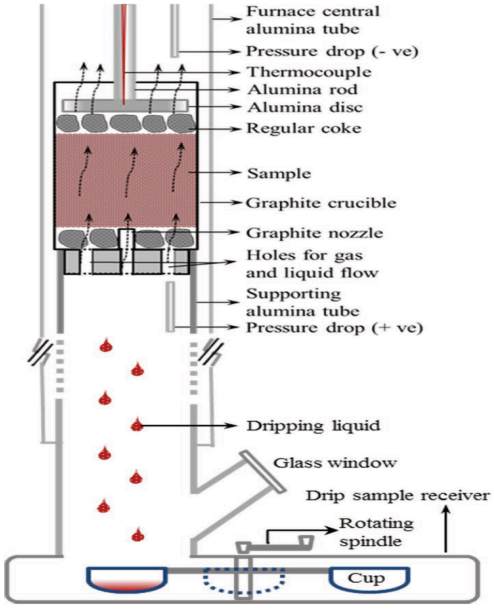

Figure 3.3. Schematic of the RSM furnace, sample arrangement and dripped liquid collection system [2].

The samples are heated from 20°C to 1550°C with different rates and corresponding gas compositions as shown in Table 3.1. The ferrous burden heats, reduces, softens, melts and then finally drips. The dripped samples are collected into the sample collector. After the experiment the samples are removed and subjected to analysis like XRF and XRD. The arrangement of RSM furnace is shown in Figure 3.3.

3.3. Raw Materials

The iron ore pellets used in the present study are commercial pellets used for production in the blast furnace, the XRF analysis of the three pellets used in the present study is given in Table 3.2.

Sample	Fe (Total)%	SiO_2, %	CaO, %	MgO, %	MnO, %	TiO_2, %	Al_2O_3, %
Pellet 1	64.12	4.05	1.57	1.25	0.21	0.24	0.81
Pellet 2	63.62	4.00	1.39	1.43	0.28	0.24	1.37
Pellet 3	63.30	3.77	1.39	1.28	0.46	0.34	1.85

Table 3.2. Chemical analysis of iron ore pellets (wt.%).

The non-ferrous mineral contribution mainly comes from CaO, MgO, SiO_2, and Al_2O_3 (CMAS), but the pellets also contain MnO and TiO_2, though in small quantities. The chemical composition of the first two pellets is almost similar in MnO and TiO_2. The pellet 3 contains a relatively higher quantity of both MnO and TiO_2. The assumption here is that MnO and TiO_2 in such a small quantity (0.2 – 0.5%), does not bear much effect on reduction softening and melting behaviour of the pellets. But this is not entirely correct because it is well known that both MnO and TiO_2 act as a fluxing agent, even in small quantities, reducing the liquidus temperature of primary slags by as much as 100°C [1] causing reduction retardation.

Especially MnO, which is used for slag thinning and avoiding re-solidification due to rapid reduction of FeO. It is mainly used as an aid for desulphurization and also affects the viscosity of slag. TiO_2 in the blast furnace slags behave as a basic oxide, hence act as a network modifier, reducing the viscosity of slags [2]. The distribution of gangue components in CMAS (normalized as 100%) is shown in Table 3.3, with basicity B2 (CaO/SiO_2) and B3 ($(CaO+MgO)/SiO_2$) mentioned as well.

Sample	SiO_2, %	CaO, %	MgO, %	Al_2O_3, %	B2	B3
Pellet 1	52.7	20.4	16.3	10.5	0.39	0.70
Pellet 2	48.8	17	17.5	16.7	0.35	0.71
Pellet 3	45.5	16.8	15.4	22.3	0.37	0.71

Table 3.3. Chemistry of CMAS (wt.%), obtained from Table 3.2.

From Table 3.2, it can be seen that alumina increases in pellets from 1 to 3, and basicity B3 is almost constant, whereas the basicity B2 varies a little, which may or may not affect the behaviour. In chapter 5, in addition to alumina, the effect of basicity B2 will also be explored. Additionally, since the variation of alumina on pellets with constant basicity is being studied here, chapter 5 will also serve to underline the possible change in the pellet behaviour as the basicity increases.

3.4. Characterization

X-ray diffraction is used for the identification of different phases (Hematite, Magnetite, and Quartz) present in the pellets, and the analysis is carried out with Cu Kα radiation with an accelerating voltage of 45 kV and filament current of 40 mA. Bragg-Brentano geometry is applied for the analysis. The scanning rate is 1.8 degree/min and the diffraction angle (2θ) is between 10° - 110°. The microstructure of pellets is analysed with the Scanning Electron Microscope (Jeol JSM IT-100), where the composition is semi-quantitatively analyzed using Energy Dispersive Spectroscopy (EDS), an accelerating voltage of 20kV and probe current of 60 nA is applied. The XRF analysis of the dripped slag was performed with a Panalytical Axios Max WD-XRF spectrometer.

3.5. References

[1] Q. Song, Effect of nut coke on the performance of the ironmaking blast furnace, PhD Thesis, Delft University of Technology, 2013.

[2] Gavel, D. J., Adema, A., Van Der Stel, J., Kwakernaak, C., Sietsma, J., Boom, R., & Yang, Y. (2020). Melting behaviour of iron ore pellet bed under nut coke mixed charge conditions. *ISIJ International*, *60*(3), 451–462.

[3] Biswas, A. K. (Anil K. (1981). Principles of blast furnace ironmaking : theory and practice / Anil K. Biswas. Cootha Publishing House.

[4] Sohn, I., & Min, D. J. (2012). A review of the relationship between viscosity and the structure of calcium-silicate-based slags in ironmaking. Steel Research International, 83(7), 611–630.

[5] Chaigneau, Renard & Sportel, Heiko & Trouw, J. & Vos, R. & Droog, J.. (1997). Blast furnace burden quality: Laboratory simulation. Ironmaking & Steelmaking. 24. 461-467.

4. Experimental Results

First the nature of results obtained from the analysis of the data from the RSM experiments is presented in section 4.1. An attempt would also be made to gain further understanding of the reduction softening and melting behaviour of pellets. Then the reproducibility of the experiment is showcased in section 4.2 and finally the results of three pellets with different levels of alumina content are compared in section 4.3. The discussion on these results is made in chapter 5.

4.1. Nature of Reduction, Softening and Melting (RSM) Experimental Results

The pressure drop and displacement curves for one of the pellets is shown in Figure 4.1. The Figure depicts that a steep rise in pressure drop across the bed coincides with a high rate of bed contraction at high temperatures, highlighting the effect of melting and exudation of slag from pellets.

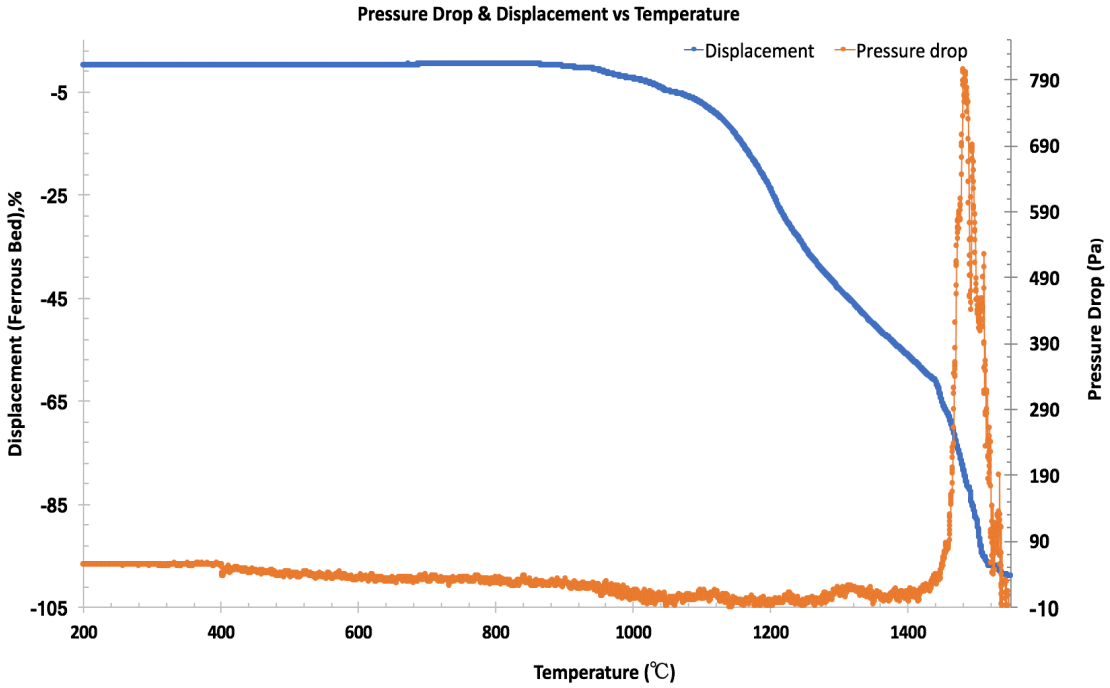

Figure 4.1. Combined pressure drop and bed contraction for pellet 3.

To gain insight on the softening and melting behaviour of the pellets, each displacement and pressure drop profiles are analyzed separately, and for this, the work of Gavel et al [4] has been used as a reference. Figure 4.2 shows that displacement can be divided into three stages. As mentioned in reference [4], stage 1 is associated with pellets shrinking because of (1) indirect reduction, (2) sintering of gangue minerals, and (3) densification of the thin iron shell formed on the periphery of the pellets due to combined effect of load and temperature. The beginning of this stage is taken as the end temperature of the thermal reserve zone, that is 1000°C (T0).

Stage 2 begins at the temperature T1, when pellets start to soften, because of the formation of primary slag in the pellet core which consists of FeO, gangue, and fluxes. This primary slag fills the micropores causing them to collapse, also due to the presence of liquid further densification of iron shell takes place. Softening causes the voids between the pellets to decrease in size, bringing pellets in intimate contact, resulting in sintering. Initially in stage 2, pellets contract at a higher rate, due to

the advent of liquid formation, which then decreases with temperature because of an increase in shell thickness, densification of plastic mass [5], and depletion of micropores [4].

Melting of iron shell brings upon stage 3, starting at temperature T2. In stage 3, the melting of each pellet layer takes place in a stepwise manner (Figure 2.7), causing the entrapped liquid to flow out into the voids below. Liquid slag comes in intimate contact with coke, resulting in direct reduction of FeO rich primary slag and further carburization of liquid iron. Once all the layers have been melted the displacement reaches a minimum at the end of stage 3 (T3).

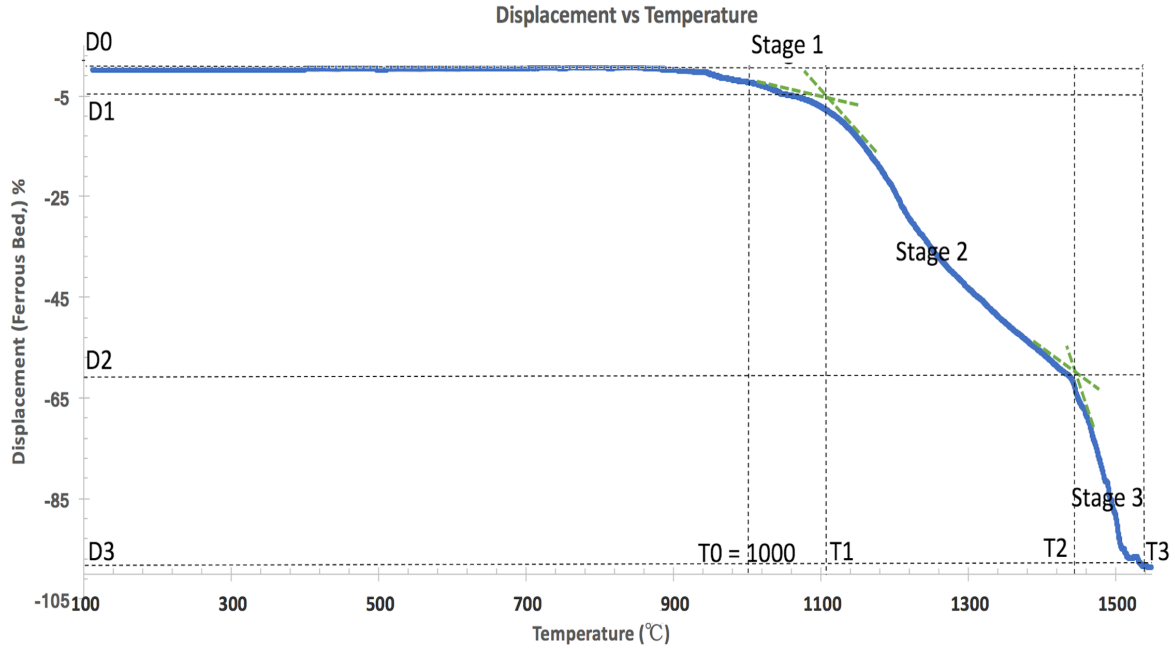

Figure 4.2. Stages of Sample bed contraction for pellet 3.

The list of physicochemical phenomena which occur in these stages is given in Table 4.1, as has been summarized by Gavel et al [4]

Stage 1	Stage 2	Stage 3
Swelling of Individual ferrous raw material	Gaseous reduction	Iron carburization (solid state)
Gaseous reduction	Metal (Iron) Formation	Burden deformation and collapse
Metal (Iron) formation	Shrinking of individual ferrous raw materials	Melting and dripping
Shrinking of individual ferrous raw materials	Sintering of ferrous raw material	Direct reduction
-	Iron carburization (solid state)	Iron carburization (liquid state)

Table 4.1. Physicochemical phenomena occurring at various stages of sample bed contraction [4].

Figure 4.3 shows the raw data of pressure drop curve with its smoothened version superimposed. The fluctuations in the raw data are due to the stochastic behaviour of burden and gases, especially at high temperatures. These fluctuations can be taken care of by using mathematical smoothing of the

curve. The exponential smoothing [11] is used here, it is commonly applied to smooth data in signal processing to remove high-frequency noise. The simple form of exponential smoothing is given by;

$$\bar{S}_t = B.S_t + (1 - B).\bar{S}_{t-1} \quad (4.1)$$

Where, B is the damping factor with a value between 0 to 1, S_t is the t[th] observation of raw data, and $\bar{S}_t$ is the corresponding estimate of the expected value of the distribution. $\bar{S}_{t-1}$ is the previous data obtained from smoothing. For the case in hand, a damping factor of 0.8 was chosen with trial and error, the aim was to make sure that the temperature at which curve starts to rise and drop matches with the raw data.

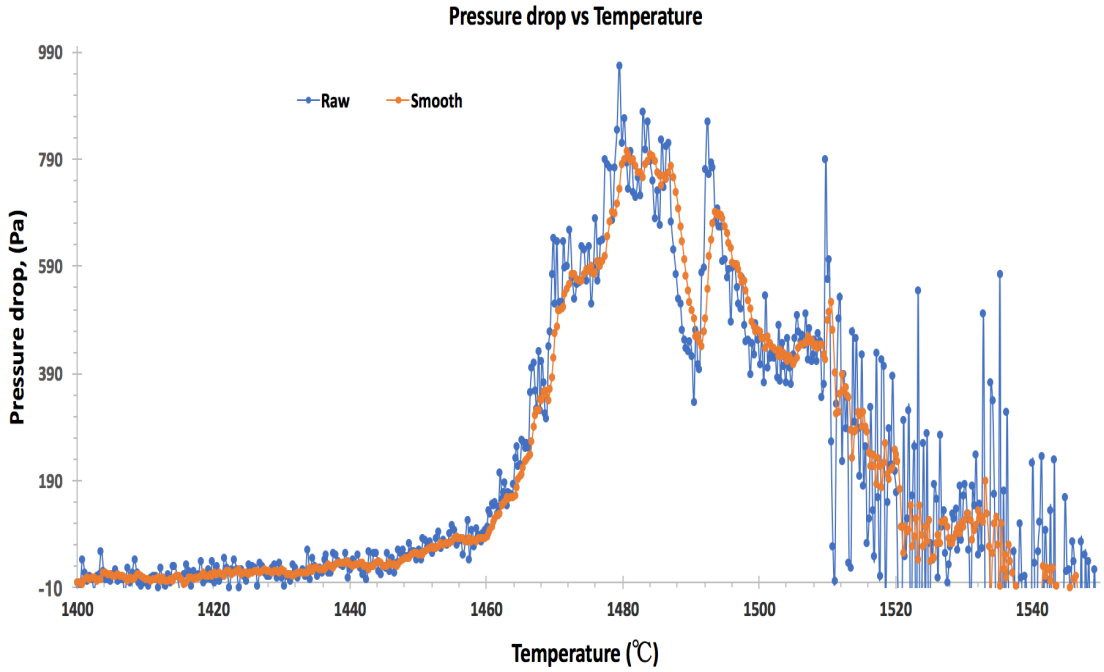

Figure 4.3. Pressure drop across bed with raw and smooth data for pellet 3.

Coming to the pressure drop, Figure 4.4 shows that at melting temperature (Tm), the pressure drop rises above the base value (P-Base) and reaches its peak (P-Peak) at flooding temperature (Tf). This is because melting causes melt exudation and filling of the voids, resisting the gas flow severely. The fluctuation in the curve is due to the dynamic behaviour of gas and the heterogeneous nature of the burden. The pressure drop starts falling after the first drop is seen from the glass window of the RSM apparatus at temperature Txf. This happens because the flow of liquid out of bed creates space for gas flow, ultimately reaching the base value at dripping temperature (Td). An important parameter quantifying the resistance to gas flow is the area under the pressure drop curve, above the base value, from melting to dripping temperature and is called S-Value.

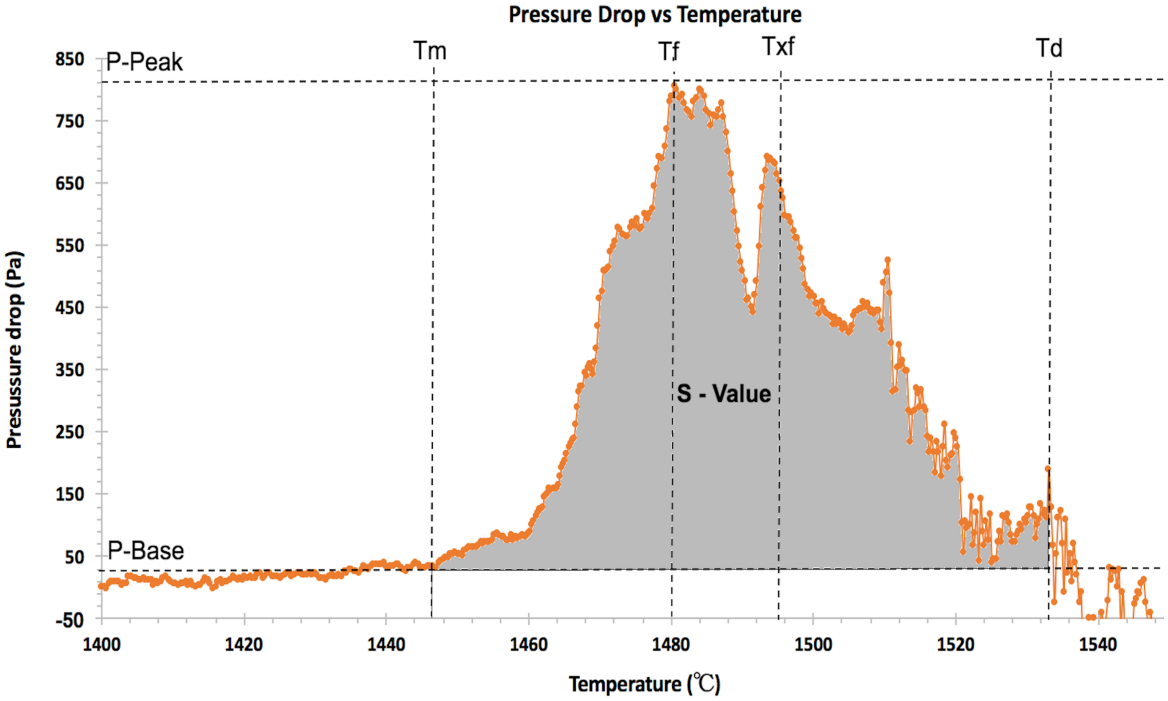

Figure 4.4. Pressure drop across bed for pellet 3.

Moving on to the reduction of iron ore pellets, Figure 4.5 showcases the nature of reduction degree as it evolves with temperature. As explained in section 3.1, the reduction degree is estimated on the basis of oxygen content in the raw iron ore pellets and that removed during the RSM experiment. The slope of the curve varies throughout, where in general the trend is that reduction degree increases gradually with temperature, except at very high temperatures. To be able to expound on this behaviour, the rate of reduction is presented in Figure 4.6.

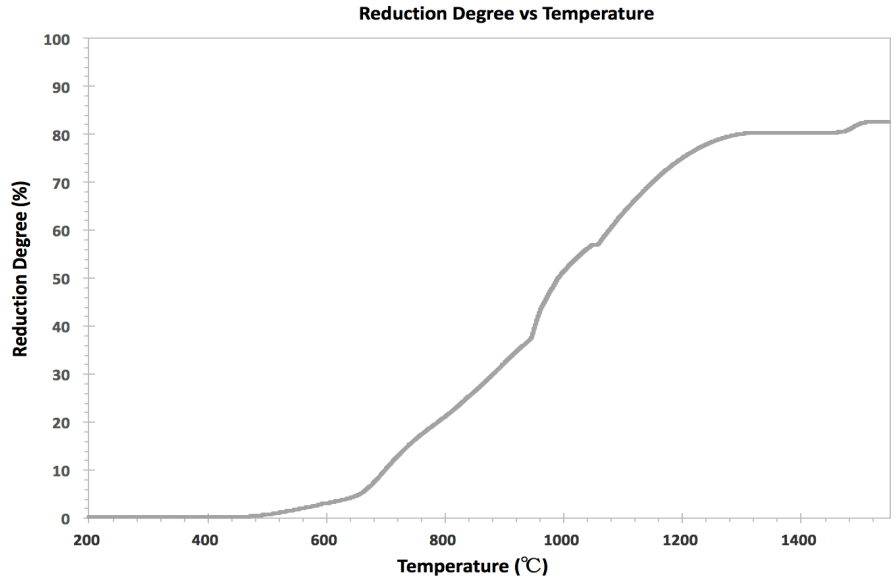

Figure 4.5. Estimated reduction degree of pellet 3.

In Figure 4.6 unit of the reduction-rate is illustrated with the grams of oxygen removed per minute per total grams of oxygen associated with iron oxide in the raw pellet. From this Figure, it is easier to

see why the slope of reduction degree changes throughout, as the rate of reduction does not increase continuously with temperature.

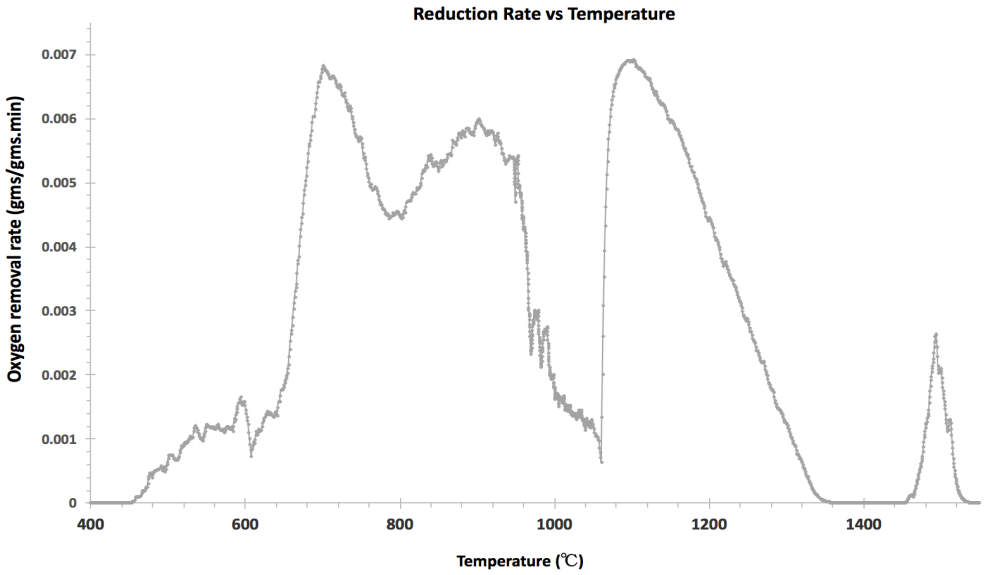

Figure 4.6. Estimated reduction rate of pellet 3.

To delineate the reason behind such behaviour, bed contraction is juxtaposed with the reduction rate in Figure 4.7. Starting from the high temperature end, the peak in reduction-rate matches with bed contraction of stage 3, which is exudation and dripping of the slag. Hence this rise in reduction rate can be attributed to the direct reduction of FeO rich primary slag by coke. At the beginning of stage 2, the reduction rate starts to fall and falls to a very low level before the end of stage 2. As mentioned earlier, stage 2 is associated with melting of partially reduced core and densification of the iron shell, both of which causes reduction retardation, explaining the fall of reduction rate until it is resumed again due to direct reduction.

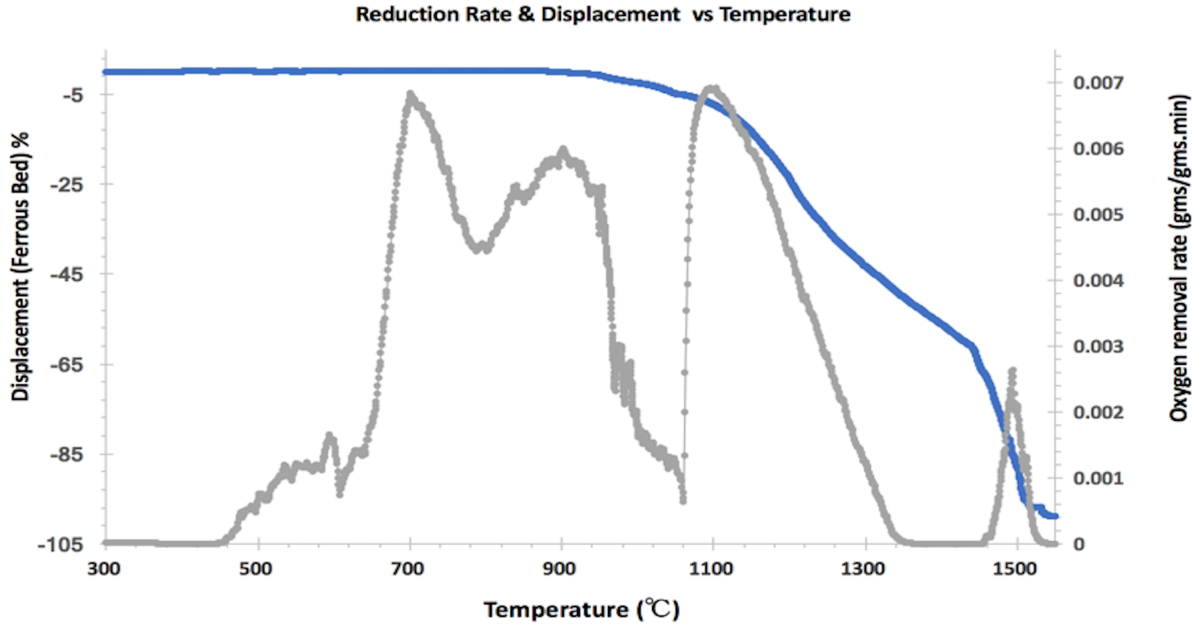

Figure 4.7. Estimated reduction rate and Bed contraction of pellet 3.

So, broadly the curve can be divided into two main regions, indirect and direct reduction as shown in Figure 4.8. The indirect reduction can be further divided into two parts, one occurring at lower temperatures, whereas the reduction retardation being part of the high-temperature region. The curve in the low-temperature region (450 °C – 1060 °C) is quite interesting. This is because, here, in addition to increase in temperature the reduction potential (%CO) of the incoming reducing gas also increases, both of which are suitable for the increasing rate of reduction. Therefore, rise and then fall in reduction rate at low temperatures where the formation of any liquid is highly unlikely to happen, is intriguing.

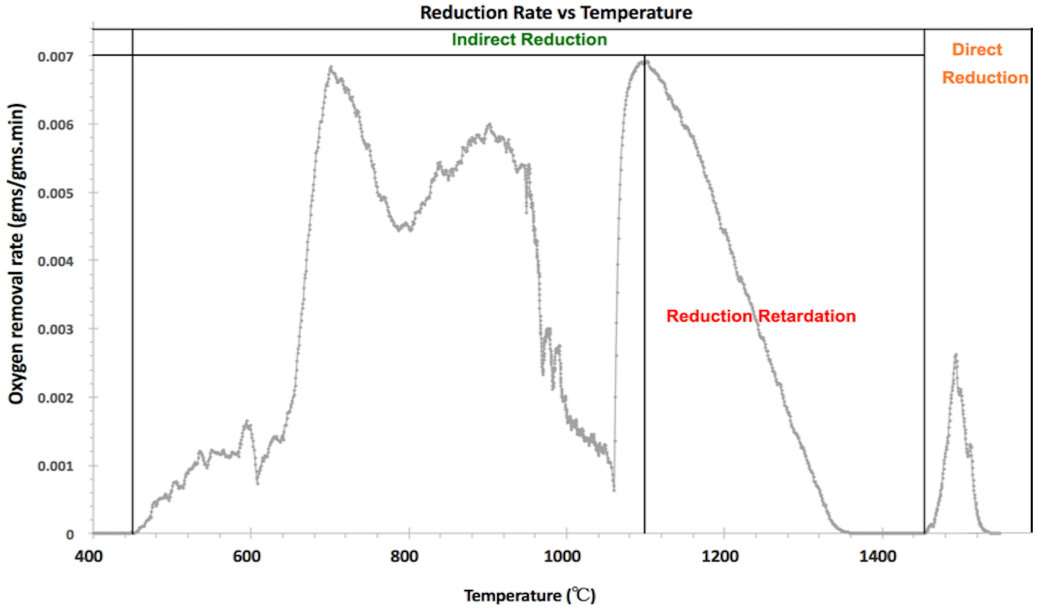

Figure 4.8. Estimated reduction rate of pellet 3.

With the help of Figure 4.9, it can be seen that reduction rate increases at temperatures corresponding to 1'/1, 2'/2 and 7'/7, these are the temperatures where reduction potential of the gas is increased by increasing proportion of CO and H_2 in incoming gas. Whereas at 6'/6, even with an increase in reduction potential the reduction rate still decreases. At temperatures corresponding to 3 and 5, reduction rate decreases, and at 4 it increases, and at all these points the incoming gas composition remains the same. This can be probed further with the help of Bauer Glaessner diagram with input CO and H_2 gas profile used in the furnace superimposed on the curve (Figure 4.10). H_2 is only a small fraction of total gas in the RSM furnace but due to no humidification of the input gas, the H_2 percentage is 100%. Hence the H_2 will cause the reduction throughout though its impact is not as significant as CO. The points marked in Figure 4.9 are also depicted in Figure 4.10.

Naturally there is no reduction before reducing gases are introduced, before point 1'. At point 1', after introducing reduction gasses in the furnace, the reduction rate increases but stays low. This is because the % CO ($100.CO/(CO + CO_2)$) value for inlet gas (55%) is very close to equilibrium values for both Fe_3O_4/Fe and FeO/Fe equilibrium system. Additionally, the kinetics of reactions are slow at low temperatures. As soon as reduction potential is increased at 2', the reduction rate jumps to high values due to an increase in the difference between imposed CO and equilibrium CO (FeO/Fe). According to Le Chatelier's principle the tendency of reduction of FeO will increase, and also the farther away a system is from equilibrium the greater is the rate of reaction. Another reaction which is thermodynamically possible here is Naumann reversion:

$$2CO \rightarrow C + CO_2 \qquad (4.2)$$

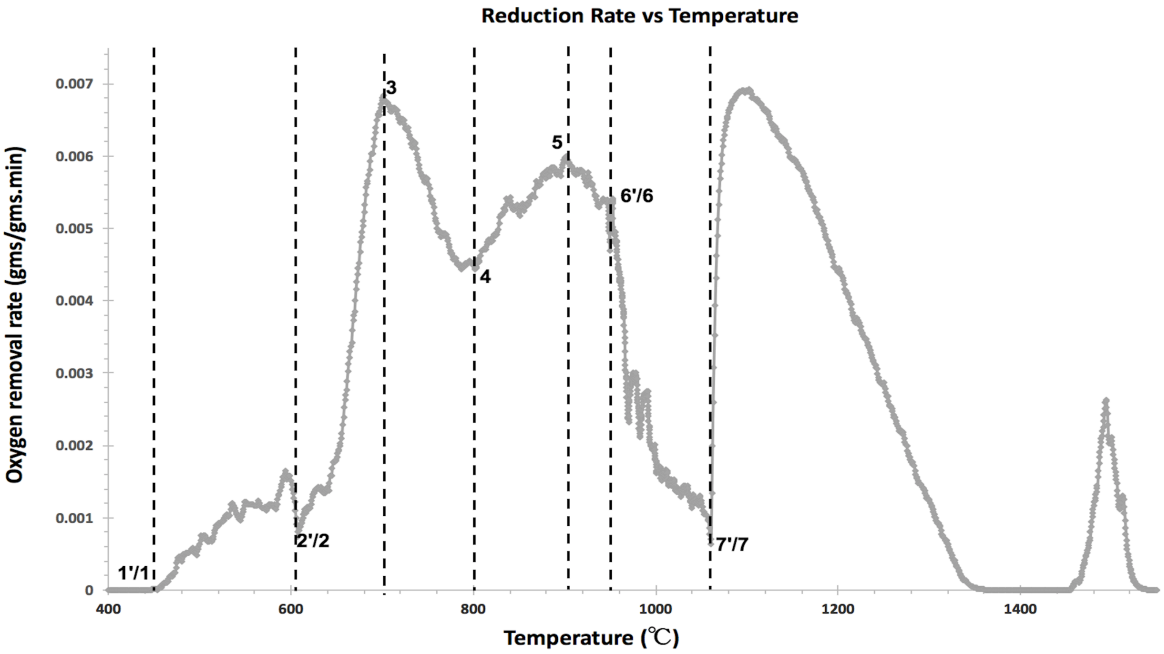

Figure 4.9. Estimated reduction rate with transition points in gas for pellet 3.

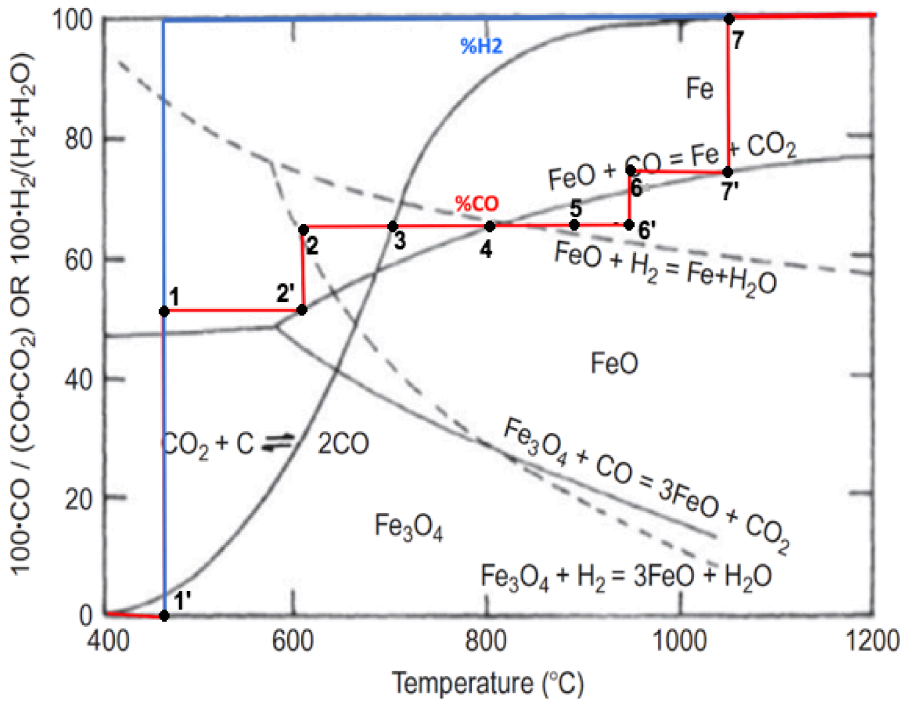

Figure 4.10. Equilibrium %CO (100. $CO/(CO+CO_2)$) and $\%H_2$ ($100.H_2/(H_2+H_2O)$) in contact with oxides of iron at various temperatures and imposed %CO and $\%H_2$ of gas in furnace for pellet 3 [6].

Reaction 4.2 can cause a decrease in the reduction rate as it decreases the reduction potential of the gas by consuming CO and depositing carbon soot on the bed. According to reference [7], the Naumann reversion (4.2) is kinetically sluggish, though it can be catalyzed by Fe and FeO. A small amount of soot does deposit at 300 - 600°C which then also takes part in reduction at higher temperatures.

As the temperature increases the difference in CO in equilibrium with FeO/Fe system and inlet CO gas decreases and at point 3 the rate of reduction starts decreasing (Figure 4.9), this is interesting because point 3 is also the intersection with Boudouard equilibrium line. Hence, thermodynamically after point 3 the solution loss reaction must cause an increase in the reduction potential of the gas and should actually result in an increase of reduction rate. It seems kinetically solution loss is not fast enough at these low temperatures which is widely accepted [6] [7], hence reduction is governed by FeO/Fe system only. Once the point 4 is reached the reduction rate increases again, point 4 also happens to be the point of intersection Fe/FeO equilibrium system with both H_2/H_2O and CO/CO_2 and input CO gas. On one hand, after point 4 the tendency for reduction of FeO by CO should actually decrease. On the other hand due to 1) large increase in Boudouard reaction line and 2) increase in the tendency of reduction with H_2, the reduction rate must increase. It seems the effect of the latter two is greater than the first, causing a net increase in the rate of reduction.

At almost 900°C (point 5) the rate reduction shows a decreasing trend again which continues till 1060°C (point 7') even when the reduction potential of the gas is increased slightly at 6'/6. It is worth reminding that in the region from point 6' to point 7' the furnace temperature is increased at a very low rate (1.2°C/min) and since these temperatures fall in the range of reserve zone, sufficient time and suitable conditions are present for equilibrium to be established for system FeO/Fe. This might explain the decrease in reduction rates, as, at equilibrium, the rate of the forward reaction becomes equal to the rate of backward reaction. Once the system comes out of reserve zone at point 7'/7 the rate of reduction steeply rises because of an increase in reduction potential and temperature. From Figure 4.5 it can be seen that the net reduction degree at point 7'/7 is 57%. This is in the range reported for pellets at the end of the reserve zone [8].

The above discussion can be summarized by looking at the inlet-outlet gas profile, Figure 4.11. Soon after changing gas profile at point 2'/2, both the CO and CO_2 outgas start moving away from their respective inlet values, which is caused by indirect reduction, resulting in an increase of the rate of reduction from 2'/2 to 3. Point 3 is the local maximum for the reduction rate (Figure 4.9), as at this point both CO and CO_2 out gas values are farthest away from their input values. From point 3 onwards both CO and CO_2 outlet moves towards their respective inlets, since kinetically solution loss reaction is sluggish at these temperatures. This causes a decrease in the rate of reduction, which is due to the CO approaching equilibrium for FeO/Fe system.

At point 4 the curves for outlets bend again, though slightly, in the opposite direction, also the H_2O starts increasing. As mentioned earlier, this might be due to an increase in the rate of solution loss reaction. From temperature at point 5 and onwards both CO and CO_2 outlet gases continuously approach the respective inlet gases. Since the rate of reduction also decreases here (Figure 4.9), this means the system approaches the chemical reserve zone from 5 onwards reaching ultimately to equilibrium at the temperature corresponding to point 7'/7. At 7'/7 the gas profile is changed, causing an abrupt increase in reduction rate. One possible reason for the decrease in the rate of reduction from point 5 to 7'/7 can be that with an increase in reduction degree the shell thickness increases also its morphology changes as at higher temperatures, increase in diffusion causes densification of the iron shell. After 7'/7 the reduction is renewed as material comes out of reserve zone. It is worth

noticing that even after stopping CO_2 input to furnace at 7'/7, the CO_2 outlet still stays above the zero, indicating the reduction of FeO and slow rate of solution loss reaction. As the temperature increases, because of reduction retardation and increased solution loss reaction, the CO_2 profile falls and CO rises continuously. And finally, after the melt exudation direct reduction takes place, but still no CO_2 peak is observed in the off-gas, because at these temperatures CO is the stable gas phase and not CO_2.

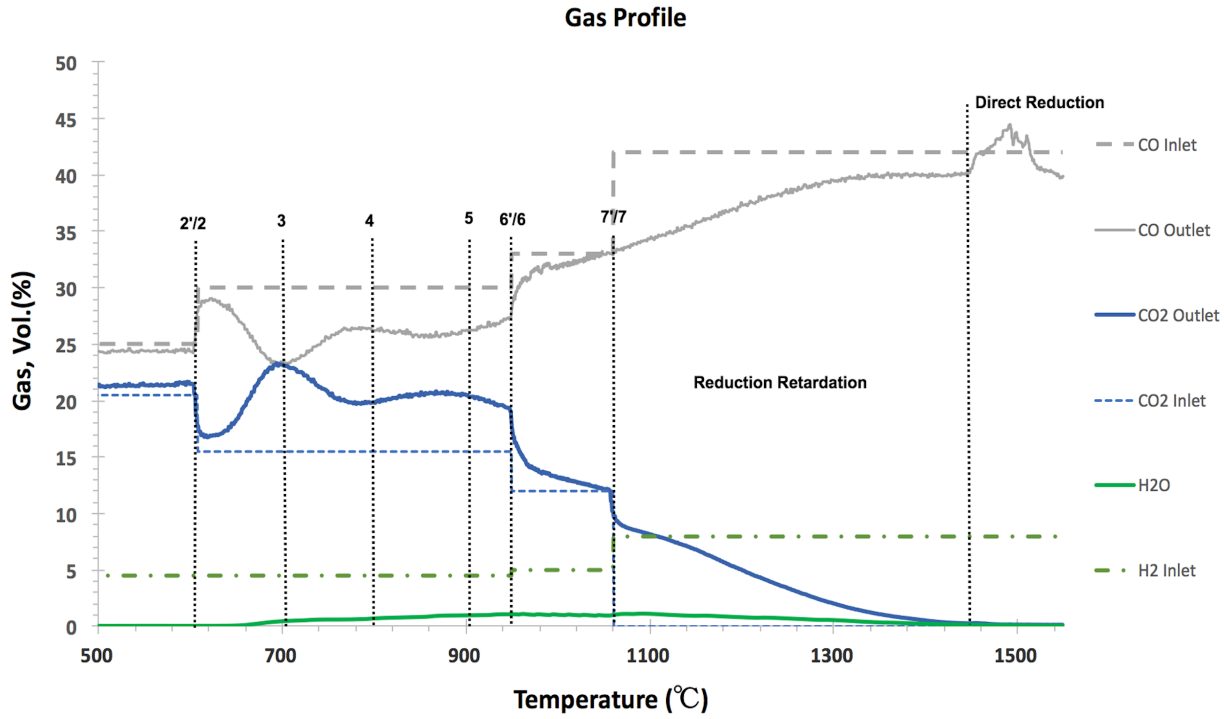

Figure 4.11. Gas inlet and outlet profile during experiment for pellet 3.

4.2. Reproducibility of RSM Results

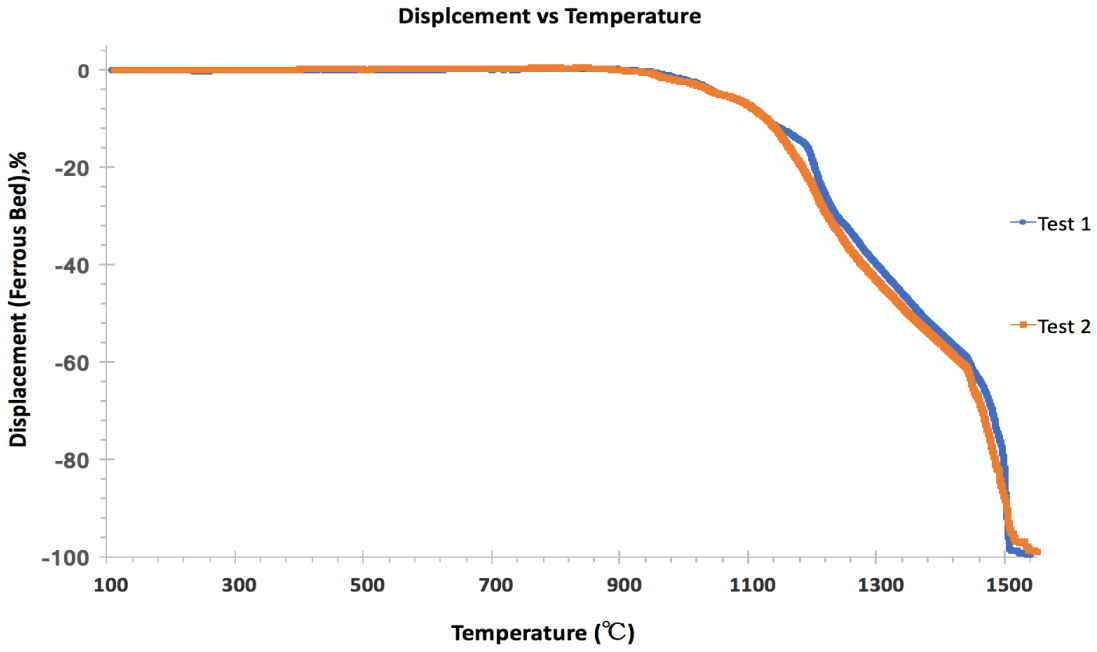

Figure 4.12. Sample bed contraction for pellet 3.

In order to confirm the reproducibility of the Reduction Softening and Melting apparatus, an experiment with one of the pellets (pellet 3), was repeated. Figure 4.12 and 4.13 depict that both bed contraction and pressure drop behaviour exhibit a good match. Table 4.2. compares the parameters defined in section 4.1 for the two experiments. The temperatures at which three stages of softening, steep rise of pressure drop, and dripping occur are in very close proximity for the two experiments. Additionally, the estimated reduction degree (Figure 4.14) also exemplifies the reproducibility of the experiment.

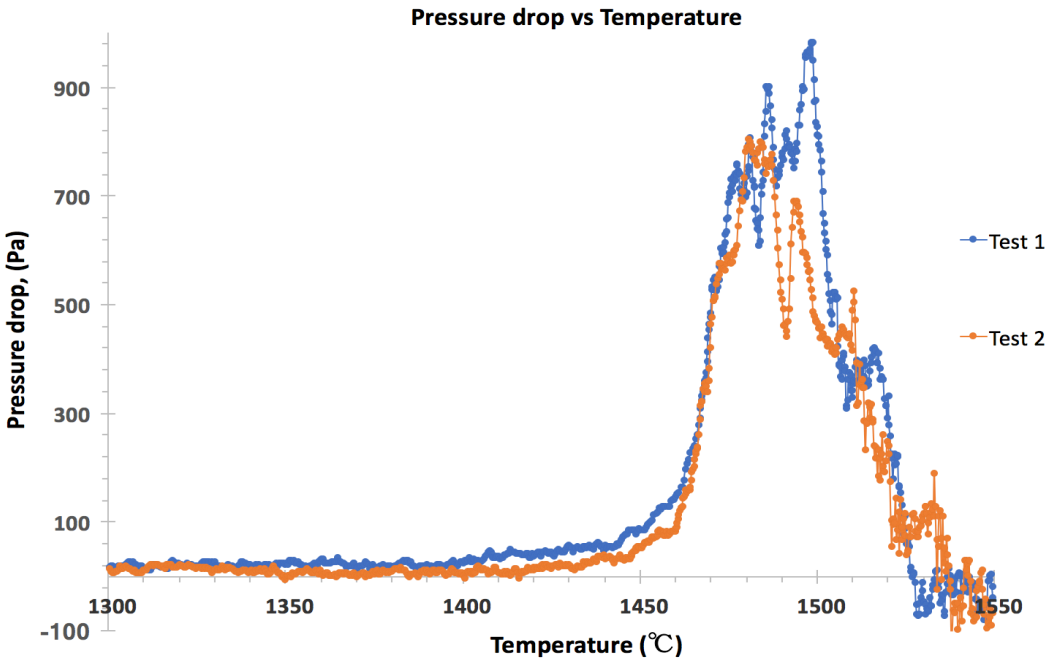

Figure 4.13. Pressure drop curve for pellet 3.

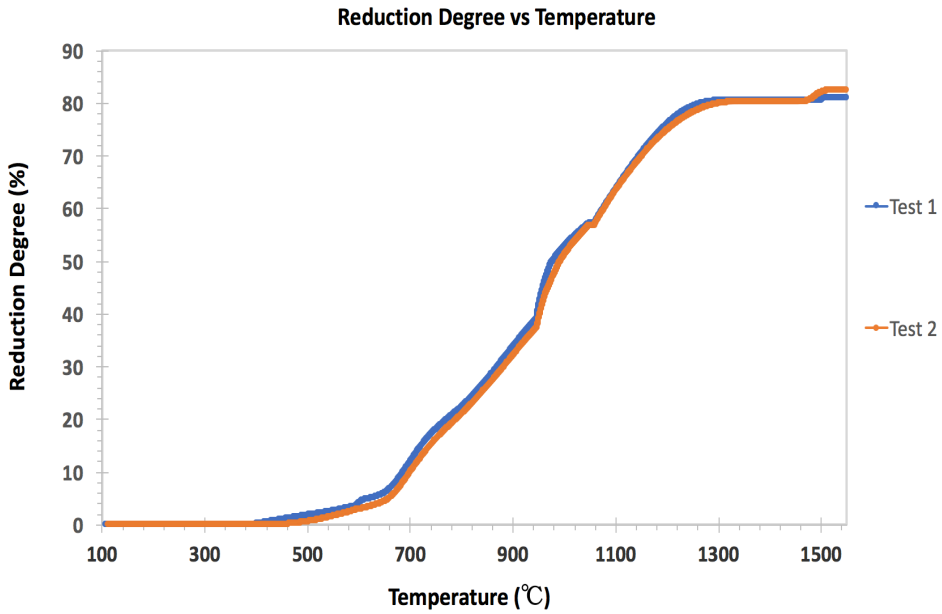

Figure 4.14. Estimated reduction degree for pellet 3.

Parameter	Test 1	Test 2
T1	1106 °C	1102 °C
T2	1448 °C	1446 °C
T3	1517 °C	1519 °C
Tm	1448 °C	1446 °C
Td	1527 °C	1530 °C
S - value	32 (kPa .°C)	29 (kPa .°C)
Reduction Degree	81%	82%

Table 4.2. Parameters obtained from RSM experiment on pellet 3.

4.3. Experimental Results

Characterization of iron ore pellets is discussed in section 4.3.1 followed by comparison of the RSM results in section 4.3.2.

4.3.1. Raw Material

X-ray diffraction pattern of the raw iron ore pellet 3 is shown in Figure 4.15, and the rest two pellets also showed the same major peaks. These are hematite pellets with small amount of magnetite (blue), quartz (pink) and a trace amount of complex mineral Augite ($(Mg,Fe,Al,Ti)(Ca,Na,Mg,Fe)(Si,Al)_2O_6$) (green) present in it.

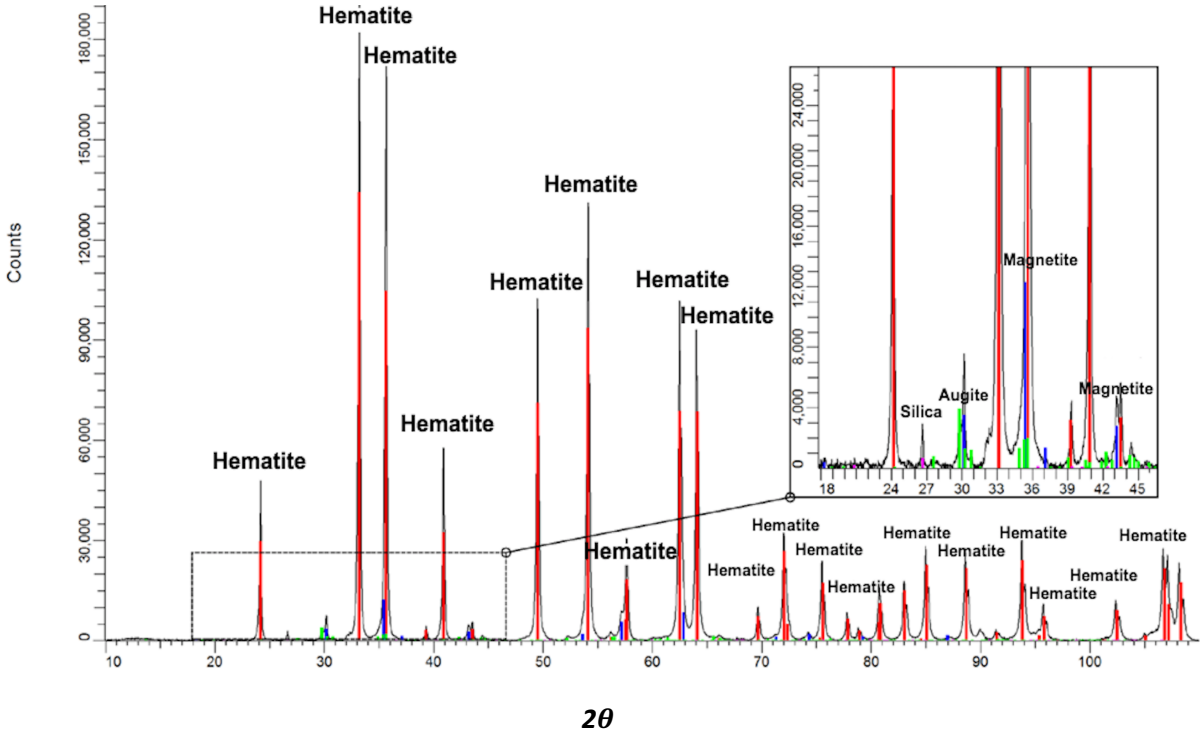

Figure 4.15. X ray diffraction (XRD) of a raw iron ore pellet 3.

Figure 4.16 (a) shows the typical microstructure of fired pellet 3, where hematite grains surrounded by a network of slag, formed during induration can be clearly seen. Additionally, microstructure also shows regions with particles, undissolved, or precipitated, into the matrix, as can be seen in Figure 4.16 (b). The mapping of different elements for this region is shown in Figure 4.17. There are two types of particles visible, silica, and a complex mineral containing Al, Si, Ca, and even a small amount of Mg.

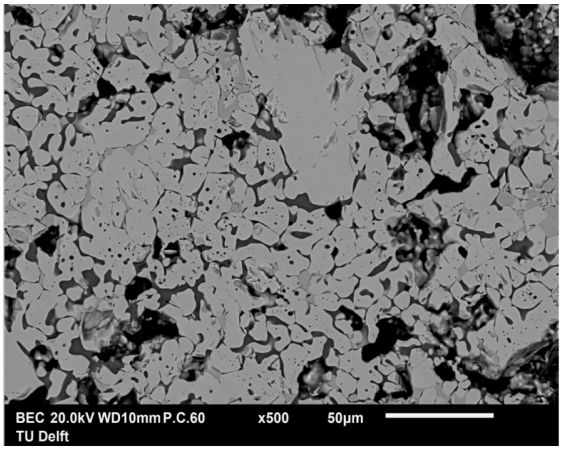

(a)

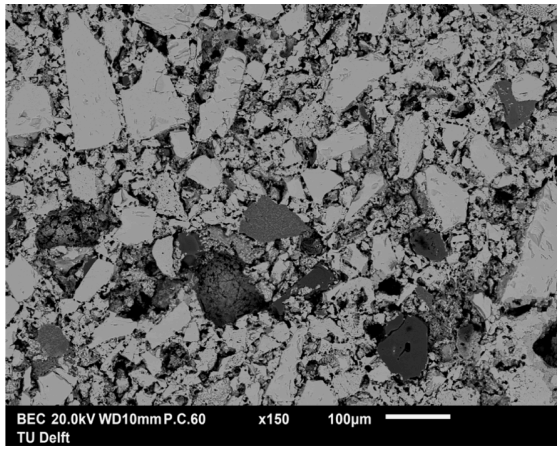

(b)

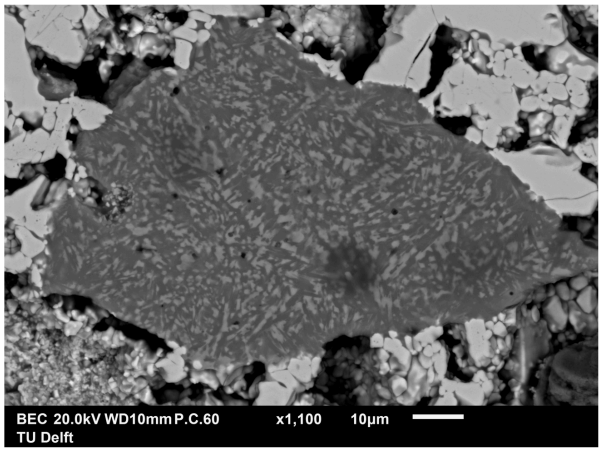

(c)

Figure 4.16. Back-scattered electron images of indurated pellet 3 (Al_2O_3 = 1.85%).

One of the Aluminum rich particles is shown separately in Figure 4.16 (C), where it looks like the particle consists of two different phases. A light phase distributed in a matrix of a dark phase. Alumina accompanies iron ore as a gangue mineral in the form of either kaolinite ($Al_2O_3 \cdot 2SiO_2 \cdot 2H_2O$) and/or gibbsite ($Al(OH)_3$) [9]. Hence the presence of Ca (Figure 4.17) suggests that this might have formed during firing.

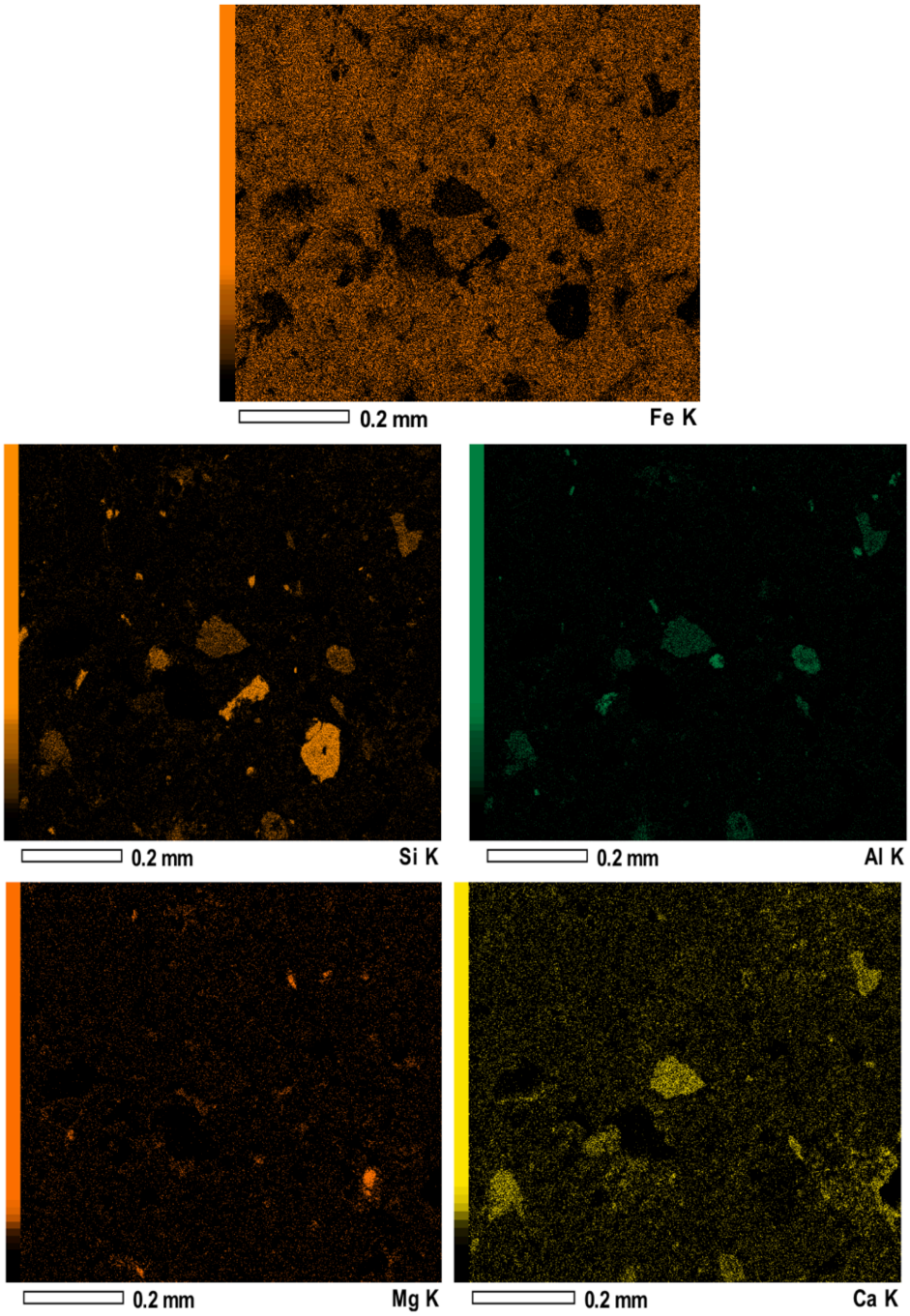

Figure 4.17.EDS scan of region depicted in Figure 4.16 (b) for pellet 3 (Al_2O_3 = 1.85%).

Hematite matrix surrounded by a network of slag can be seen again in Figure 4.18 (a) for pellet 2. Like pellet 3, there are regions with undissolved particles, as can be seen in Figure 4.18 (b). EDS point analysis showed that most of these particles are silica (points 1, 3, 6 and, 8) while some being forsterite (2MgO. SiO_2) (points 2 and 4). Point 5 is the particle rich in aluminum, this particle is magnified in Figure 4.18 (c).

Like the particle observed in 4.16 (c), for pellet 3, this particle also consists of two phases, a light phase distributed in a dark matrix. Moreover, it seems during induration, part of this particle formed liquid

and penetrated the hematite matrix adjacent to it, as slag like network shows morphology similar to that of particle which is not visible for slag anywhere else in the microstructure.

Figure 4.19 shows the distribution of elements for the region shown in Figure 4.18 (c), where similar distribution is seen as was seen in Figure 4.17. The particle is a complex phase consisting of Al, Si, Ca, and Mg as was seen for pellet 3.

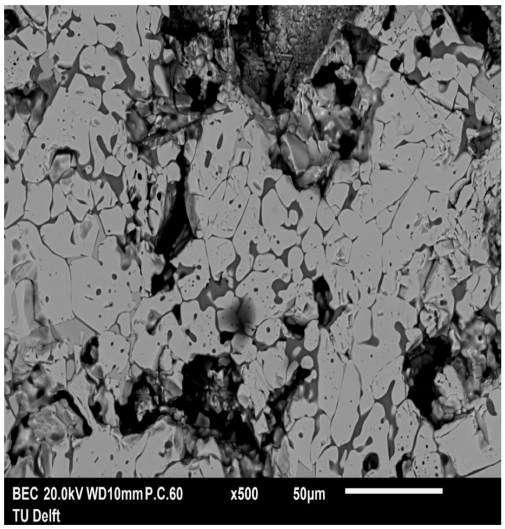

(a)

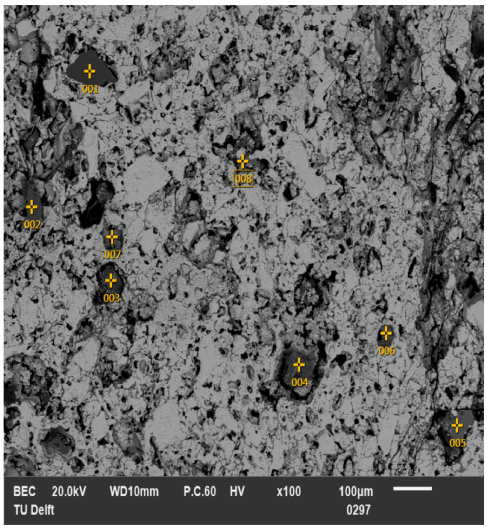

(b)

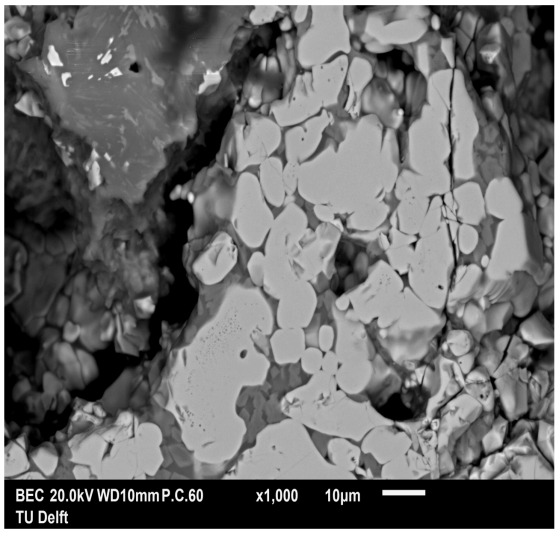

(c)

Figure 4.18. Back-scattered electron images of indurated pellet 2 (Al_2O_3 = 1.37 %).

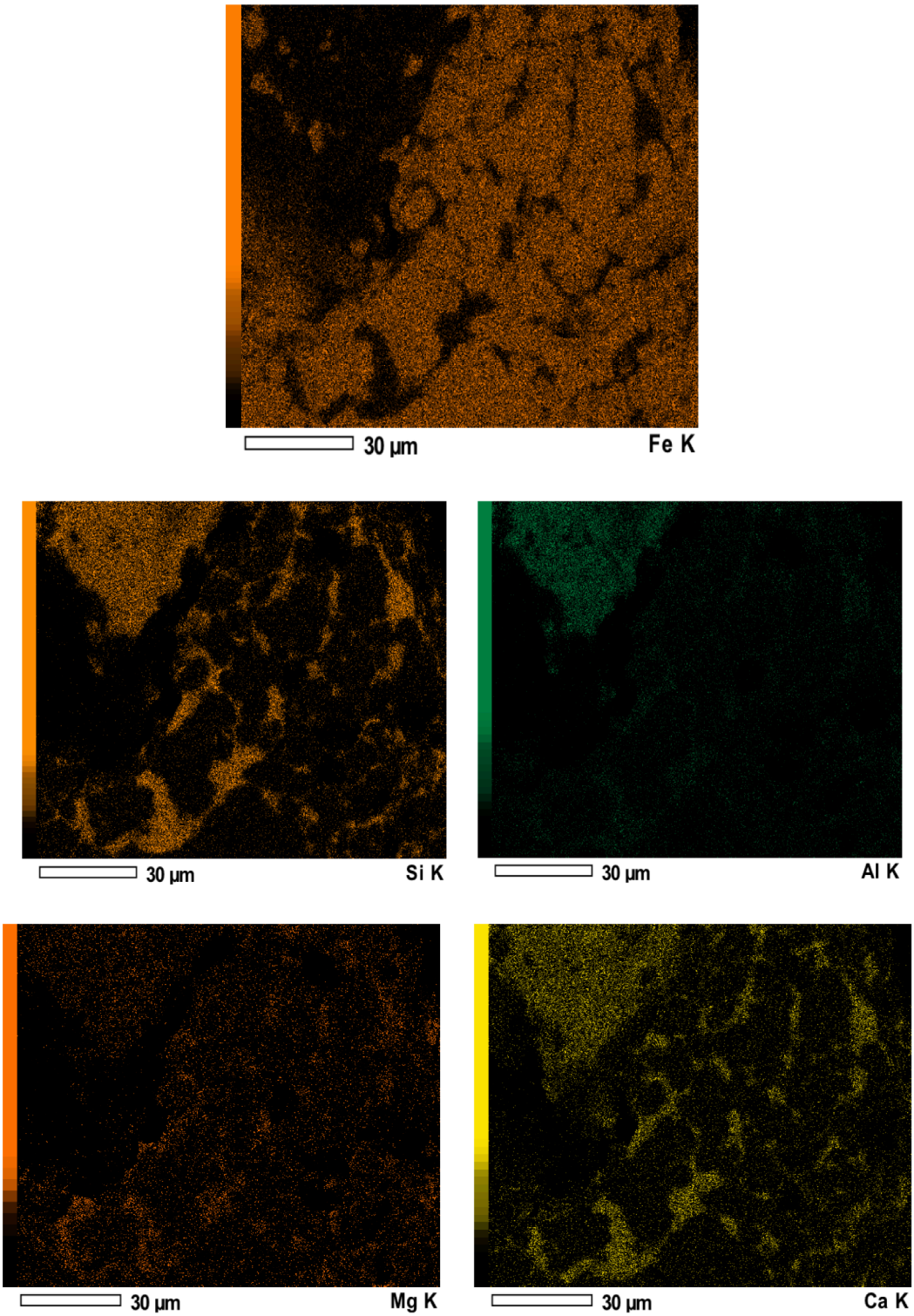

Figure 4.19. EDS scan of region depicted in Figure 4.18 (c) for pellet 2 (Al_2O_3 = 1.37 %).

Coming to indurated pellet 1, which contains the least amount of Alumina (Al_2O_3 = 0.81%), it shows features similar to the other two pellets mentioned above; a hematite matrix surrounded by slag and regions with undissolved (or precipitated) particles.

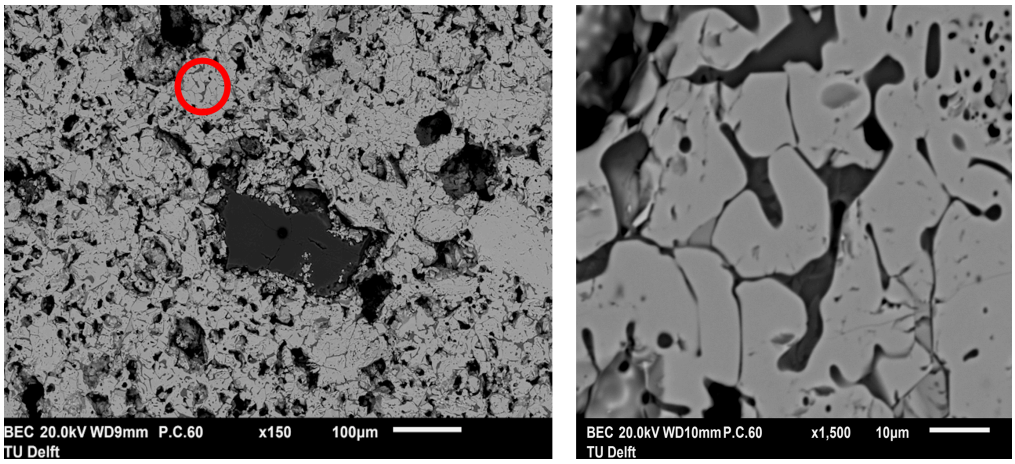

(a) **(b)**

Figure 4.20. Back-scattered electron images of indurated pellet 1 (Al_2O_3 = 0.81 %).

Here interestingly no alumina rich particles were observed, at least for the two different samples selected at random. The particle is shown in Figure 4.20 (a) is silica as confirmed by the EDS map shown in Figure 4.21. Coming to the slag part, Figure 4.20 (b) is the magnified image of one of the hematite grain highlighted in Figure 4.20 (a). The mapping of this slag is shown in Figure 4.22. It can be seen that slag consists of mainly Si and Ca and small amounts of Mg and Al.

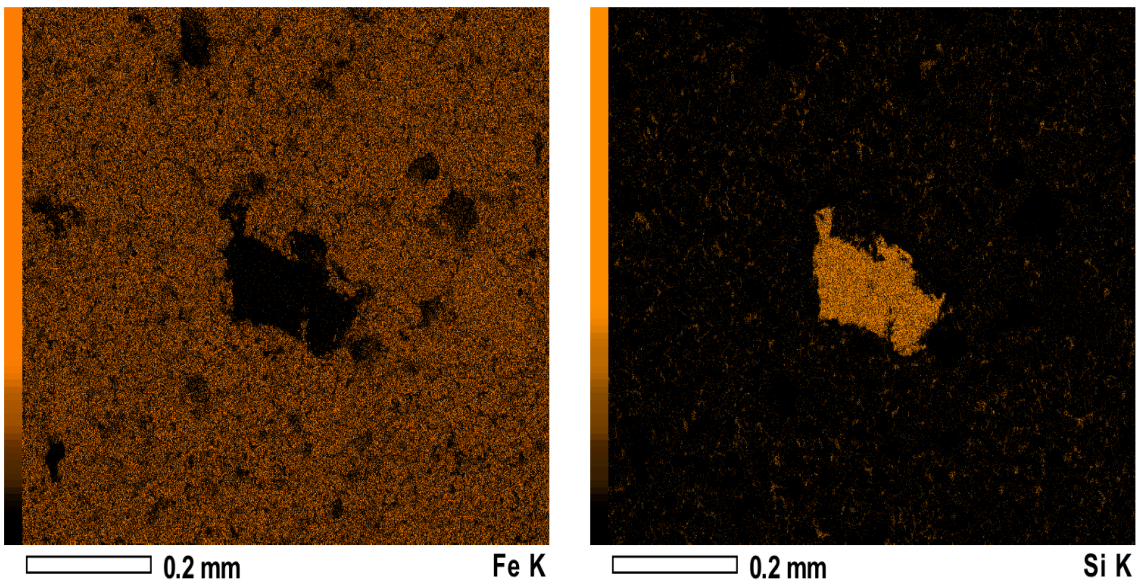

Figure 4.21. EDS scan of region depicted in Figure 4.20 (a) for pellet 1 (Al_2O_3 = 0.81 %).

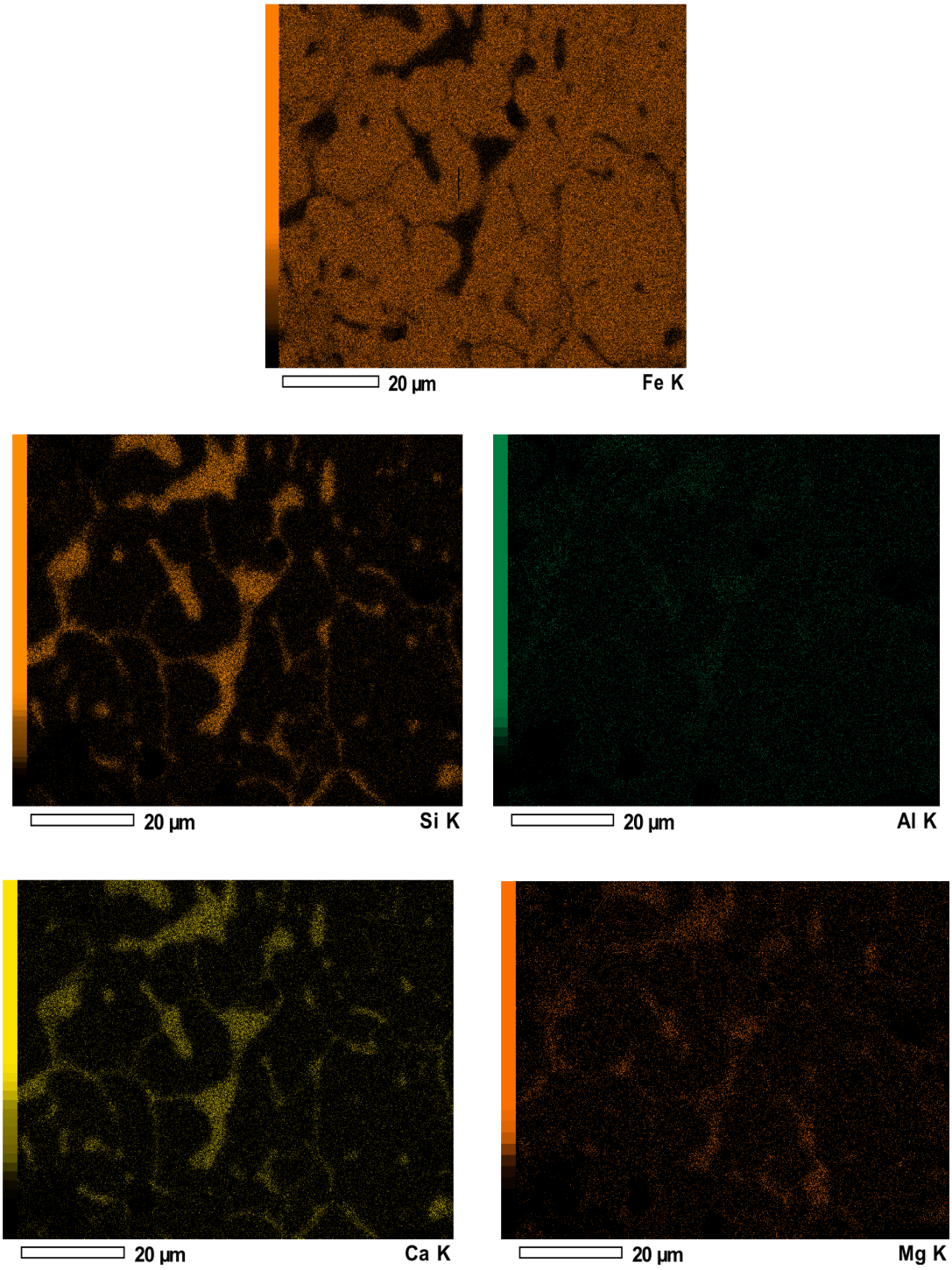

Figure 4.22. EDS scan of region depicted in Figure 4.20 (b) for pellet 1 (Al_2O_3 = 0.81 %).

4.3.2. Reduction, Softening and Melting Experiments

The pressure drop and displacement curves of all three samples are compared in Figure 4.23 and 4.24 respectively. It seems that the melting point of the sample bed shifts to lower temperatures with an increase in Al_2O_3 content. In reference [12] and [3], authors obtained similar Softening and Melting trends for pellets and sinters respectively, with variation of alumina. Figure 4.23, for bed contraction, shows an obvious difference in stage 2, where it seems that with the increase in Al_2O_3 the rate of

softening increases. To highlight the effect of Al_2O_3 on three stages of bed contraction, the various parameters defined in section 4.1 are compared in Figures 4.25, 4.26 and 4.27.

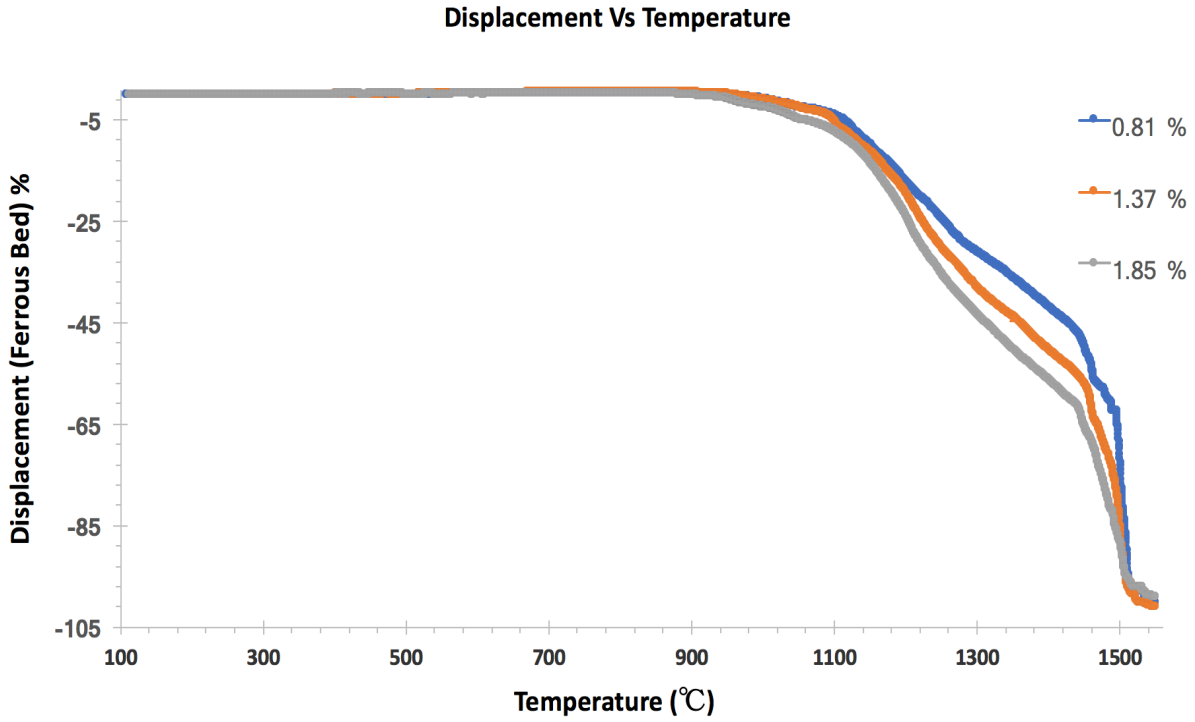

Figure 4.23. Effect of Al_2O_3 on bed contraction.

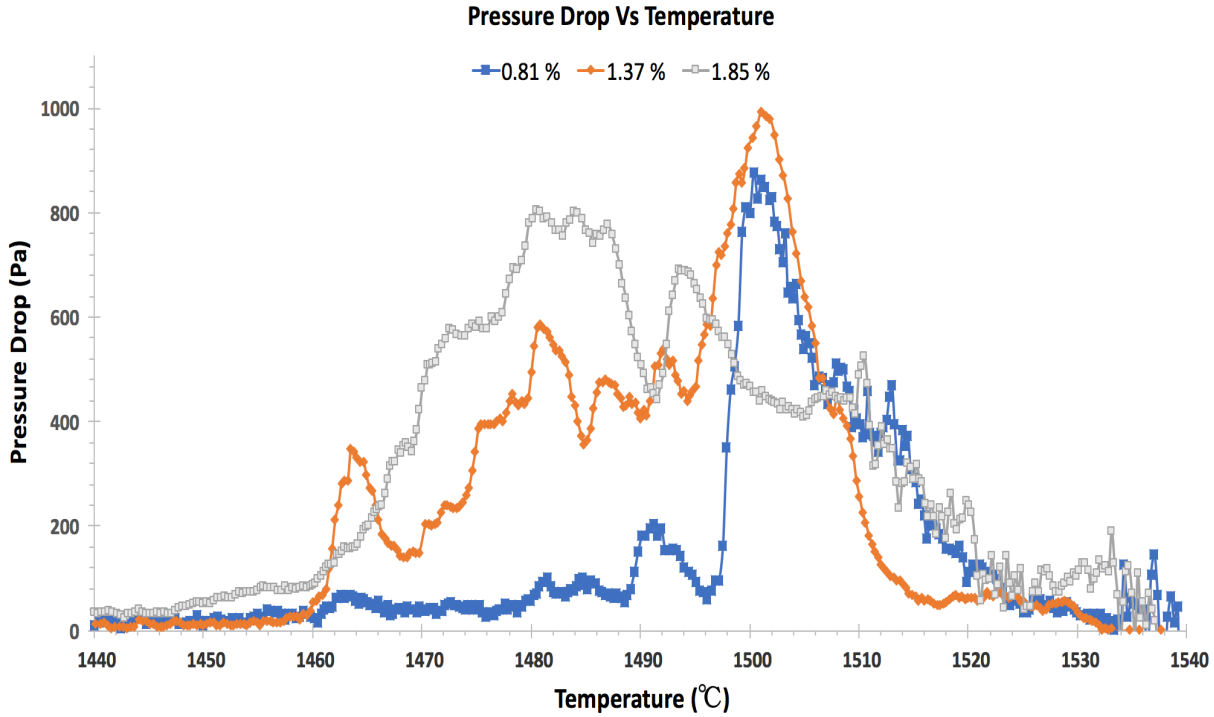

Figure 4.24. Effect of Al_2O_3 on pressure drop.

Temperatures T1, T2, T3, and contractions D1, D2, D3 at those respective temperatures are summarized in Table 4.3. The effect of Al_2O_3 on softening start temperature and respective contraction doesn't seem to be substantial. Whereas the end of stage 2 shows a clear distinction as not only does the temperature (T2) decreases with Al_2O_3, but also the amount of contraction occurred (D2) increase. Finally, for the end of stage 3, T3 is close for pellet 1 and pellet 2 whereas the pellet 3 shows the lowest T3 temperature, all three reaching the maximum contraction at their respective T3 temperature.

Parameters associated with the pressure drop curve are shown in Figure 4.28 and 4.29. It can be seen from Figure 4.28 that the melting temperature (Tm) decreases considerably with the increase in Al_2O_3 and the dripping temperature (Td) increases slightly with the increase in Al_2O_3, resulting in the increase of the melting dripping zone.

Sample	Al_2O_3 (wt.%)	T1 (°C)	T2 (°C)	T3 (°C)	D1 (%)	D2 (%)	D3 (%)
Pellet1	0.81	1099	1491	1525	-2.7	-54	-98
Pellet 2	1.37	1100	1458	1529	-3.1	-57	-100
Pellet 3	1.85	1102	1446	1519	-4.5	-61	-97

Table 4.3. Parameters pertaining to three stages of bed contraction.

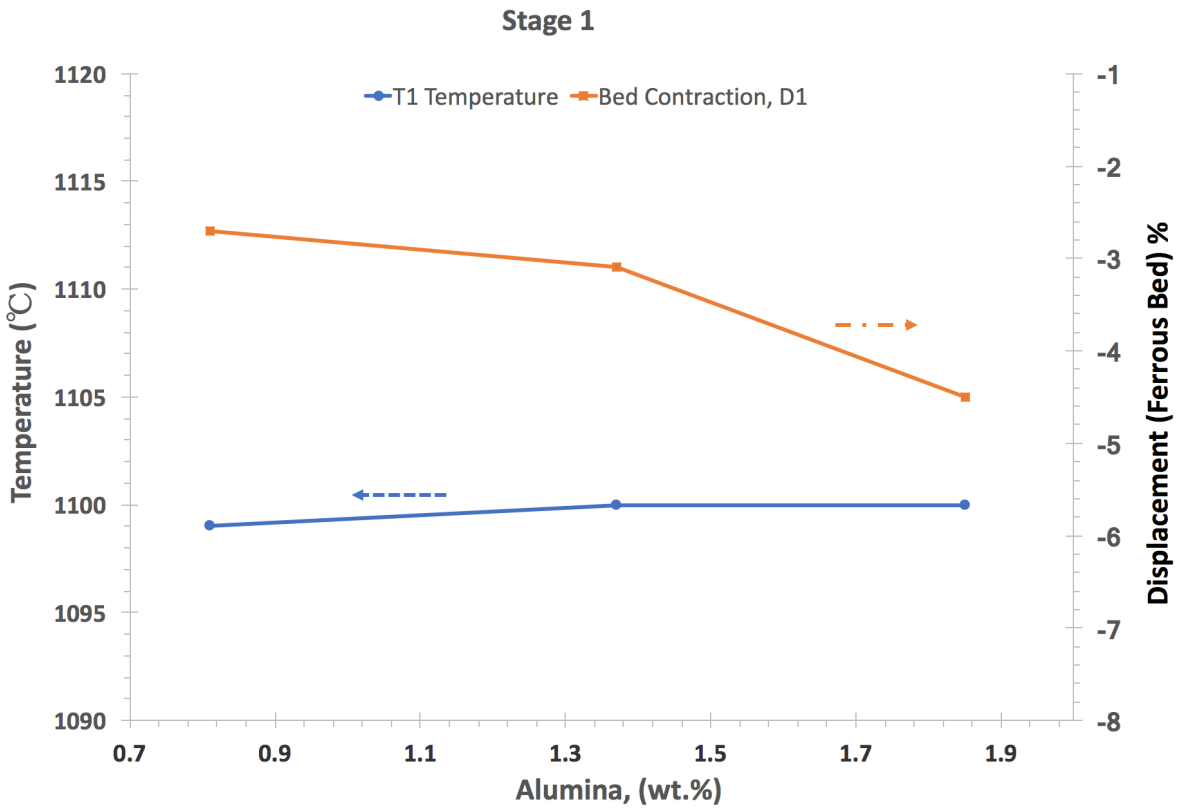

Figure 4.25. Effect of Al_2O_3 softening start temperature (Stage 1).

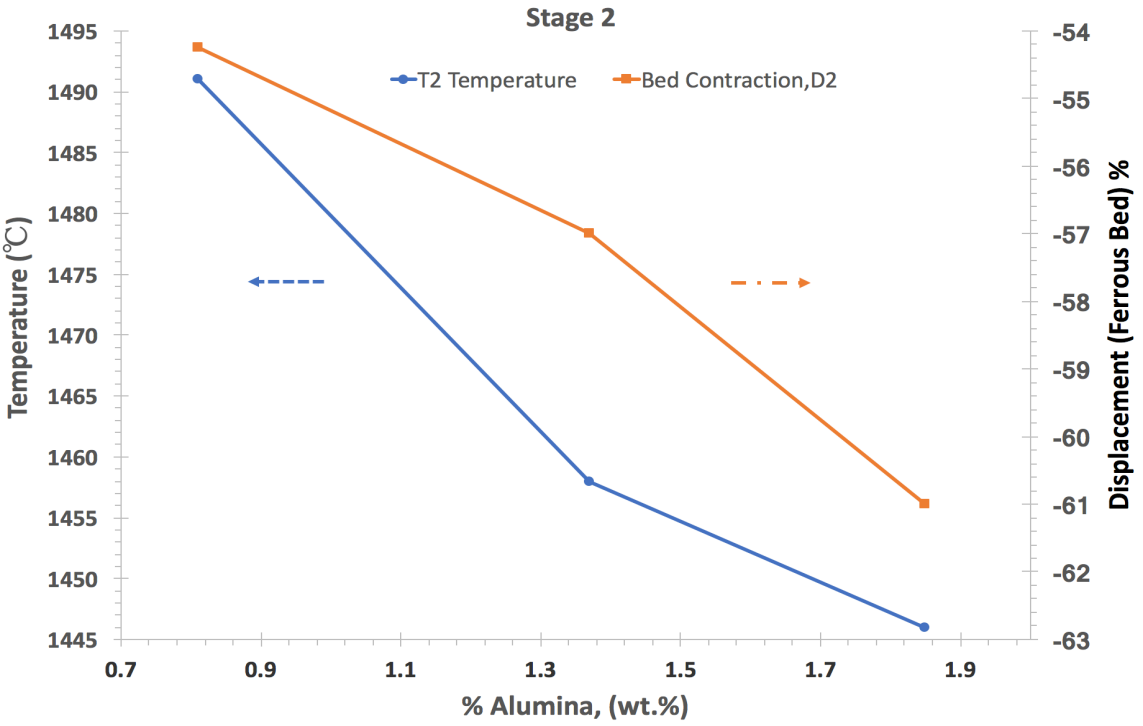

Figure 4.26. Effect of Al_2O_3 on temperature T2.

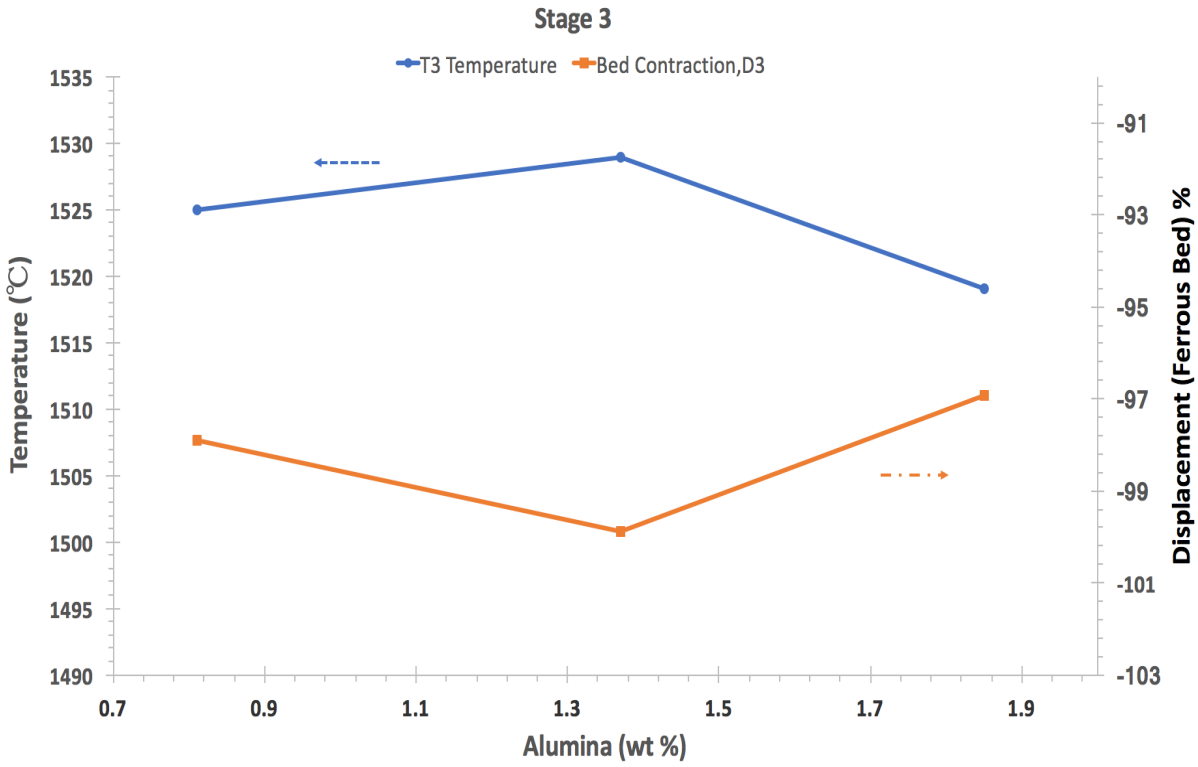

Figure 4.27. Effect of Al_2O_3 on temperature T3.

Sample	Al_2O_3 (wt.%)	Tm (°C)	TD (°C)	S-Value (k Pa.°C)
Pellet 1	0.81	1491	1525	13.21
Pellet 2	1.37	1458	1529	22.81
Pellet 3	1.85	1446	1530	29.34

Table 4.4. Parameters associated with pressure drop curve.

S-Value as depicted in Figure 4.4, is compared in Figure 4.29. The area under the pressure drop curve increases with increasing Al_2O_3, adversely affecting blast furnace efficiency. Finally, the thickness of cohesive zone, softening dripping range, is shown in Figure 4.30. indicating the negative impact of increasing Al_2O_3 on pellets softening melting behaviour. These values are also tabulated in Table 4.4.

The pellets of all three samples are reduced to different levels, as shown in Figure 4.31. It can be seen that the pellet with the lowest Al_2O_3 (pellet 1) reduces the most, but interestingly one with the highest (pellet 3) doesn't reduce the least. It is the sample with 1.37 % Al_2O_3 (pellet 2) that reduces the least, and also the difference is substantial. Figure 4.32 makes things further intriguing, as the reduction rate for pellet 2 shows the lowest reduction in the low-temperature region (800 to 1060°C), whereas it shows the highest rate of reduction at higher temperatures (1060 to 1350 °C).

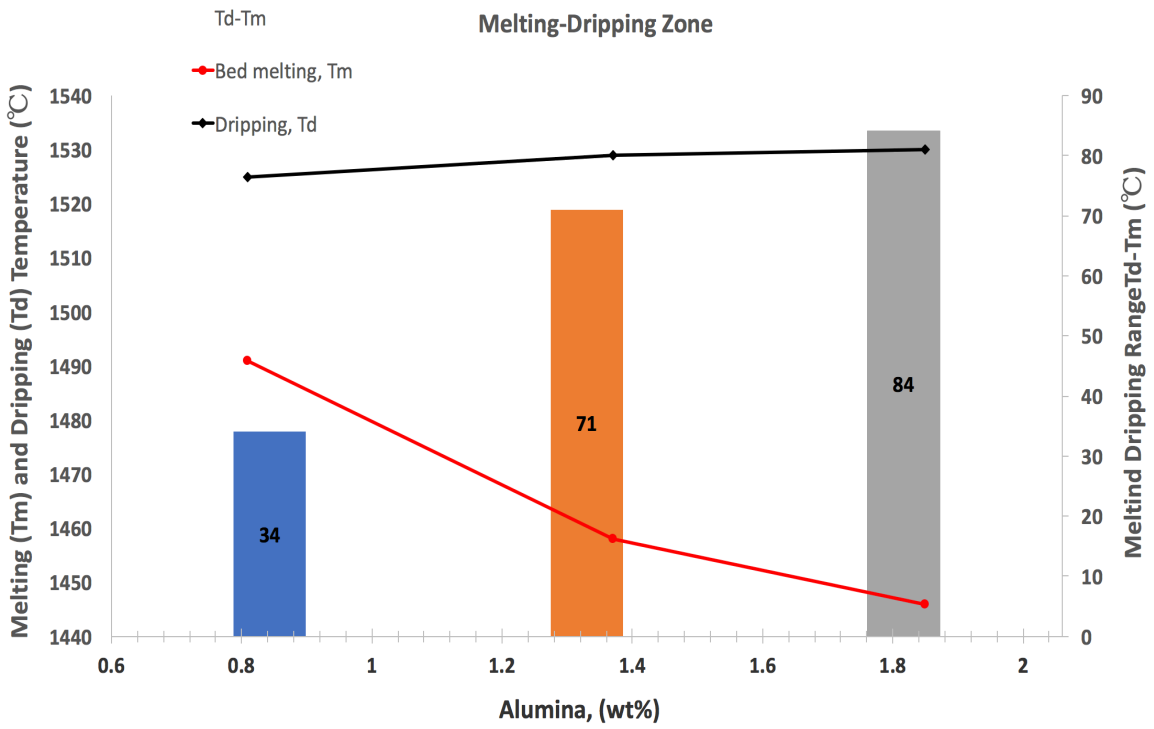

Figure 4.28. Effect of Al_2O_3 on melting and dripping temperatures.

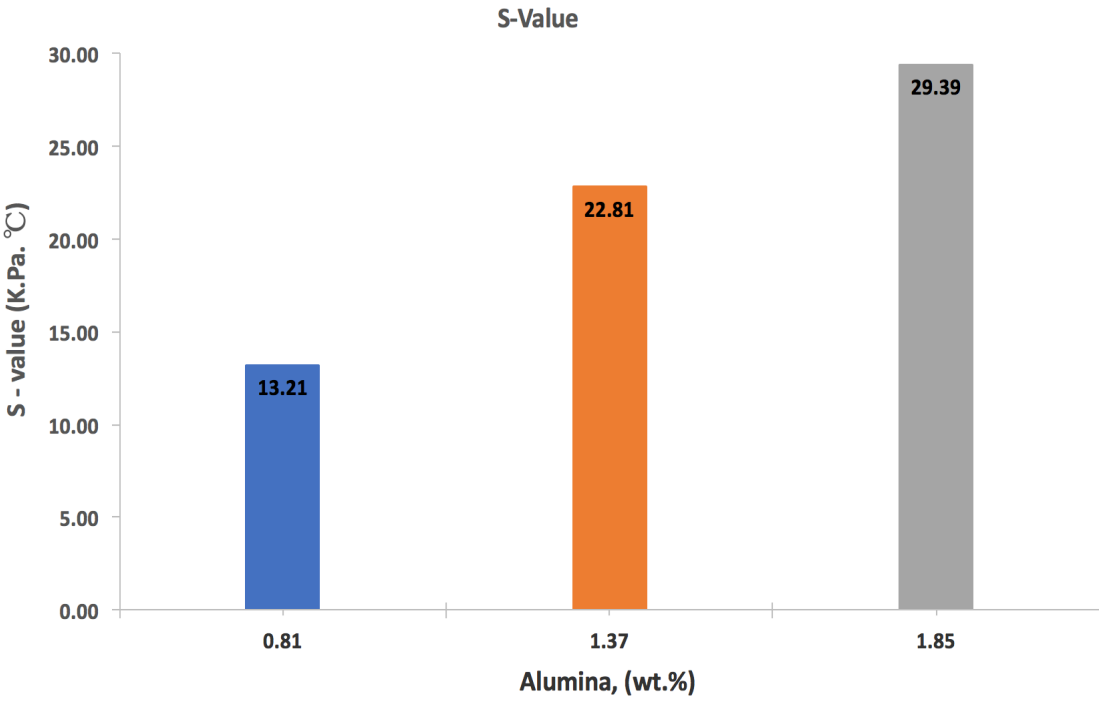

Figure 4.29. Effect of Al_2O_3 on S-Value.

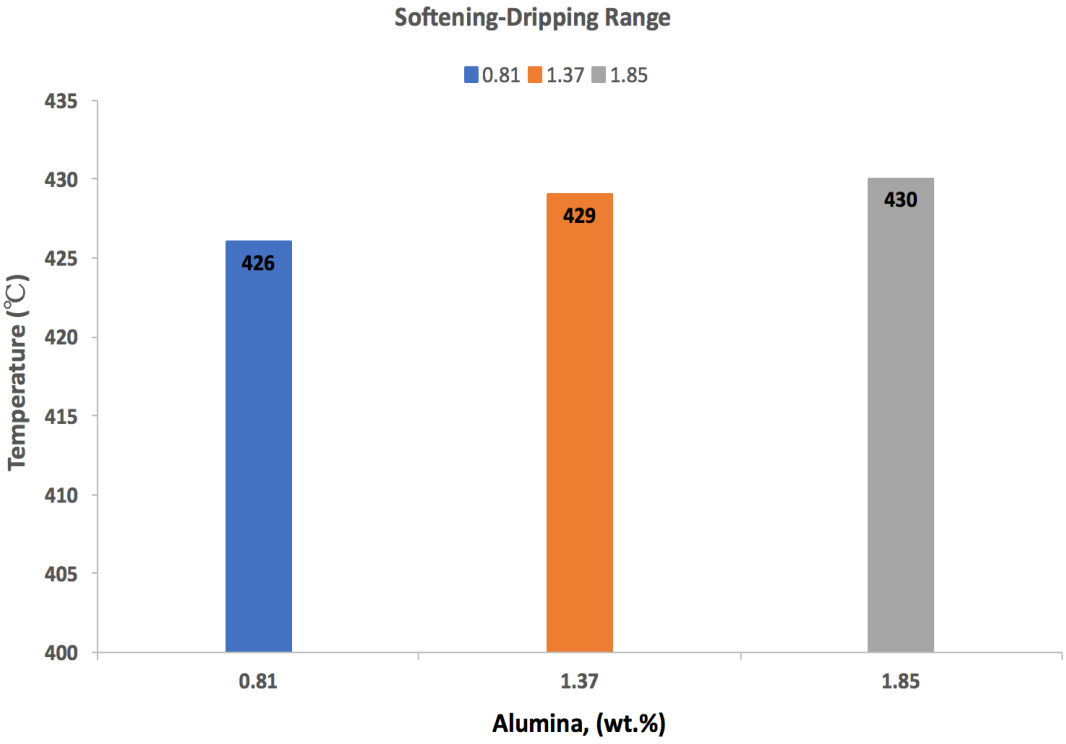

Figure 4.30. Effect of Al_2O_3 on cohesive zone thickness.

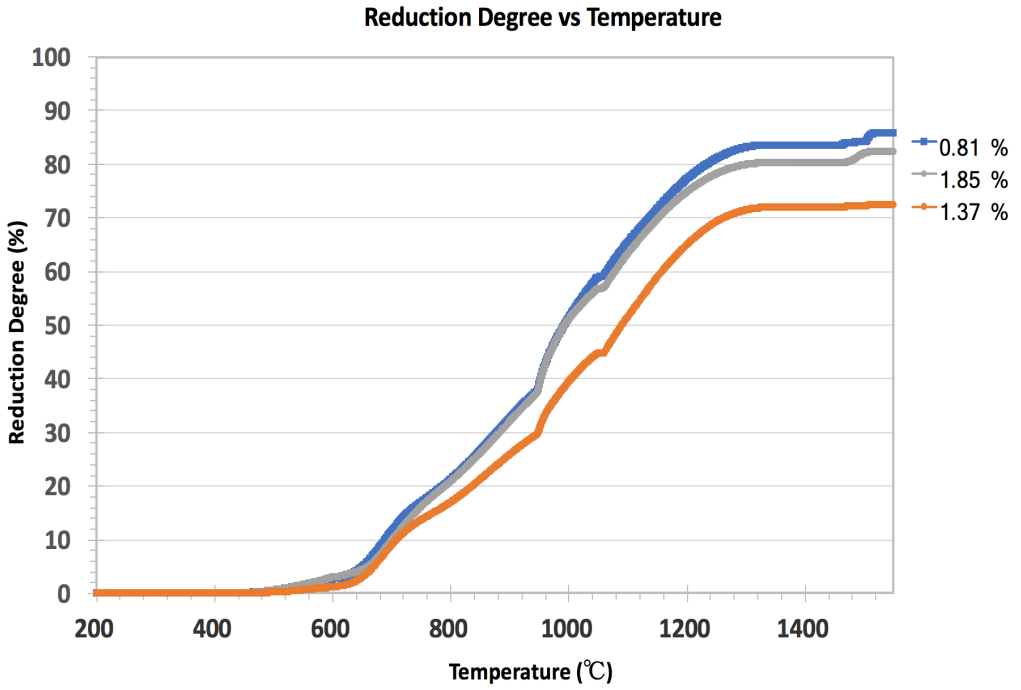

Figure 4.31. Effect of Al_2O_3 on reduction degree.

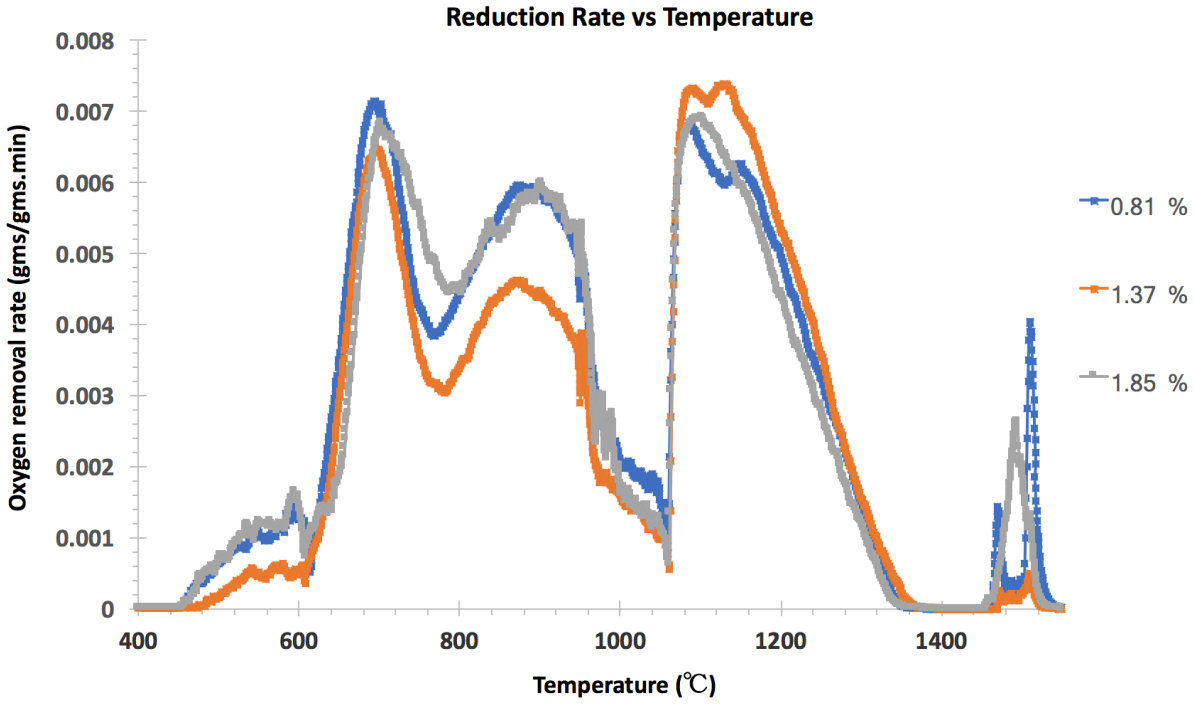

Figure 4.32. Effect of Al_2O_3 on rate of reduction.

Figure 4.33 shows the chemistry obtained from the XRF analysis of separately collected slag droplets. Since the slag drips in a discontinuous manner, each drop was collected separately over time. Since for samples with 0.81% Al_2O_3, the pressure drop peak is very sharp, it was possible to only collect first and final drop. For the other two, four slag samples were collected and analyzed for each pellet type. From 4.33 (e), on average the FeO content in slag from pellet 2 (1.37% Al_2O_3) shows higher values than the other two confirming the result of the estimated reduction degree. Since FeO shows an erratic trend, the rest of the components are normalized to 100 excluding the FeO. Figure 4.33 (c) depicts that the values of alumina in the dripped slag falls in the same range as in the raw pellets. The values are slightly higher because some small amount of silica reduces as seen from Figure 4.33 (d) where silica shows the same trend as raw pellets, but a bit smaller values. Similarly, both CaO and MgO also maintain the chemistry in line with original pellets. Interestingly, in addition to all this, some amount of alkalis is also observed in pellets, with the slag of pellet 3 showing the maximum amount of well above 1 wt.%.

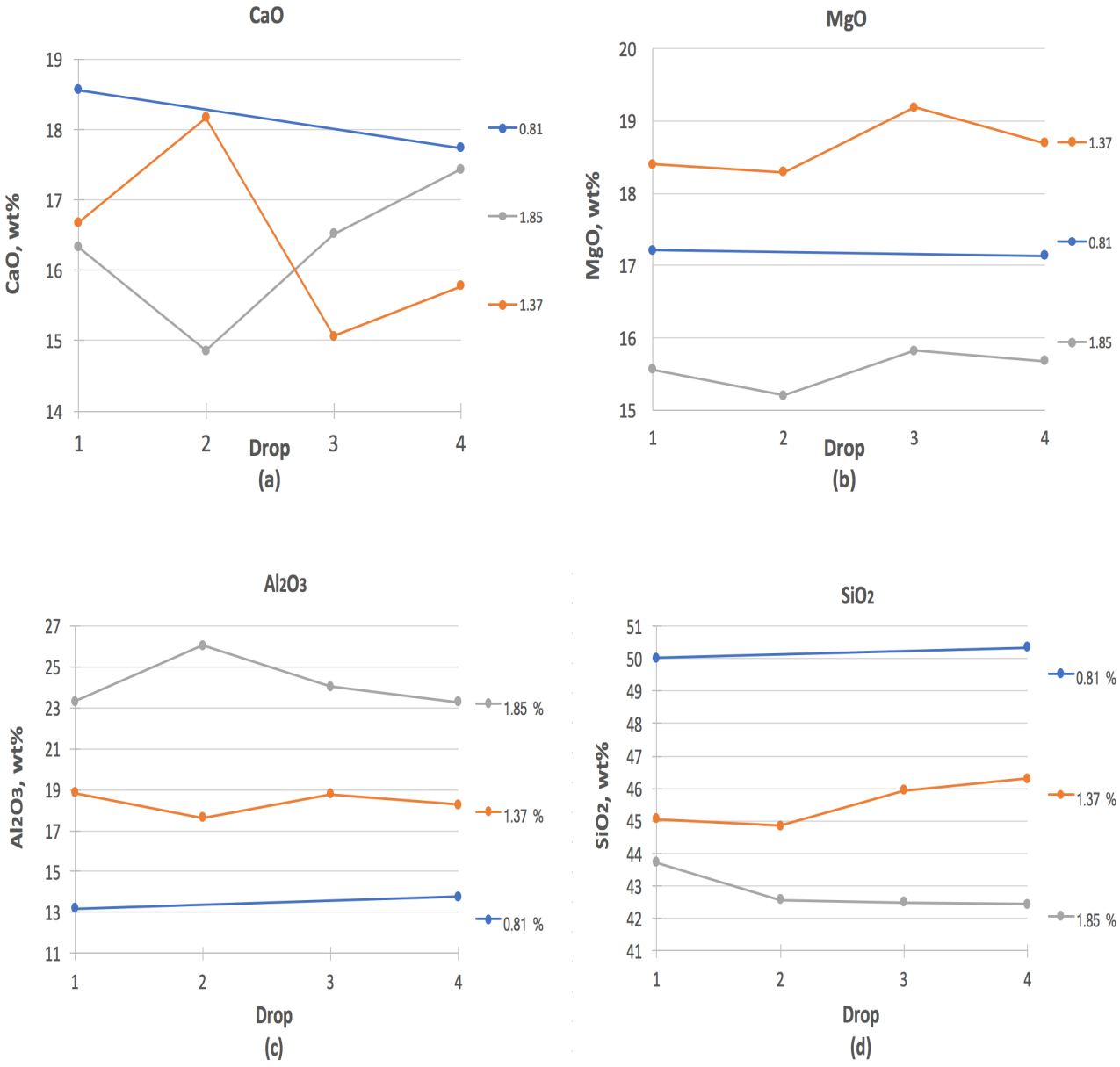

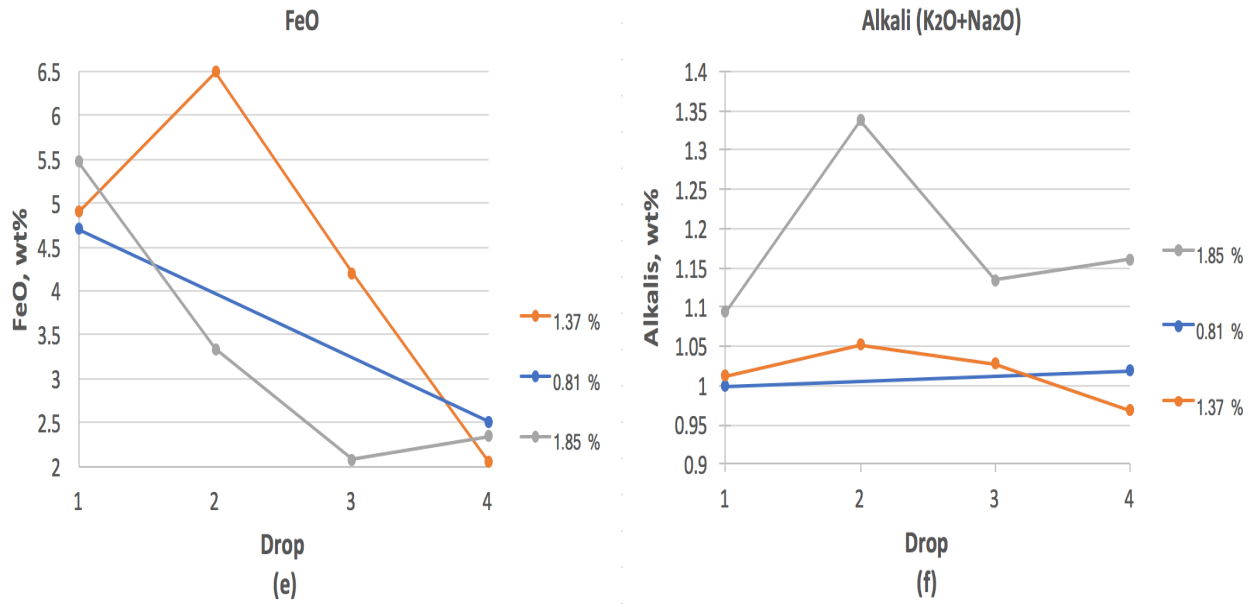

Figure 4.33. Weight percent of (a) CaO (b) MgO (c) Al_2O_3 (d) SiO_2 (e) FeO (f) Alkalis. dripped slag.

4.4. References

[1] Biswas, A. K. (Anil K. (1981). Principles of blast furnace ironmaking : theory and practice / Anil K. Biswas. Cootha Publishing House.

[2] Sohn, I., & Min, D. J. (2012). A review of the relationship between viscosity and the structure of calcium-silicate-based slags in ironmaking. Steel Research International, 83(7), 611–630.

[3] Meng, F. Y., Wang, Z., Zhang, J. L., & Wang, R. B. (2015). Fundamental study of high Al2O3 sinter softening and melting behaviour. TMS Annual Meeting, 2015-March, 643–650.

[4] Gavel, D. J., Adema, A., Stel, J. Van Der, Sietsma, J., Boom, R., & Yang, Y. (2019). Effect of nut coke addition on physicochemical behaviour of pellet bed in ironmaking blast furnace. ISIJ International, 59(5), 778–786.

[5] Shatokha, V., & Velychko, O. (2012). Study of softening and melting behaviour of iron ore sinter and pellets. High Temperature Materials and Processes, 31(3), 215–220.

[6] Yang, Y., Raipala, K., & Holappa, L. (2014). Ironmaking. In Treatise on Process Metallurgy (Vol. 3). Elsevier Ltd.

[7] Tupkary R.H (2010), An Introduction to Modern Iron Making. Physical-thermal- chemical processes in a blast furnace, Khanna Publishers

[8] Nogueira, P. F., & Fruehan, R. J. (2005). Blast furnace burden softening and melting phenomena: Part II. Evolution of the structure of the pellets. Metallurgical and Materials Transactions B: Process Metallurgy and Materials Processing Science, 36(5), 583–590.

[9] Lu, L., Holmes, R. J., & Manuel, J. R. (2007). Effects of alumina on sintering performance of hematite iron ores. ISIJ International, 47(3), 349–358.

[10] Q. Song, Effect of nut coke on the performance of the ironmaking blast furnace, PhD Thesis, Delft University of Technology, 2013.

[11] Holt, C. C. (2004). Forecasting seasonals and trends by exponentially weighted moving averages. *International Journal of Forecasting*, *20*(1), 5–10.

[12] Higuchi, K., Naito, M., Nakano, M., & Takamoto, Y. (2004). Optimization of chemical composition and microstructure of iron ore sinter for low-temperature drip of molten iron with high permeability. *ISIJ International*, *44*(12), 2057–2066.

5. Discussion

This chapter discusses the various ways in which alumina affects the different factors important for softening and melting behaviour. Section 5.1 deals with the influence of alumina on the degree of reduction of pellets. The phenomena of reduction retardation as seen in both heterogeneous (5.1.1) and homogenous (5.1.2) state of the ferrous burden are presented, additionally the possible reasons behind the ambiguous behaviour of pellet 2 are explored in (5.1.3). In section 5.2 the possible effects of alumina on the degree of carburization of the iron shell are listed. Section 5.3 presents a detailed analysis of alumina's influence on the viscosity of slag, this is done by using the thermodynamic software FactSage. Finally, section 5.4 highlights the influence of alumina on surface tension and wettability of slags.

5.1. Effect of Alumina on Reduction Degree

In section 2.1 the possible effect of reduction degree on the softening melting behaviour was discussed. Based on the literature it seems that, with increase in reduction degree the melting temperature (Tm) shifts to higher temperatures, because of the combined effect of increase in shell thickness and decrease in amount of slag in the core. Where on one hand, the effect of reduction degree on softening start temperature is not certain but on the other hand, the rate of softening decreases with increase in reduction degree. Unfortunately or fortunately, for one of the experiments on pellet sample 1, leakage was observed. The gas leaked from the gap created between the graphite crucible and alumina tube due to misalignment of load, and because of which pellets didn't reduce to the limit they should have. This problem was recognized and mended just in time, by manually re-adjusting the load, so the pressure drop peak was observed.

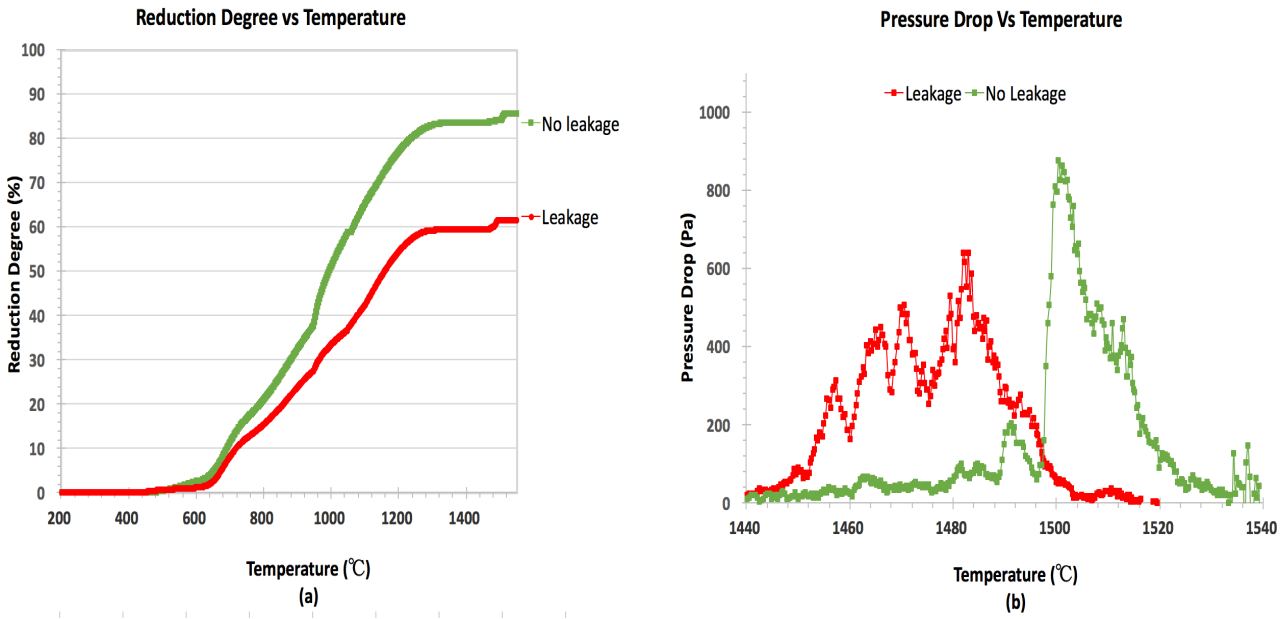

Figure 5.1. Effect of leakage on (a) Reduction degree (b) softening melting behaviour, for pellet 1 (Al_2O_3 =10.5% (CMAS)).

Figure 5.1. can be used to highlight the effect of the reduction degree on melting behaviour. Obviously, the pellet in the experiment which witnessed leakage show a lower reduction degree (Figure 5.1 (a)), more importantly the melting dripping zone for this pellet shifted to lower temperature (Figure 5.1

(b)). This has been observed by numerous authors as mentioned in section 2.1. Unfortunately, nothing can be said about the bed contraction, as for the case with leakage the displacement curve was discontinuous due to misalignment of load which in turn also caused a gap to appear between graphite crucible and alumina tube causing the leakage.

Having established that there is indeed an effect of reduction degree on the melting dripping behaviour. Next, the effect of alumina on the reduction degree of pellets will be explored. This can be done by looking at the effect of alumina in two parts. Firstly, when pellets are in heterogeneous conditions, that is before the formation of liquid slag. Secondly, alumina affects the reduction degree when the microstructure in the core is homogenizing, this initially leads to a microstructure of solid wüstite and slag in the core and then finally to complete liquid, as has been observed by numerous authors.

5.1.1. Effect in Heterogeneous State of the Ferrous Burden

The basis of this section is that in the iron ore pellets the melting starts from a condition in which solid phases are heterogeneously distributed. Therefore, the distribution of the phases affects the melting mechanisms due to the formation of low melting interfaces. This melt then acts as a barrier for reducing gases causing reduction retardation. The point to note here is that the “homogenous” is a relative term as the same distribution can be considered as homogenous in one scale and heterogeneous in another. It is more appropriate to use quasi-homogeneous than homogenous. The intention of evoking the terms heterogeneous and homogenous is that they are linked to equilibrium/non-equilibrium thermodynamics. In homogenous conditions the Gibbs free energy of the system is minimised as the activities of individual components are the same in all the phases present, and farther away one moves from this, the free energy of the system increases. This is schematically shown in Figure 5.2. It depicts the increase in Gibbs free energy of a system as the distribution changes from quasi homogenous to heterogeneous. Another way of understanding this is that in relatively homogenous distribution, the specific surface area of reaction surfaces is higher and diffusion distance is shorter, therefore, it is closer to the equilibrium state.

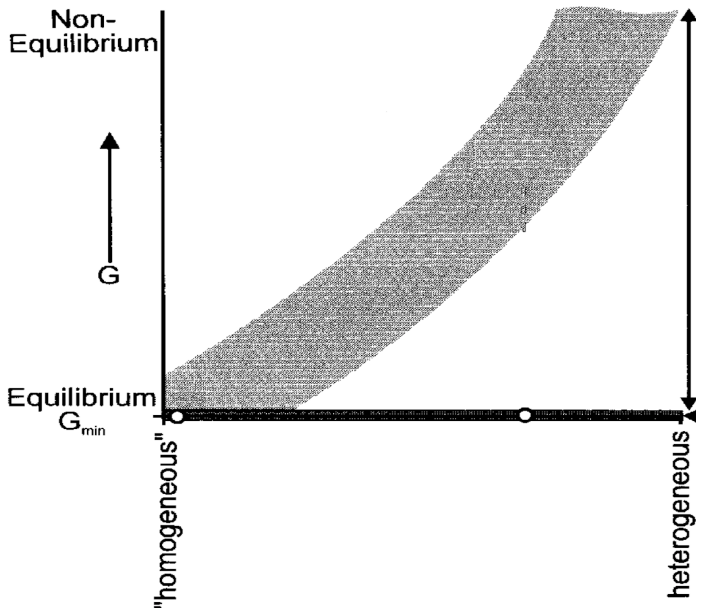

Figure 5.2. Relation between distribution and equilibrium [3].

Though a heterogeneous state is far away from global equilibrium, still local equilibriums could be formed. That is, two (or more) phases which are not in equilibrium with one another react (very locally) and form an interface in-between which is in equilibrium with both the phases. With an increase in the temperature it is the high energy local interfaces that starts to melt first, and once the liquid is formed the homogenizing rate increases as the liquid phase mass transfer is faster than solid-state diffusion [4]. So, even if a particular phase is high melting, it is the melting temperature of the interface which determines the overall solidus temperature. A similar argument has also been presented in the reference [5], where according to authors long-range mass transport is too slow for global equilibrium to be achieved, but short-range mass transport is rapid enough to allow equilibrium at the interfaces between phases in the pellets. According to the reference [6], the initial liquid does not directly influence softening; rather, it acts to improve mass transport and push the system towards homogenization. They further add that the initial liquid is formed at the interface of the lowest melting point, usually between an iron oxide particle and another oxide. After the first melt is formed, it tends to wet the ore particles due to the reduction of the interfacial energy. Furthermore, as the liquid spreads, it may encounter other oxide particles and would react with them if that results in lowering of the free energy, and thus pushes the system towards equilibrium.

In references [3] and [6] authors observed that the liquid onset temperature increase with increasing homogeneity for customized pellets. And irrespective of the starting microstructure, the microstructure reaches the same point at higher temperatures, which is the slag matrix surrounding wüstite islands at around 1250°C. In reference [7], a very local liquid slag was observed even at 980°C. In the reference [6], for a basic pellet, interesting features were observed; a very local slag appeared at 1028°C which then disappeared at 1034°C and then finally again appeared at 1082°C, which then grew slowly till 1185°C. This highlights the erratic behaviour of early local slags forming at low melting interfaces. As soon as the dissolution of one of the phases takes place, mostly a non-wüstite component as it is low in quantity, slag may re-solidify. This makes it difficult to ascertain the impact of local slag on the reduction retardation.

To summarise, the sample evolves from an ‘‘as-fired’’ microstructure to a semisolid throughout the heating process. The liquid acts to improve the mass transport of the heterogeneously distributed components; thus, this evolution is controlled by the quantity of liquid present. The bigger question is how much initial liquid is necessary to lead the system to equilibrium. Another important point is that this very local liquid slag is insufficient to cause softening but can result in reduction retardation as local liquid acts as a barrier for reducing gases. In section 5.1.1.1 possible phases present in the pellets are analysed using the thermodynamic software FactSage. The information obtained from section 5.1.1.1 is utilised in section 5.1.1.2 to understand the role of alumina in causing reduction retardation in the heterogeneous state.

5.1.1.1. Equilibrium Phase Relations in Heterogeneous State of the Ferrous Burden

Coming to the case in hand, as was showcased in Figure 4.16, the pellet sample with 1.85 % alumina (pellet 3) contains numerous particles rich in alumina scattered in the pellet. The microstructure of the alumina rich particle (Figure 4.16 (c)) revealed that it consists of a dark matrix with light phase distributed in it. The EDS point analysis of the particle shown in Figure 4.16 (c) was taken at several points for both light and dark phases, it was observed that on an average the dark phase is richer in aluminium and the light phase is slightly leaner but contains magnesium and higher amount of iron. The typical chemistry of both light and dark phases is shown in Table 5.1.

Phase	Al (wt.%)	Si (wt.%)	Ca (wt.%)	Mg (wt.%)	Fe (wt.%)	O (wt.%)
Dark	16	18	19	-	8	39
Light	8	16	17	2	23	34

Table 5.1. Typical chemistry of phases present in alumina rich particle in pellet 3 obtained from EDS point analysis.

The chemistry of Table 5.1, was studied using the computational thermodynamic software FactSage version 7.0. Three types of solution phases were considered in the FactSage calculations: a liquid oxide phase (FToxid - SLAG), a solid monoxide phase (FToxid-MeO), and a solid olivine-type phase (FToxid-Oliv). Authors in reference [8] used the same selection for acid and olivine pellets and found a good correlation with experimental results.

The analysis of dark phase shows that it mainly consists of grossularite ($Ca_3Al_2Si_3O_{12}$), around 65%. The grossular can be part of iron ores [9] or can even form from anorthite ($CaAl_2Si_2O_8$) during cooling. Anorthite can in turn be formed at induration temperatures with the reaction of Al_2O_3 and slag, interestingly no free alumina was seen in the microstructure. Apart from the grossularite, the dark phase also seems to consist of corundum (Al_2O_3) and anorthite. Coming to the sparsely distributed light phase, it seems again the major phase is grossularite (50%), additionally, it contains olivines like fayalite (Fe_2SiO_4) and kirschsteinite ($CaFeSiO_4$), also a small amount of $CaMg_2Al_{16}O_{27}$, due to the presence of magnesium.

Coming to the particle of pellet 2 (Al_2O_3 = 1.37 %), the microstructure can be seen in Figure 4.18, the chemistry of dark and light phases is shown in Table 5.2. The dark phase has a chemistry similar to that observed for the particle in pellet 1. The light phase is also similar to that observed in pellet 3, the only difference being it contains a greater content of magnesium, which is in line with the overall chemistry of pellet 2. This might suggest that the original particle is mainly the dark phase and the light phase is formed during induration.

Phase	Al (wt.%)	Si (wt.%)	Ca (wt.%)	Mg (wt.%)	Fe (wt.%)	O (wt.%)
Dark	17	18	15	-	5	45
Light	6	18	16	4	16	40

Table 5.2. Typical chemistry of phases present in alumina rich particle in pellet 2 obtained from EDS point analysis.

Naturally since the chemistry of aluminium rich particle in pellet 2 is similar to that in pellet 3, so would be the phases obtained from thermodynamic calculations. The dark phase consists mainly of grossularite and anorthite (more than 80%) while a small amount of corundum and almandine ($Fe_3Al_2Si_3O_{12}$) is also suggested to be present. The light phase is made up of 50% grossularite and 40% olivines like fayalite and kirschsteinite. Also, $MgFeSiO_4$ is another olivine phase suggested. It is a phase formed between two olivine end members namely fayalite and forsterite (Mg_2SiO_4). Higher content of magnesium would explain the formation of such a phase. A very small amount of diopside ($CaMgSi_2O_6$) is another probable phase. In pellets 1 (Al_2O_3 = 0.81 %) no such aluminium rich particle was observed. An important thing to note here is that these phase calculations are based on the assumption that thermodynamic equilibrium exists between the components, which happens rarely in real systems, so that this can only be taken as an approximate analysis.

Since, the light phase is sparse and non-uniformly distributed in the dark matrix it can be neglected and the particle can be assumed to be grossularite or even anorthite, as grossularite any way converts to anorthite at higher temperatures. It is more appropriate to consider the phase as grossularite because anorthite is rarely found on earth as a naturally occurring mineral but is abundant on the moon [10]. For both the pellets 2 and 3, as the temperature increases during the experiment, the hematite gradually converts to magnetite and further to wüstite, and as grossularite converts to anorthite, the phases in contact will be wüstite and anorthite. The phase diagram of the anorthite-wustite system is shown in Figure 5.3. At the anorthite rich end, the phases present at low temperatures are anorthite, corundum, and grossularite, as was also seen for the chemistry of dark phase in the particle. The fayalite appears as FeO content increases.

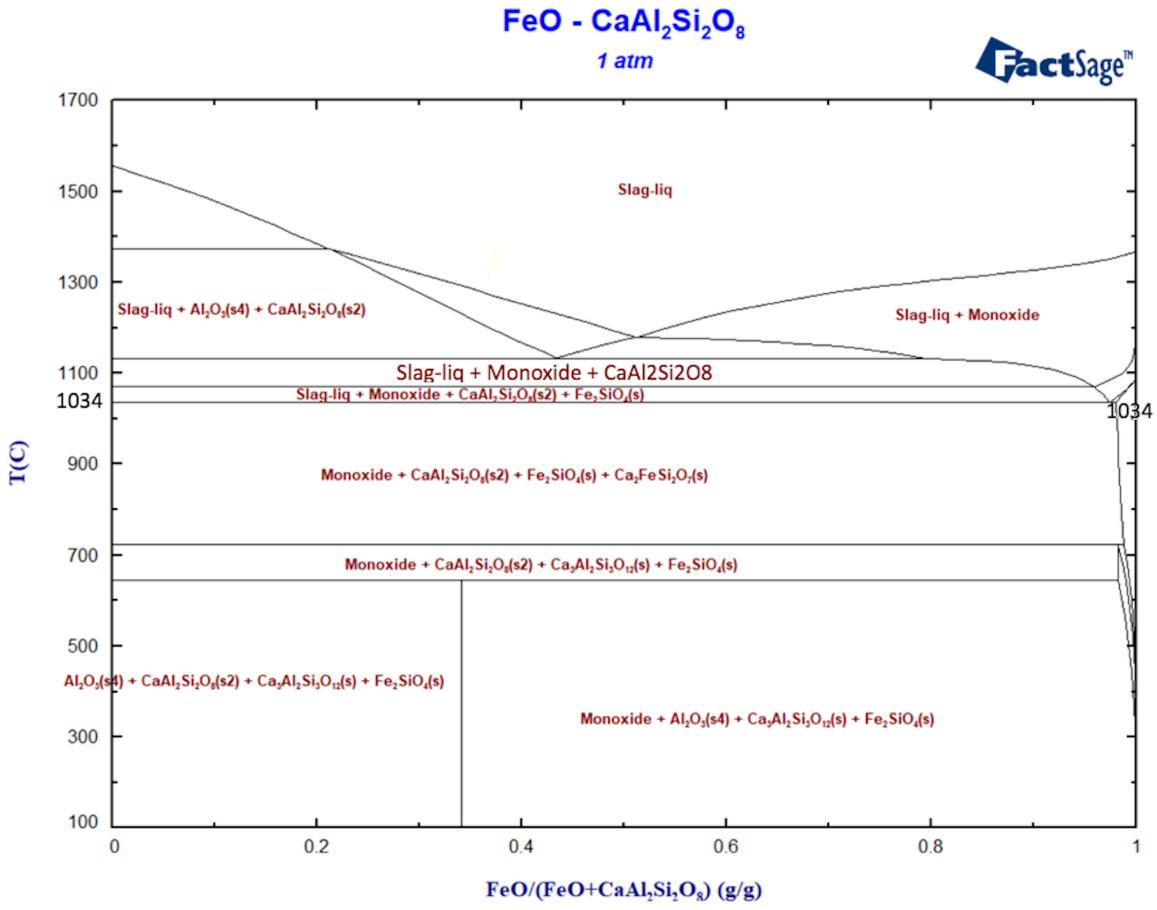

Figure 5.3. Anorthite – Wüstite binary phase diagram obtained from FactSage.

It can be seen that though FeO is not soluble in anorthite, some amount of anorthite is soluble in FeO. More importantly anorthite is a high melting phase (1553 °C) but as soon as it comes in contact with a small amount of FeO the solidus temperature drops to 1034°C. On the other extreme, that is at the FeO rich end the solidus temperature decreases gradually from 1377 °C to 1034 °C as anorthite dissolves in it. At temperature, close to solidus, the phases present are anorthite, monoxide (FeO), fayalite (Fe_2SiO_4), and iron akermanite ($Ca_2FeSi_2O_7$). This means that anorthite and wüstite react to form an interface consisting of fayalite and iron akermanite, and it is this interface that melts at low temperatures.

It is difficult to predict the nature of the interface. It can either be a layered structure of fayalite and iron akermanite, or it is also possible that the interface is some complex mixture of both fayalite and

iron akermanite. A logical guess can be made by looking at the binary phase diagrams of relevant systems one by one.

From Figures 5.4 to 5.6, it can be seen that all relevant combinations of the binary system have a solidus temperature greater than 1034°C, hence the interface at wüstite – anorthite system on anorthite side is a mixture or some complex arrangement of these three phases. This is further confirmed from the ternary phase diagram of anorthite, iron akermanite, and fayalite (Figure 5.7) which shows the advent of liquid at 1040 °C already, and hence interface is not some layered structure.

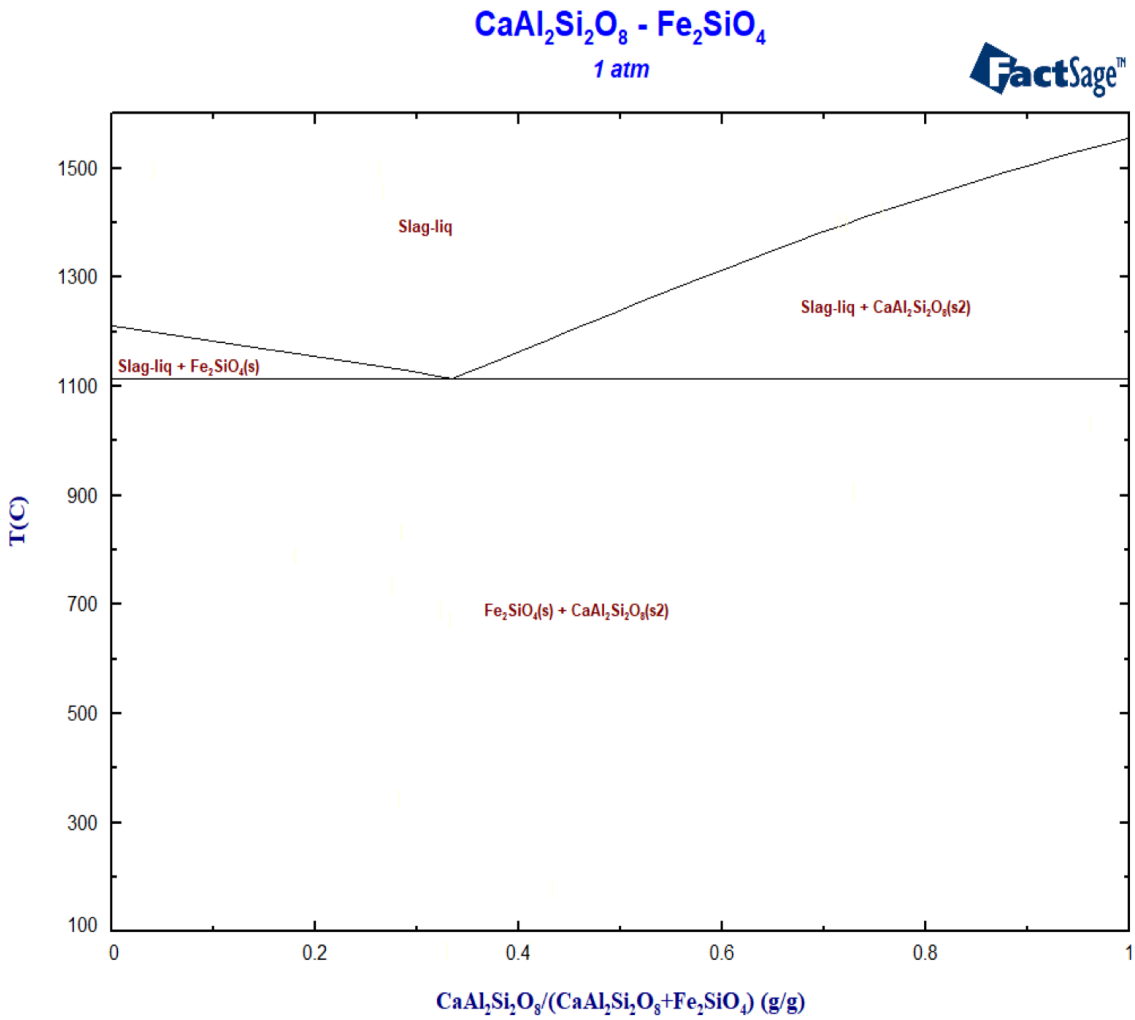

Figure 5.4. Binary phase diagram Anorthite – Fayalite obtained from FactSage.

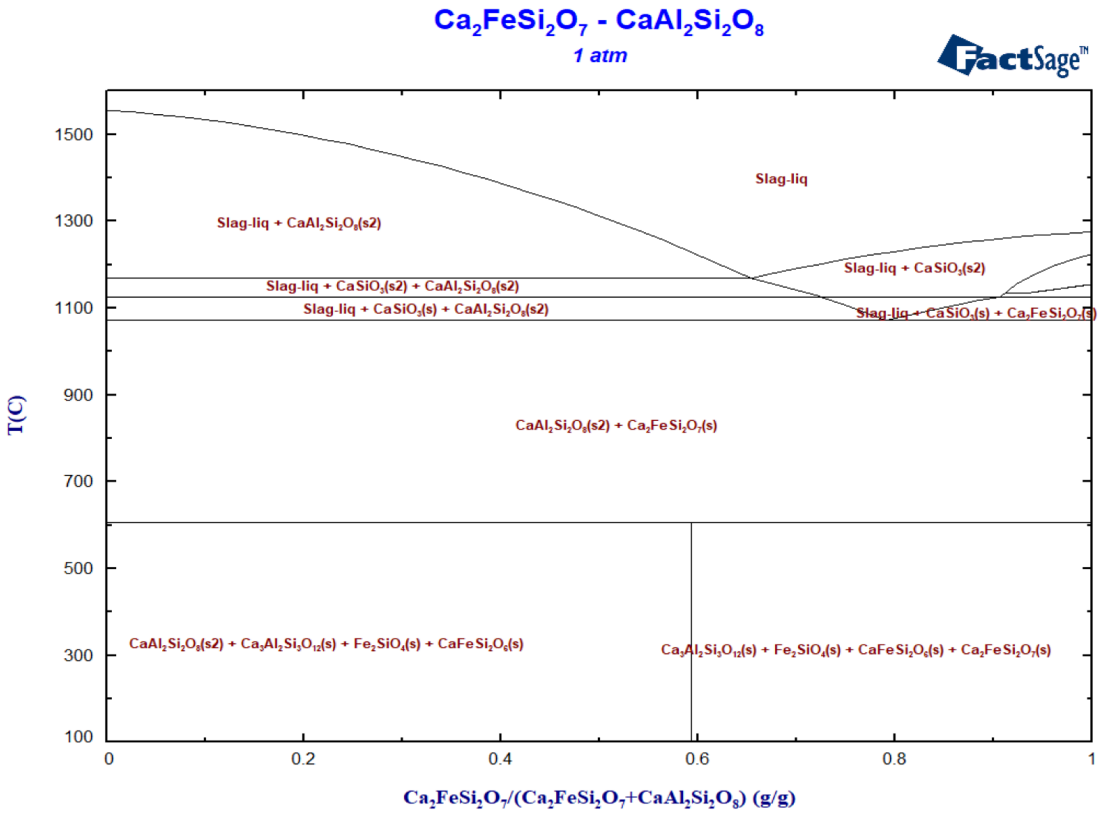

Figure 5.5. Binary phase diagram of Anorthite – Iron akermantite obtained from FactSage.

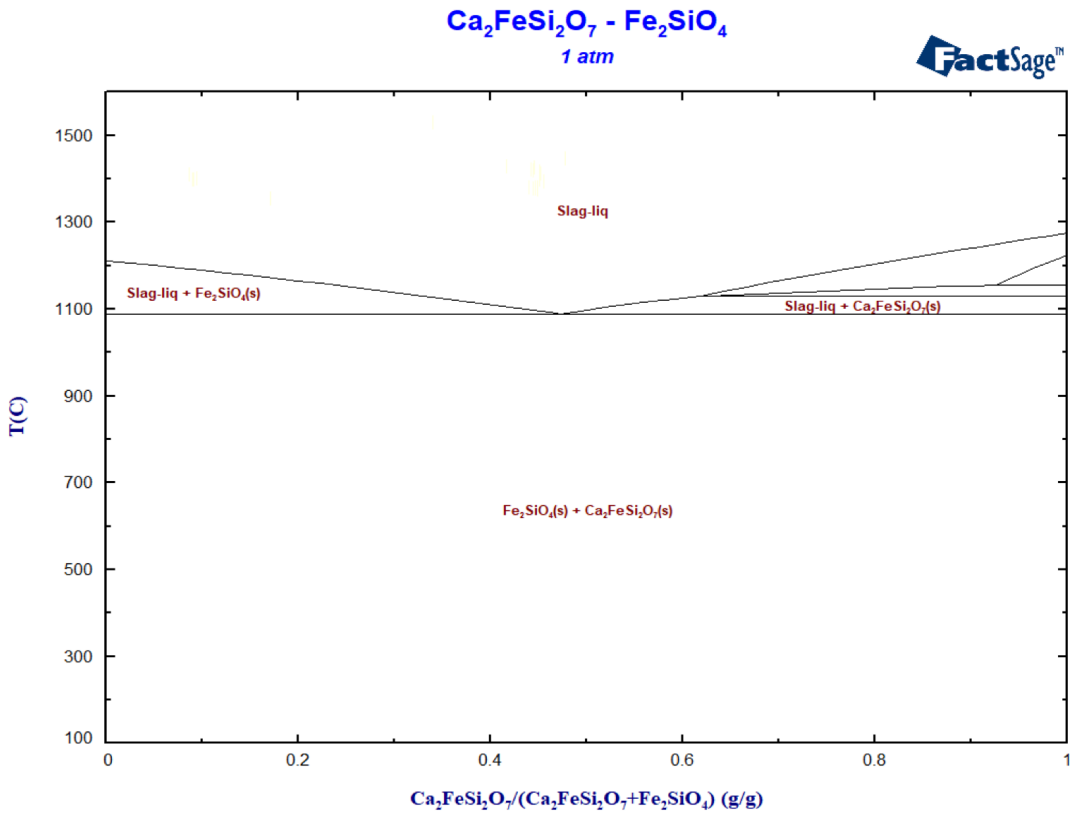

Figure 5.6. Binary phase diagram of Iron akermanite – Fayalite obtained from FactSage.

Coming back to Figure 5.3, the first liquid will appear at the interface on the anorthite rich end. This is because, on the wüstite rich end a certain amount of anorthite is required to dissolve in wüstite to reduce its solidus temperature to the same level as at anorthite rich end (1034 °C). This is difficult due to the slow rate of solid-state diffusion. But once the liquid has formed it becomes easier for anorthite to transport across and dissolve in wüstite. Since the size of the wüstite matrix surrounding the anorthite particle is much greater, it can accommodate the entire anorthite. As the anorthite dissolves in wüstite the net composition shifts towards the wüstite end ultimately leading to a final configuration of wüstite and slag. This is how the system transforms from a heterogeneous state towards a homogenous state.

Another type of particle that was observed in all three pellets is silica. Figure 5.8 shows the binary phase diagram of the FeO-SiO_2 system. The liquid starts forming at 1183°C at FeO rich end and 1185°C at SiO_2 rich end, both higher than the solidus temperature at anorthite - wüstite interface.

Sample	Al (wt.%)	Si (wt.%)	Ca (wt%)	Mg (wt%)	Fe (wt%)	O (wt%)
Pellet 1	2	21	16	4	18	39
Pellet 2	4	24	14	4	12	42
Pellet 3	5	20	11	3	21	40

Table 5.3 Typical chemistry of slags obtained from EDS point analysis.

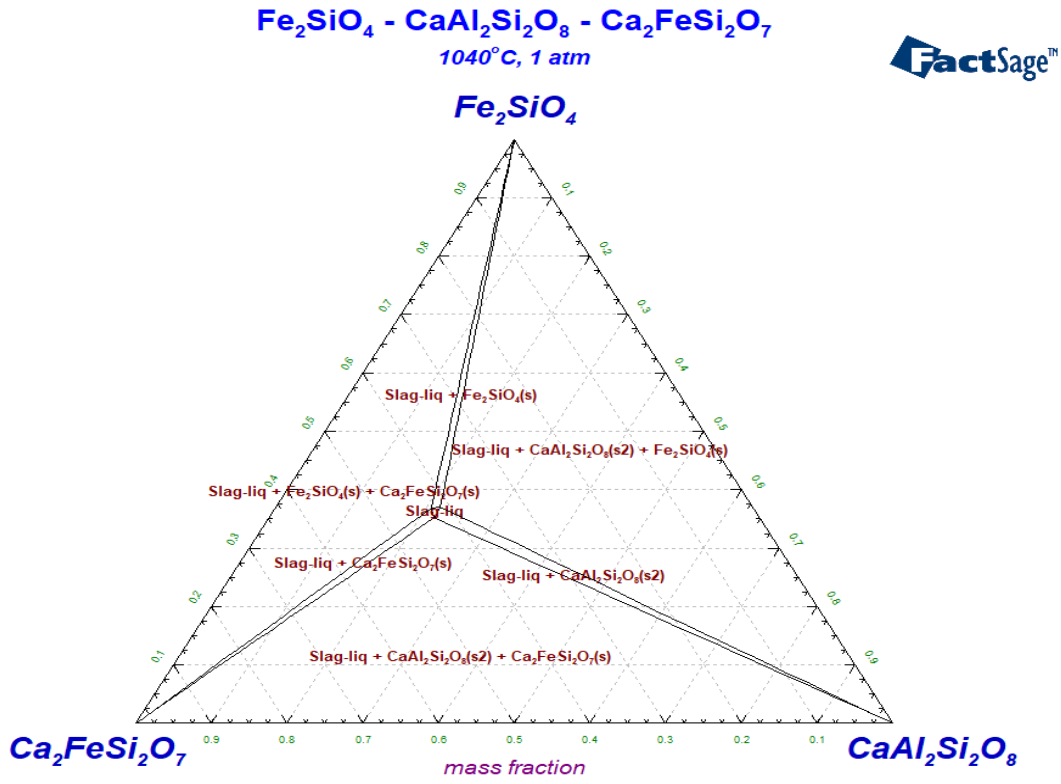

Figure 5.7. Ternary phase diagram of Fayalite, Iron-akermanite and anorthite system at 1040°C showing presence of liquid slag obtained from FactSage.

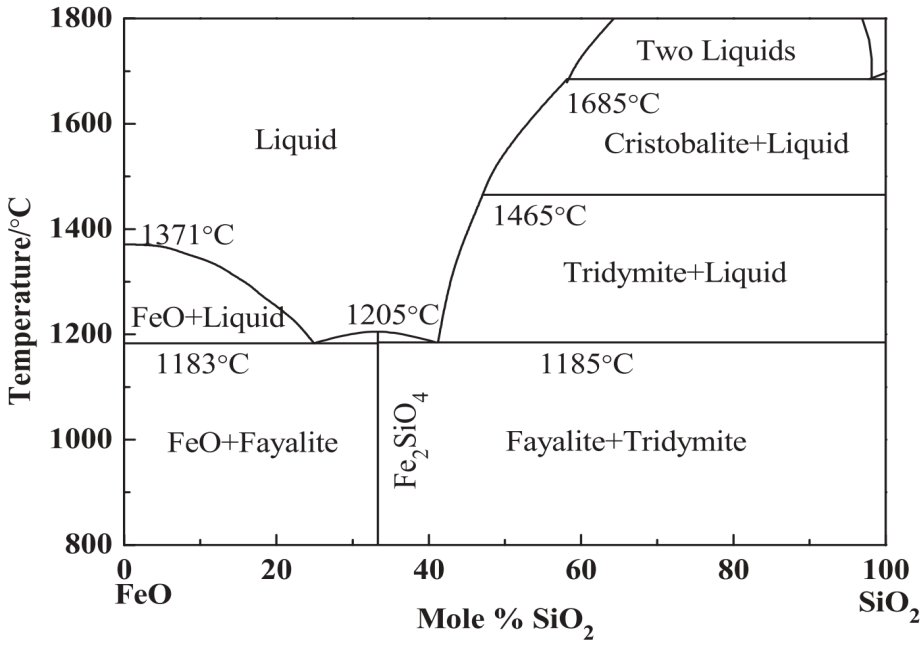

Figure 5.8. Binary phase diagram FeO – SiO_2 [11].

Coming to the chemistry of the slag, Table 5.3 shows the slag chemistry in three cases is quite similar as the values for all elements fall in the same range. The obvious difference being the increase in aluminium content from pellet 1 to pellet 3, and also pellet 2 consistently showing higher content of Mg. The suggested phases by FactSage are the same for three cases, which is an almost equal proportion of fayalite (Fe_2SiO_4), diopside ($CaMgSi_2O_6$), grossularite ($Ca_3Al_2Si_3O_{12}$), hedenbergit ($CaFeSi_2O_6$), forsterite (Mg_2SiO_4) and also a small amount of almandine ($Fe_3Al_2Si_3O_{12}$).

5.1.1.2. Reduction Retardation in Heterogeneous State of the Ferrous Burden

Now moving onto the effect of these low melting interfaces. Figure 5.9 shows the reduction rate in the temperature range of interest as taken from Figure 4.32, depicting the difference in the rate of reduction in three samples at relatively low temperatures.

The pellet 3, with the highest alumina content (Al_2O_3 = 1.85 %), reduces at a similar rate to one with the lowest, pellet 1 (Al_2O_3 = 0.81 %), until about 1000 °C. After around 1000 °C, the rate for pellet 3 drops to lower levels. Interestingly this is in the vicinity to temperature at which anorthite particles start to dissolve. The temperature (998°C) at which the fall in reduction rate for the sample containing the highest alumina (pellet 3) happens is lower than what is expected from thermodynamics (1034°C). This can be explained by the presence of impurities like alkalis, which are notoriously known for decreasing solidus temperatures of phases. From Figure 4.33 (f), it was confirmed that the pellet 3 on an average contains a larger amount of alkalis. This highlights another indirect effect of alumina.

The pellet 2 (Al_2O_3 = 1.37 %) reduces at much lower rates than the other two in the low-temperature range (Figure 4.32) and it stays low in 1000 to 1050°C as well. An attempt will be made in section 5.1.3 to explain this ambiguous behaviour of pellets with 1.37 % alumina.

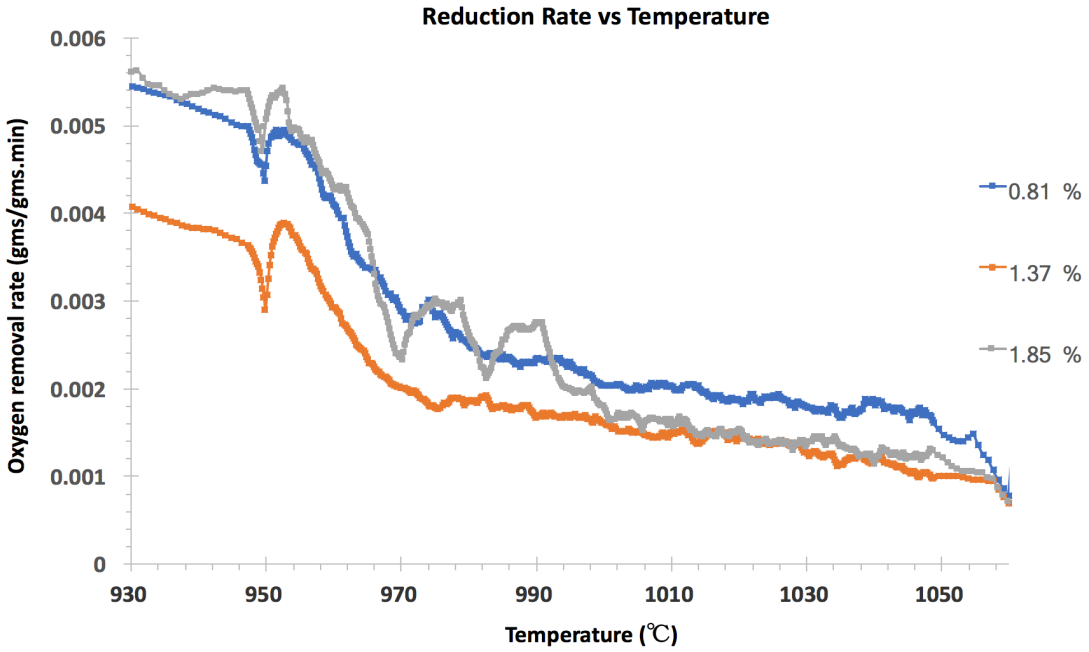

Figure 5.9. Possible effect of alumina on reduction retardation at low temperatures.

The reason for showing the curve till 1060°C only, is that, at 1060°C the reduction potential of the incoming gas is increased causing sudden a rise in rate of reduction for all three samples, hence nullifying any effect on reduction rate due to alumina. Another point to note here is that at these temperatures the rate of reduction is already very low, hence the influence of difference in reduction rate on net reduction degree is not substantial. The aim here is to show that there is an effect on reduction rate in heterogeneous condition even at these low temperatures, and this will continue to higher temperatures which will be seen in the next sub section 5.1.2.

5.1.1.3. Effect of Basicity in Heterogeneous State of the Ferrous Burden

According to reference [2], CaO dissolves in wüstite, decreasing the activity of FeO in the primary slag forming process hence delaying reduction retardation. Another indirect effect is that, with the increased basicity, alkalis which are prone to forming the low-melting compounds, are bound to stable silicates, hence again increasing the solidus temperature of the system. According to reference [6], in basic pellets homogenization takes place at higher temperatures because of the lack of low melting interfaces.

Seeing the effect of CaO in a heterogeneous system is difficult as it depends on the distribution of CaO in the system. On one hand, it can be uniformly distributed in the microstructure, on the other hand, it can be present as discrete CaO rich particles. Assuming that CaO is present uniformly, then the effect of CaO on solidus temperature can be seen with the help of the pseudo-binary phase diagram (Figure 5.10). It depicts the anorthite end of the anorthite-wüstite interface. The amount of anorthite is taken as a constant high value (95%).

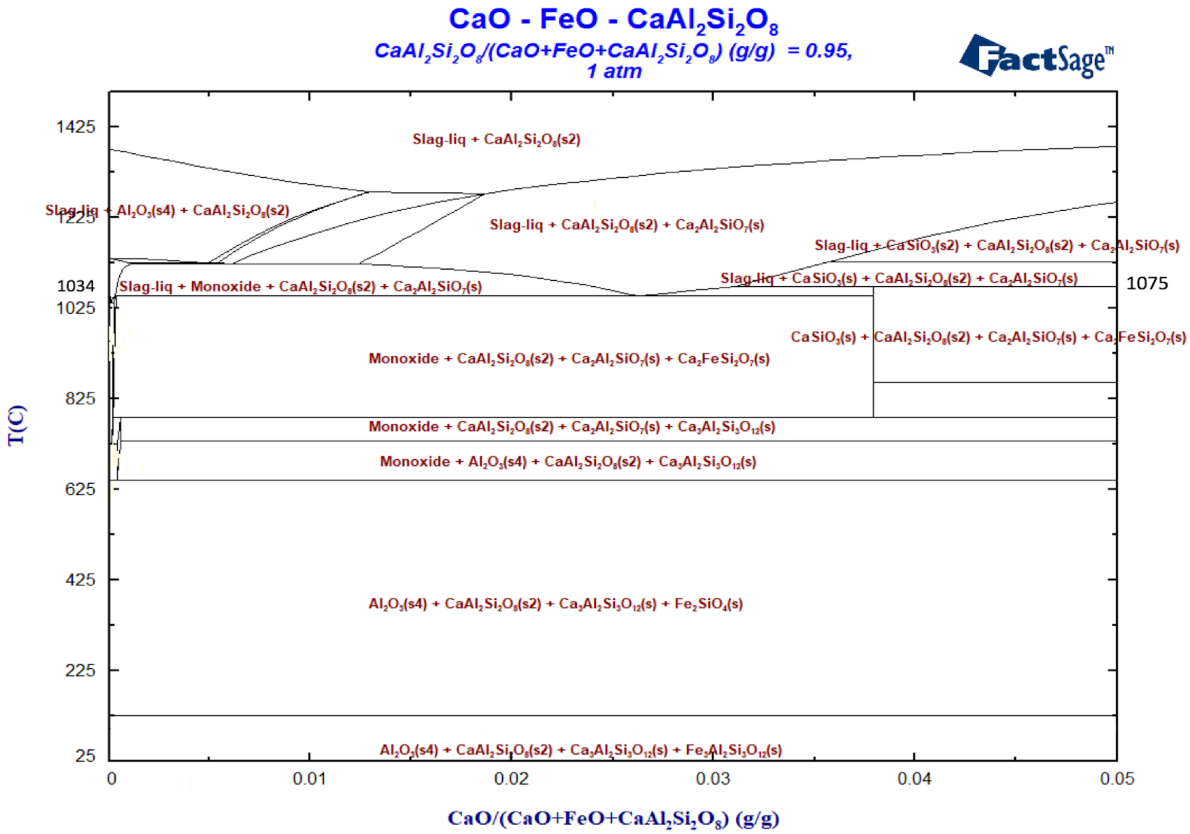

Figure 5.10. Effect of CaO on anorthite - wüstite interface obtained from FactSage.

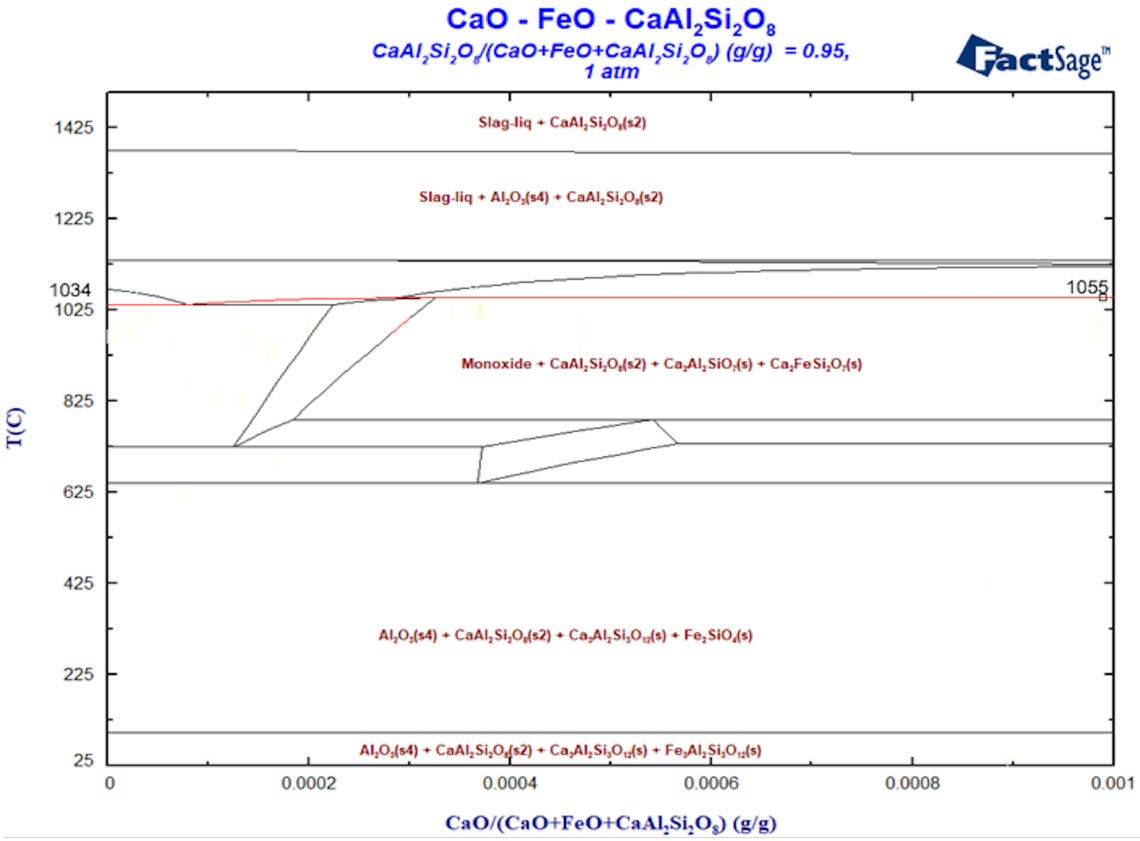

Figure 5.11. Effect of CaO on anorthite – wüstite interface obtained from FactSage.

Though not visible clearly in Figure 5.10, with an increase in CaO the solidus temperature initially increases from 1034 °C to 1055°C and then finally to 1075°C. The increase to 1075°C happens only when CaO reaches 0.037%. The early increase can be seen properly in Figure 5.11. Where the slight increase in solidus temperature can be seen from the solidus line highlighted in red. It seems that with an increase in CaO the solidus temperature increase only slightly.

In the case where CaO is present heterogeneously in the pellets, a FeO – CaO interface would exist, this can be visualised using Figure 5.12. The solidus temperature at both CaO and FeO rich end is higher than the anorthite – wüstite system. This means that the CaO will have to diffuse in the solid-state towards the anorthite – wüstite interface, the rate of which is again dependent on the CaO distribution. As in the microstructure with a fine distribution the diffusion distance is smaller in comparison with a coarser distribution.

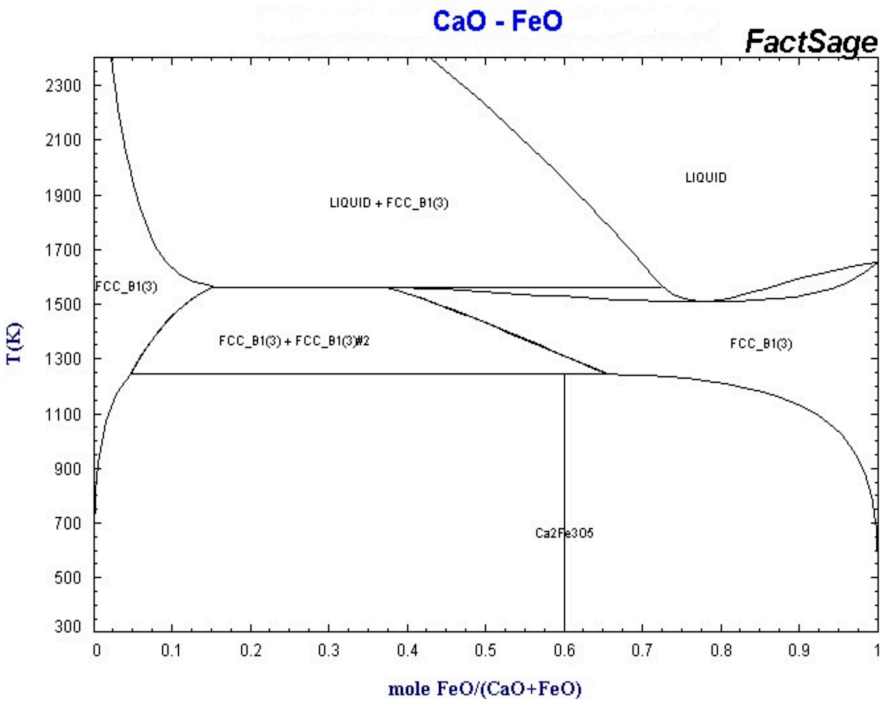

Figure 5.12. CaO – FeO phase diagram obtained from FactSage.

5.1.2. Effect in Homogenous State of the Ferrous Burden

In literature [5], the pellet structure showed the presence of gangue, individual silica particles, and very local coarse pocket of slags at 1150°C. The microstructure was still heterogeneous at 1150°C, but only in the next 100 °C, the structure changed to that of liquid slag surrounding the wüstite islands. This emphasises how fast the homogenisation takes place once liquid slag starts forming in the pellets. This is where local liquid formed at the low melting interfaces becomes important as they increase the rate of homogenization. Once homogenization occurs, the system consists mainly of (magnesio)wüstite (Fe,Mg)O, Fayalitic slag $(Fe,Mg,Ca)_2SiO_4$, and the metallic iron Fe [1]. In addition to the core the metallic iron periphery also gets impregnated by slag. The slag from the core can reach the metallic shell due to the difference in surface energies, and this results in the reduction retardation in the homogenous state.

Reduction retardation of pellets is attributed to the disappearance of the micropores caused by the sintering of iron under the presence of a liquid exuded from the wüstite core. The mechanism of reduction retardation in the homogenous state has been summarised in literature [13];

1) At first, the melt formed in the wüstite core exudes into the iron shell under the influence of surface energy (capillary forces).
2) When the liquid phase fills the pores present between the metallic iron particles in the shell, each interparticle space becomes a capillary in which a substantial capillary pressure is developed. This pressure results in densification of the metallic iron.
3) Additionally, the presence of liquid helps in mass transfer, resulting again in the densification of the iron shell. This causes the fine pores to disappear, thereby impeding the reduction gas diffusion and consequently leading to retardation of reduction.

Regarding the last point above, in literature [5] it was also observed that as the temperature increases the metallic network coarsens. The frequency of the small pores reduces, as a result of the densification caused by the increase in the liquid slag fraction. The mass transfer across liquid is easier hence it causes coarsening of the iron shell network. So, the improvement in the pellet reduction retardation can be brought about by adjusting the chemical composition of the core part to have a higher solidus temperature [13]. The solidus temperature here is governed by overall chemistry. According to authors of reference [1], it is both solidus and liquidus temperature which governs the properties of the pellets. For a given solidus temperature, the liquidus temperature governs the rate at which the liquid phase proportion increases with temperature. It is this liquid phase proportion which causes reduction retardation and softening.

5.1.2.1. Equilibrium Phase Relations in the Homogenous State of the Ferrous Burden

Once the homogenization has taken place the chemistry of the core will be that of the unreduced wüstite and rest being the gangue and fluxes. The estimated chemistry for the partially reduced core of all three pellets is shown in Table 5.4. Here it is assumed that the iron oxide is reduced until FeO and except iron oxide, no other oxide is reduced.

Sample	FeO (wt.%)	SiO_2 (wt.%)	CaO (wt%)	MgO (wt%)	Al_2O_3 (wt%)
Pellet 1	91.5	4.5	1.7	1.4	0.9
Pellet 2	90.9	4.4	1.5	1.6	1.5
Pellet 3	90.7	4.2	1.5	1.4	2.1

Table 5.4. Estimated chemistry of partially reduced core just after homogenization.

The above chemistry has been used to calculate the liquid phase proportion at various temperatures between solidus and liquidus for each pellet sample, using “equilib” module of the FactSage. The result is shown in Figure 5.13.
The solidus and liquidus temperatures of three pellets are shown in Table 5.5. Though there is not much difference in solidus and liquidus temperatures of three pellets, still the rate of increase in liquid phase proportion differs among the pellets.

Sample	Solidus (°C)	Liquidus (°C)	ΔT
Pellet 1	1085	1387	302
Pellet 2	1086	1389	303
Pellet 3	1087	1382	295

Table 5.5. Solidus, liquidus and melting range for pellets based on FactSage calculation.

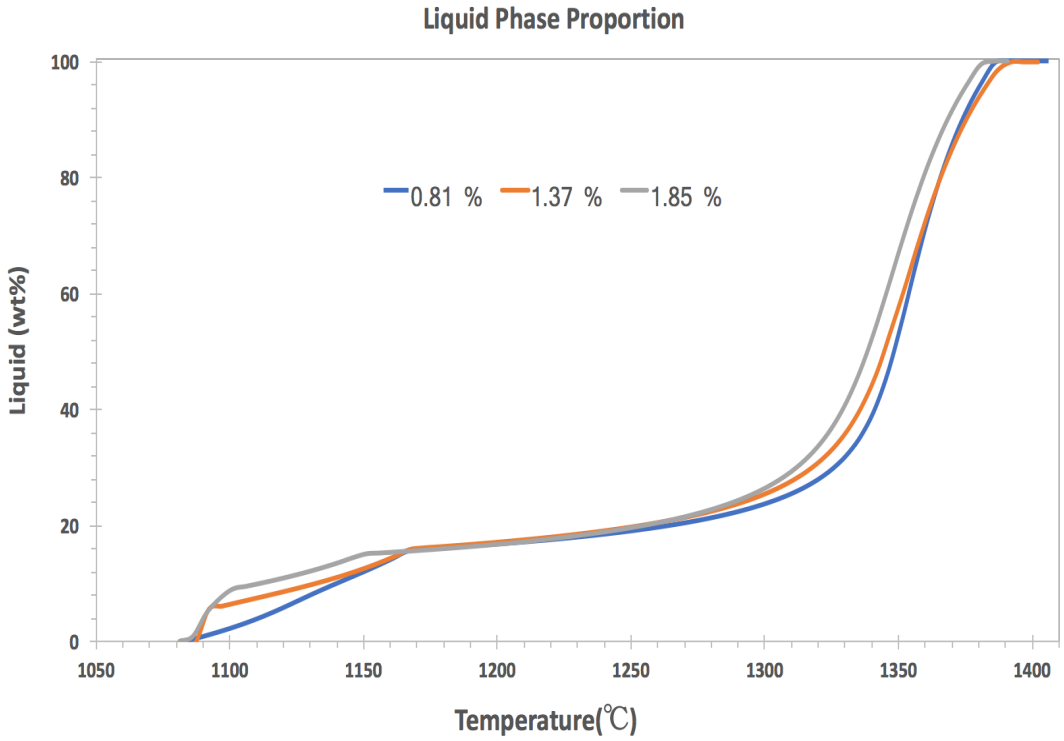

Figure 5.13. Effect of alumina on liquid phase proportion in core, obtained from FactSage.

This behaviour can be explained with the help of figure 5.14, where variation in the proportion of the phases with respect to temperature, is depicted. From Figure 5.14 (b), it can be seen that with the increase in alumina the proportion of olivine decreases. The olivine is a mixture of various silicates of calcium, magnesium, and iron. For the three pellets considered the major constituent phases of olivine here are fayalite (Fe_2SiO_4) and kirschsteinite ($CaFeSiO_4$), constituting more than 75% together. Their variation with temperature is shown in Figure 5.14 (c) and (d) respectively. Naturally, fayalite and kirschsteinite show the same trend as olivine. Additionally, the olivine also consists of a third phase, $MgFeSiO_4$, as shown in Figure 5.14 (e). It is formed between two the endmembers of olivine series, namely forsterite (Mg_2SiO_4) and fayalite (Fe_2SiO_4). The proportion of $MgFeSiO_4$ is greater in pellet 2 as it contains a higher content of Mg. Figure 5.14 (f) shows that with an increase in alumina the anorthite proportion increases. Anorthite dissolves at lower temperatures than the olivine, resulting in a high rate of increase in the liquid phase proportion for pellets containing 1.87 % alumina (pellet 3), followed by pellets containing 1.37 % alumina (pellet 2), while the pellet containing 0.81 % alumina (pellet 1) shows negligible amount of anorthite formation, hence resulting in lower liquid phase proportion at a given temperature. Figure 5.14 (a) shows that the rate of FeO dissolution also increases with an increase in alumina, which means that anorthite reacts with FeO (even olivine) to form liquid slag. Hence with an increase in alumina the proportion of liquid slag increase in the microstructure. This liquid slag causes reduction retardation.

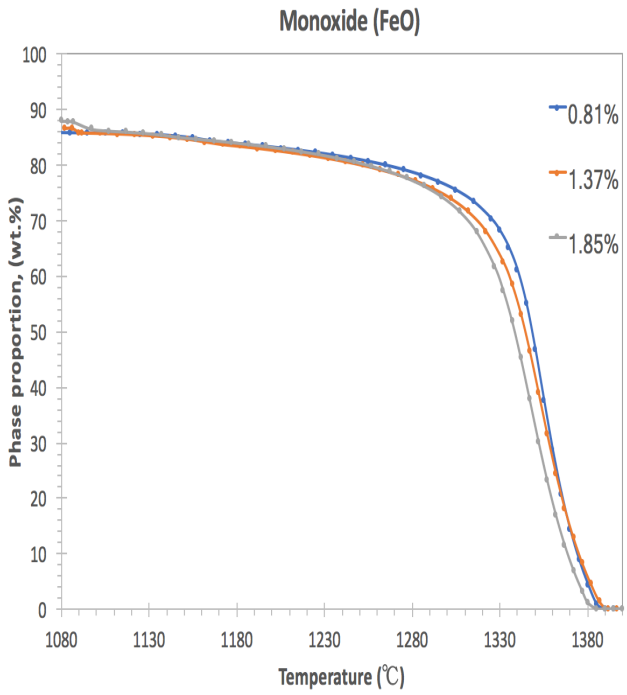
Monoxide (FeO)
Phase proportion, (wt.%)
Temperature (℃)
0.81%
1.37%
1.85%

(a)

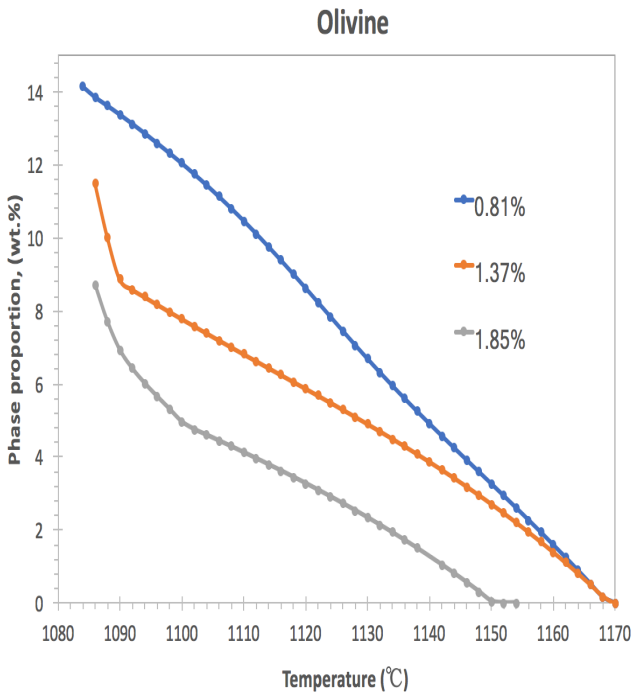
Olivine
Phase proportion, (wt.%)
Temperature (℃)
0.81%
1.37%
1.85%

(b)

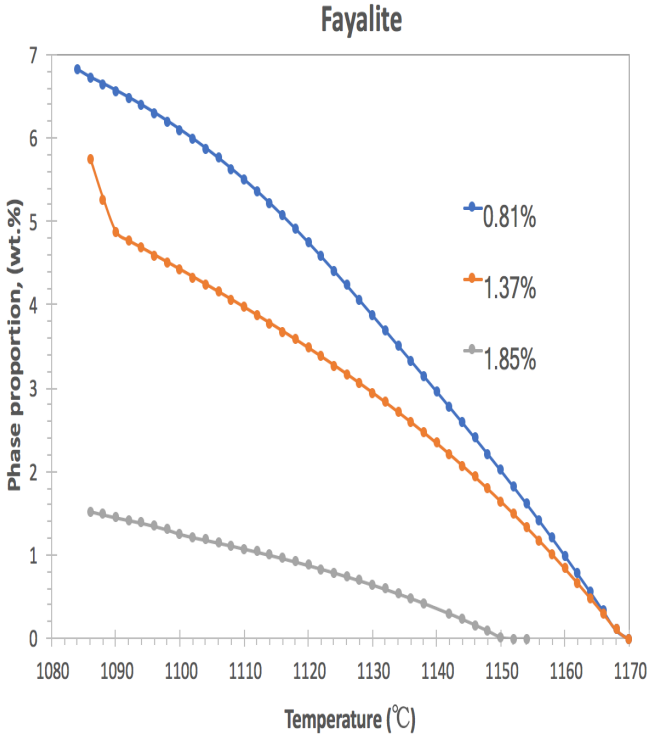
Fayalite
Phase proportion, (wt.%)
Temperature (℃)
0.81%
1.37%
1.85%

(c)

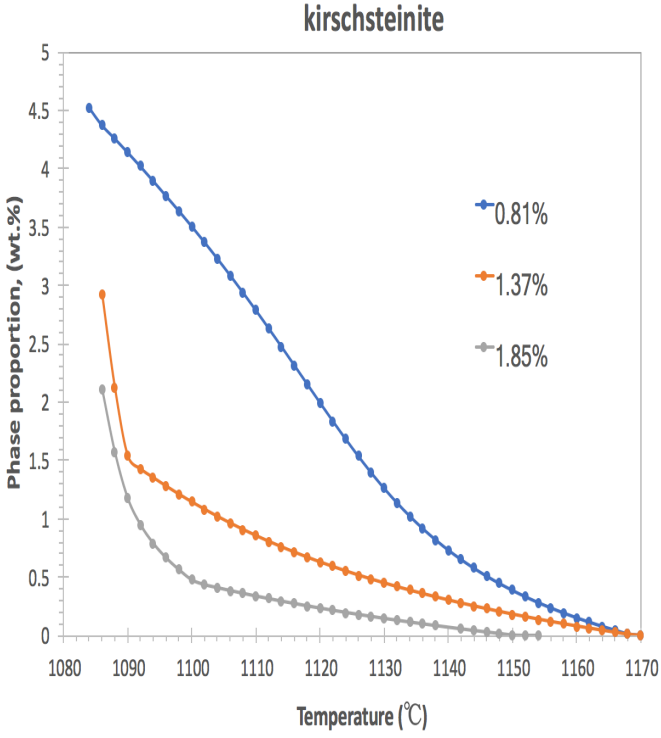
kirschsteinite
Phase proportion, (wt.%)
Temperature (℃)
0.81%
1.37%
1.85%

(d)

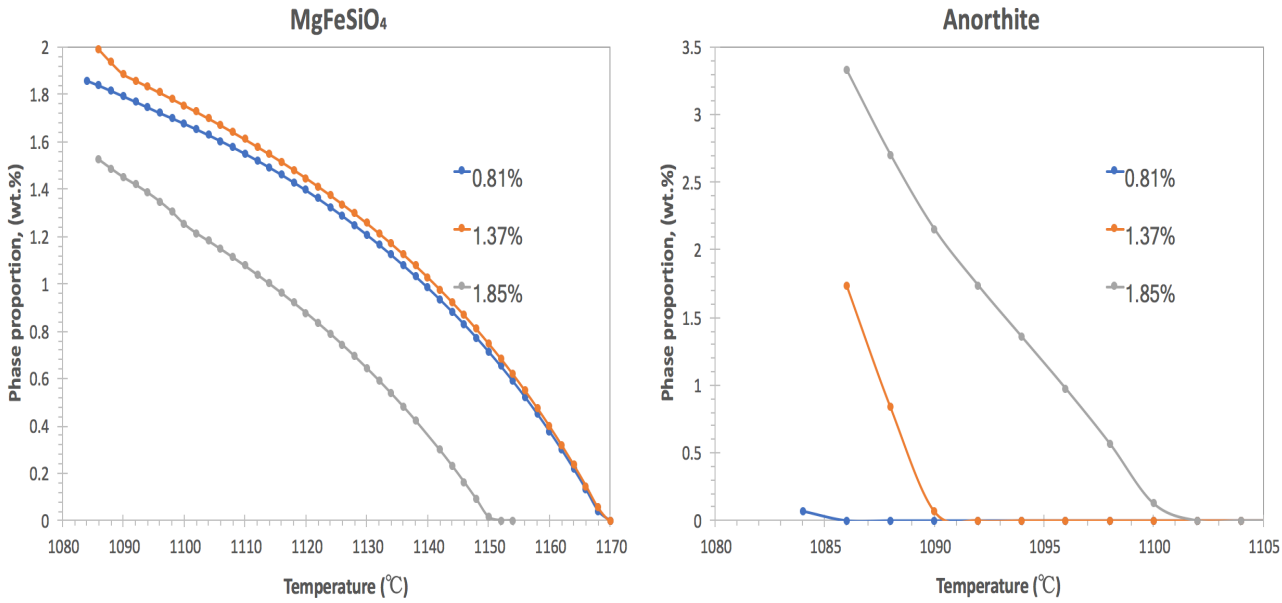

(e) **(f)**

Figure 5.14. Solid phase proportion above solidus temperature, based on FactSage calculations.

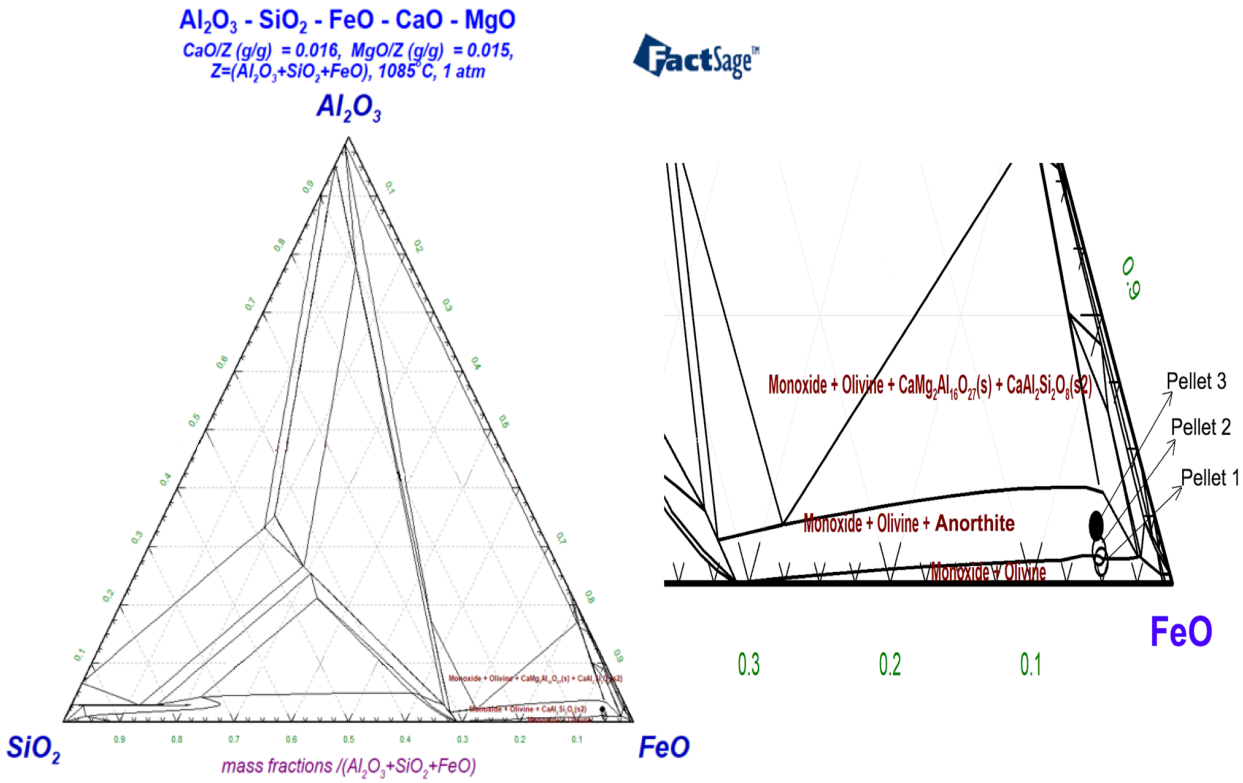

(a) (b)

Figure 5.15 Pseudo ternary phase diagram of FeO – SiO_2 – Al_2O_3 – 1.4 wt.% MgO – 1.5 wt.% CaO, obtained from FactSage (a) complete figure (b) FeO corner with three pellets chemistries.

Figure 5.15 shows the pseudo ternary diagram with constant CaO (1.5 wt.%) and MgO (1.4 wt.%) at 1085°C. Since these values are close to the amount of CaO and MgO present in for pellet 3 (Table 5.4), the chemistry for primary slag of pellet 3 is depicted in the FeO corner in the Figure 5.15 (b). For the primary slag of pellet 1 and 2, due to the difference in CaO and MgO, only an approximate chemistry can be shown in Figure 5.15 (b). The Figure depicts that with increase in alumina the tendency of formation of anorthite phase increases as the chemistry moves away from the monoxide (FeO) – olivine region and move towards the monoxide (FeO) – olivine - anorthite region.

It is important to note that the small amounts of alkalis, MnO and TiO_2 oxides are ignored in the calculation, but they can have profound effect on solidus, liquidus temperatures and the rate at which liquid phase proportion increases in the pellets. Table 3.2 shows that the MnO content increases from pellet 1 to pellet 3, whereas Pellet 3 also contains a higher content of TiO_2 (Table 3.2) and even alkali oxides as reflected from the analysis of dripped slag (Figure 4.33 (f)).

5.1.2.2. Reduction Retardation in Homogeneous state of the Ferrous Burden

Figure 5.16 shows that the reduction rate starts decreasing at around 1085°C, which is close to the solidus temperature for all three pellets (Table 5.5). Also, in section 4.3.2 it was seen that the softening for all three samples begins at around 1100°C, hence it means that the softening starts only when some reasonable amount of liquid slag has already formed in the pellet core. It can be also seen from Figure 5.13 that initially the rate at which liquid proportion increases is slow which might also explain the difference in softening start temperature and solidus temperature of the core. This indicates that the share of the liquid slag in the pellet has an important role in softening behaviour.

Coming back to the comparison of the rate of reduction, again for the most part the sample with 0.81 % alumina (pellet 1) shows a greater reduction rate than the sample with 1.85 % alumina (pellet 3). Contrary to low temperatures, here the sample with 1.37 % alumina (pellet 2) shows the maximum reduction rate. An attempt will be made in section 5.1.3 to explain this behaviour of pellets containing 1.37 % alumina.

In literature [1], authors studied the softening behaviour of acid and olivine pellets using the Advanced Reduction under Load Test, and concluded that the cause of the difference in softening behaviour is mainly due to the difference in chemistry as chemistry governs the solidus and liquidus temperature of the slag, the advent of which brings upon softening. On the grounds of this argument the softening behaviour in stage 2 for three pellets, as seen in Figure 4.23, can be explained. The rate of softening (stage 2) is greatest for pellet 3 (1.85 % Al_2O_3) followed by pellet 2 (1.37 % Al_2O_3) and the pellet 1 (0.81 % Al_2O_3) showed the least rate of softening. This can be justified by comparing the rate at which the liquid phase proportion increases with temperature. As seen in Figure 5.13, the liquid phase proportion increases with an increase in the alumina content of the pellets, hence causing an increase in the rate of softening.

According to the literature [12], the more the reduction retardation the lower is the melting temperature (Tm) of pellets. The difference in melting behaviour and correlation with the reduction degree is clear for pellet 3 and pellet 1 (Figure 4.24). Pellet 3 (1.85 % Al_2O_3) melts at lower temperature as it shows a lower reduction degree in comparison to pellet 1 (0.81 % Al_2O_3). But even though the pellet 2 (1.37 % Al_2O_3) reduces the least, it still shows the melting temperature higher than pellet 3 (1.85 % Al_2O_3). This highlights the importance of factors other than reduction degree in governing the melting and dripping behaviour of pellets.

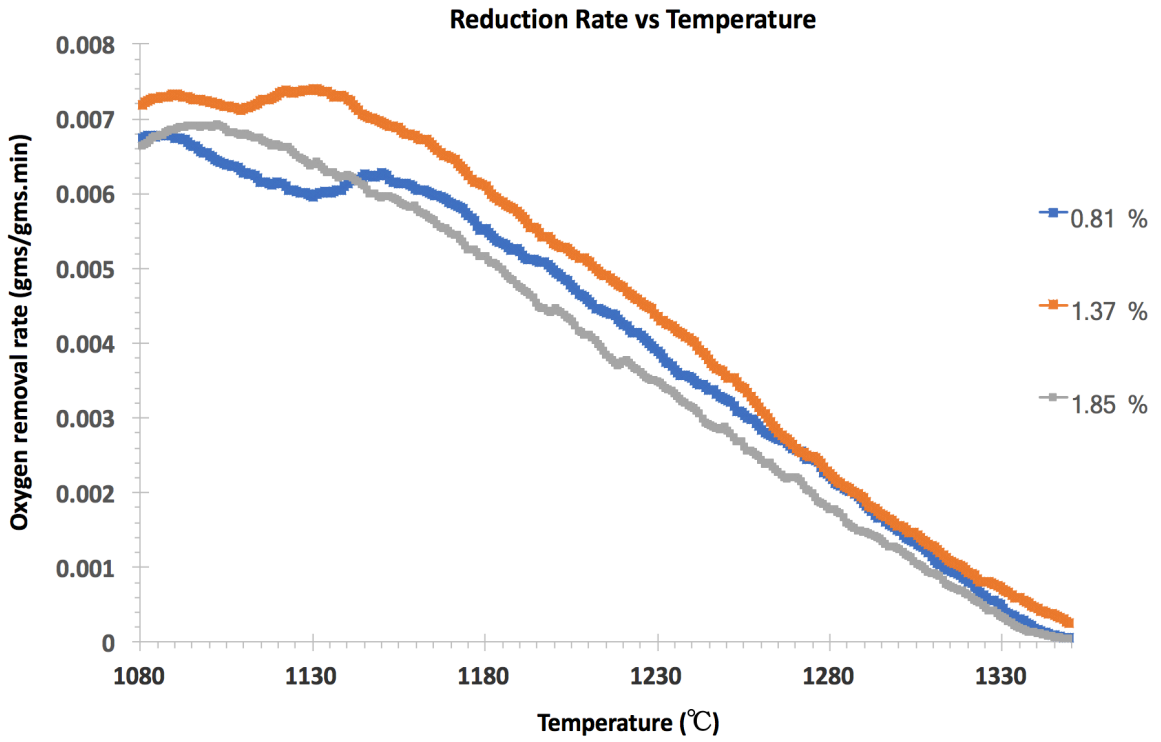

Figure 5.16. Effect of alumina on reduction retardation.

5.1.2.3. Effect of Basicity in Homogeneous state of the Ferrous Burden

In reference [6], authors observed that in basic pellets the liquid onset occurs at a temperature lower than acidic pellets, but in acidic pellets liquid fraction indicates a sharper rise in comparison to the basic pellets. Since for acidic pellets the melting and dripping occurred at lower temperatures, this implies that the rate of increase in liquid phase fraction is more important than the temperature at which the first liquid appears.

According to reference [7], the addition of fluxing agents like CaO tends to increase the reducibility of burden materials. In literature [2], the authors observed that with an increase in basicity the melting temperature increases for both sinter and pellets as it increases the temperature at which primary slag is formed. With an increase in CaO, the Ca-based olivine phases are formed which have high melting temperatures, hence increasing reducibility.

In reference [13], the authors observed that there is an optimum level of basicity in order to achieve the highest solidus temperature. Figure 5.17 depicts their result, the solidus temperature decreases on both sides of optimum basicity. More importantly according to authors of [3], for a given Al_2O_3 or MgO content, the effect of the basicity on the solidus temperature was similar to that without the presence of the respective oxides. This can also be confirmed from Figure 5.17, with the presence of MgO the solidus temperature increases but the nature of the curve still remains the same.

Similar to the observation in reference [13], authors of literature [12] also reported optimum basicity for maximum reduction degree. It was noted that the reducibility reaches a maximum at basicity of 1.3 and then decreases with increased basicity. In addition, to increase in reduction degree, they found that softening and melting range also decreases with an increase in basicity.

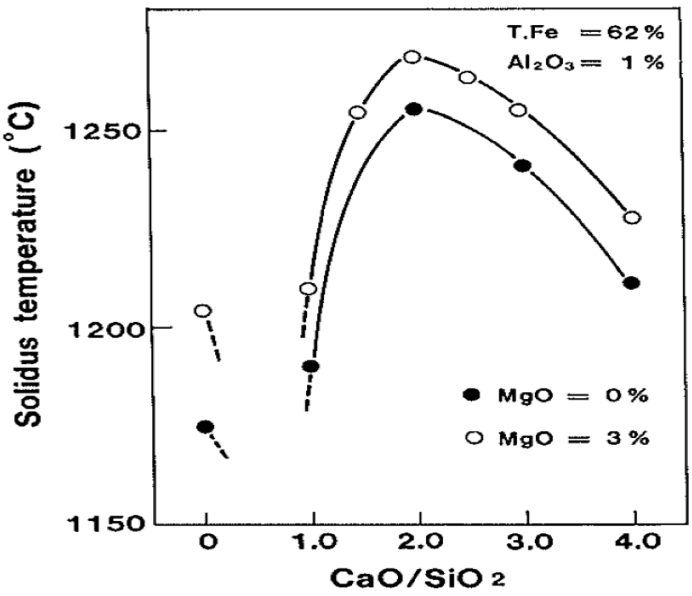

Figure 5.17. Effect of basicity and MgO on solidus temperature of specimens reduced at the wüstite stage [13].

5.1.3. Unexpected Reduction Behaviour of Pellets 2

From Figures 4.31 and 4.32, it is clearly visible that pellet 2, containing 1.37 % alumina reduces the least in low-temperature range, 700 – 1060 °C, and shows the maximum reduction rate in the higher temperature region, 1060 – 1340 °C. On the contrary it should be showing a behaviour in between the two pellets, as far as the effect of alumina is concerned. Below are the attempts to provide some explanations. Starting with low reduction at lower temperatures, the possible reasons are:

1) Pellet 2 showing a lower reduction rate at lower temperatures can be caused by higher firing temperatures, which can happen as the thermal cycle during the firing process is not consistent in industrial conditions. The higher firing temperature leads to excessive slag formation and less porous pellets [14]. These pores tend to collapse after softening [7], hence they influence only the low-temperature reduction behaviour. On the other hand, it is also important to note that pellet 2 contains a relatively higher amount of MgO (1.43%), and it is also reported that dolomite fluxed pellets exhibit higher porosity in comparison to limestone pellets as MgO increases liquidus temperature of the slag [5].

2) Authors in reference [7] observed that olivine (Mg_2SiO_4) pellets reduce less in low temperature range, specifically in the range of 800 to 1100°C. The result of their reduction experiment is shown in Figure 5.18, where the reduction degree of olivine pellet is compared with pure hematite pellet. The reason behind such behaviour is the formation of magnesium bearing ferrite, which could be formed by diffusion of MgO into FeO or Fe_3O_4. Mg bearing ferrite is known as a reduction retarding compound during the iron ore reduction process. Because of this reason, the reduction degree of pure hematite had a value higher than that of olivine based pellet. On the other hand, at higher temperatures the olivine pellets showed greater reduction because MgO increases the melting temperature of FeO, lowering the reduction retardation at higher temperatures. The MgO content of pellet 2 is only slightly

greater than that of the other two pellets, therefore, it seems unlikely that this large effect could arise from such a small difference of MgO.

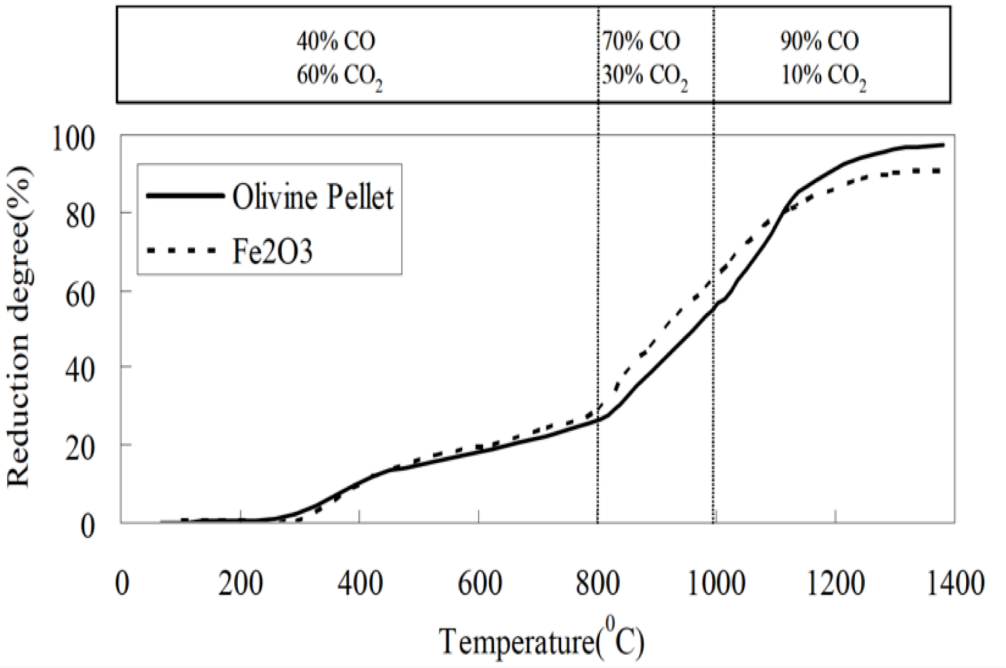

Figure 5.18. Comparison of reduction degree with temperature between pure hematite and olivine pellet [7].

Now assuming one of the above to be true, an attempt can be made on explaining the high reduction rate at higher temperature.

1) In addition to chemistry, it is the morphology of iron shell that can influence the reduction rate. One of the reasons that the pellet 2 would show a higher reduction rate at higher temperatures is that, its iron shell could be more porous when compared with those of pellets 1 and 3 at high temperatures. The reason behind this can be that pellets 1 and 3 reduce more in low temperatures, and according to reference [16], in a low-temperature region dense iron shell is formed. This is because, at low temperatures, the chemical reaction rate is slow so that the difference in iron ion concentration between the sample surface and the bulk becomes small. Therefore, the initial decomposition of the wüstite surface occurs in a planar manner leading to a dense wüstite covered with dense iron, which hinders the reduction progress at high temperatures. Additionally, according to reference [34], it is the ratio of rate of iron ion diffusion to rate of oxygen removal (dn), that governs the morphology of iron shell. At low temperatures, the rate of diffusion is lower than the rate of chemical reaction. Hence tendency for freshly nucleated iron ions to migrate to preferential sites like lattice defects is low. Therefore, a dense iron layer is formed at low temperatures.
2) Another reason could be that; due to more reduction at lower temperatures, the total iron content is greater for pellets 1 and 3. On one hand, an increase of total iron content reduces the quantity of generated melt in the wüstite stage, but on the other it promotes solid-state sintering of the metallic iron. This is because the frequency of contact of the metallic iron particles increases with an increase in reduction degree. As a result of which pore closing and hence the reduction retardation is caused at higher temperatures [13].

3) Finally, an interesting argument has been put forth by the author of reference [7]. From Figure 5.19 it seems that the reduction rate constant increases about 7 times as the FeO transforms from solid-state to liquid. So, this means that the lower the amount of indirect reduction in the solid-state, as is the case for pellet 2, the higher is the amount of liquid FeO, increasing the reduction rate at higher temperatures.

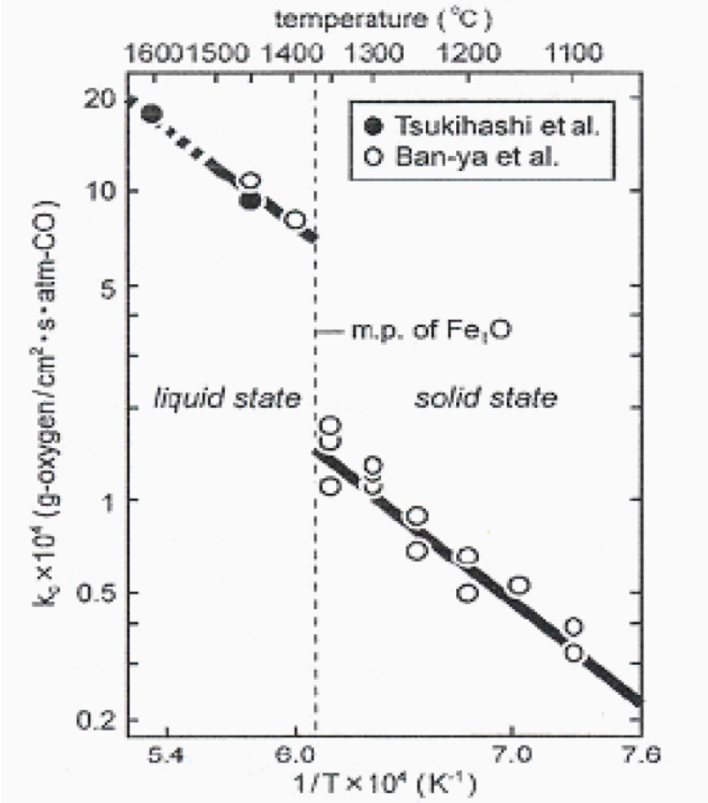

Figure 5.19. Temperature dependence of apparent rate constant of wüstite by CO gas [7].

Since the experiment on pellet 2 could not be reproduced, due to scarcity of samples, nothing can be stated with confidence. Nonetheless experiment with pellet 2 raised a very important point, that even though the pellet 2 reduced the least out of three pellets, its softening and especially melting and dripping behaviour is still better than the pellet 3. Therefore, the reduction degree is not the only parameter that governs the softening melting behaviour of the pellets and ferrous burden. To this end, in the next section the possible effect of alumina on the degree of carburization will be discussed.

5.2. Effect of Alumina on Degree of Carburization of the Iron Shell

A configuration similar to that shown in Figures 2.6 and 2.7 where slag is present in between the iron shell and coke has also been observed by the authors of reference [5], at temperatures as low as 1150°C. Large pockets of slag were observed, especially amid the metallic iron network, filling pre-existing pores, which according to authors can cause reduction retardation and also take part in carburization.

As far as the effect of FeO-rich slag on the degree of carburization is concerned, assuming the situation in Figure 2.6 to be true, where a slag layer is sandwiched between iron shell and carbonaceous material. The amount of FeO can be considered to be the single most significant factor controlling the

degree of carburization. This is because the greater the FeO content of the slag, the larger is the value of ΔC (gradient of FeO) in equation 2.8. Hence, the rate of slag flow increases with FeO, increasing the carburization degree. Also, equation 2.5 shows that with the FeO content of the slag, the rate of reduction increases. A high rate of reduction means a large number of Fe-C particles generated per unit time, therefore increasing their amount at the slag/Fe interface as well. An increase in the amount of Fe-C particle at the slag/Fe interface results in increasing the rate of diffusion of carbon in the Fe matrix (equation 2.9), hence increasing the degree of carburization again. Therefore, FeO content affects all three stages mentioned in section 2.2 and increases the degree of carburization. Anything that influences the amount of FeO rich slag and FeO content of the slag will have an effect on the degree of carburization.

According to reference [7], the carburization and melting behaviour of reduced metallic Fe in the cohesive zone can be accelerated by the formation of liquid phase rich in FeO, where authors observed that degree of carburization of metallic Fe was greater when carburization occurred via FeO rich slag as compared to carburization of solid Fe with coke. If this is assumed to be the case, then alumina can affect the degree of carburization because:

1) As discussed in the previous section, alumina can cause reduction retardation, both in the homogenous and heterogeneous states. As a result, as the Al_2O_3 content of the pellet increase, the degree of reduction decrease, and the amount of FeO rich slag increases, causing an increase in the degree of carburization.

2) Alumina is part of the gangue, as the alumina increases in the pellet, the net iron content of the pellet decreases, and so does the FeO in the slag, causing a decrease in the degree of carburization. In the present case, Table 5.4, due to small variation in alumina the variation in FeO is small among the three pellets.

On the other hand, according to the authors in literature [22], rate of carburization of iron shell directly through coke should be greater than via slag, because slag adds extra resistance, which is mass flow through the slag phase. Furthermore, since the mass transfer rate of carbon in metal is much faster than in slag, hence, the degree of carburization should decrease with an increase in slag content. In reference [2], authors observed that with an increase in gangue, hence slag, the dripping temperature increases, the reason for which is lowering of degree of carburization. The slag minimises direct contact of iron with carbonaceous material that hinders carburization. On the basis of this with an increase in alumina the degree of carburization will decrease as alumina causes reduction retardation, increasing the net amount of slag in the core of the pellets.

Yet another way alumina can affect the degree of carburization is through its effect on surface tension and wettability of slag. If it is assumed that with an increase in alumina the wettability of slag decreases, the tendency of the slag to wet the iron shell would decrease causing an increase in the degree of carburization. Section 5.4 will explore the possible effect of alumina on surface tension and wettability of slag.

Coming to the unexpected behaviour of pellet 2, it was seen that even with a lower reduction degree, 72% for pellet 2 as compared to 82 % for pellet 3, the melting temperature was still greater (1458°C) than that for pellet 3 (1446°C). This could happen due to a higher degree of carburization experienced by pellet 3, causing the melt exudation to occur at a lower temperature than that for pellet 2. An attempt can be made to explain the higher degree of reduction for pellets 3 from the above discussion:

1) A higher degree of carburization for pellet 3 can be explained by considering its higher reduction degree hence lower amount of slag present in the core as compared to pellet 2. As the slag acts as a barrier for carburization, the degree of carburization will be higher for pellet 3. But pellet 1 reduces the most (86%) and still shows the highest temperature among the three pellets for melt exudation (1491°C). This can be explained by considering the combined effect of both reduction degree and degree of carburization. For pellets 1, the greater shell thickness can compensate for a high tendency for carburization, as with an increase in shell thickness it takes more carburization to reach the same average value of carbon as in the other two pellets. This is because the carbon from the shell surface would continuously diffuse inwards. Referring to Figure 2.5, with an increase in the shell thickness, it will take more time for coke to melt the iron shell away, and since time is equivalent to temperature in the graphical expression, the melt exudation stage shifts to higher temperatures.

2) Another reason can be that; if the wettability of slag to iron shell decreases with an increase in alumina, the degree of carburization of pellet 3 would be greater than pellet 2 and pellet 1. As the tendency for the slag to form a layer between coke and the iron shell will decrease with alumina, causing an increase in the carburization rate. The effect of alumina on wettability with iron shell is discussed in section 5.4.

5.2.1. Effect of Basicity on Degree of Carburization

For the entirety of the discussion, Figure 2.9 and relevant chemical reactions from section 2.3.3.2 are repeated here.

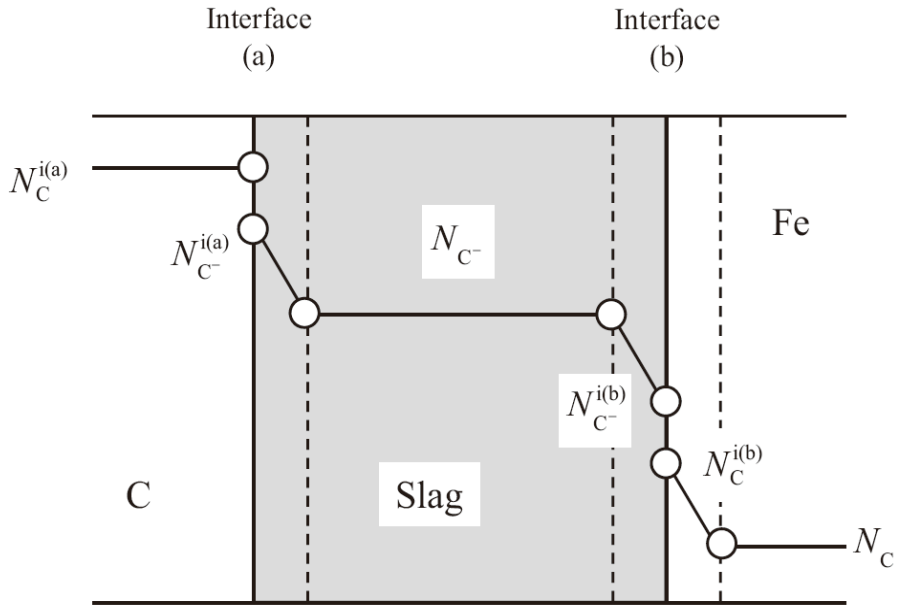

Figure 2.9. Profile of carbon contents through successive phases of carbon, slag, and iron [22].

$$C(s) + \frac{1}{2}O^{2-}(slag) \rightarrow C^{-}(\text{slag}) + \frac{1}{4}O_2(g) \quad (2.11)$$

$$CO_2 + O^{2-}(in\ slag) \rightarrow CO_3^{2-}(in\ slag) \quad (2.12)$$

The reactions above highlight the ways in which dissolution of carbon in the slag phase can take place. From equation 2.11 and 2.12 the equilibrium constants are given:

$$K_{2.11} = \frac{(a_{C^-}.(P_{O_2})^{\frac{1}{4}})}{a_C.(a_{O^{2-}})^{\frac{1}{2}}} \quad (5.1)$$

$$K_{2.12} = \frac{(a_{CO_3^{2-}})}{P_{CO_2}.(a_{O^{2-}})^{\frac{1}{2}}} \quad (5.2)$$

Where $K_{2.11}$ and $K_{2.12}$ are the equilibrium constants for reactions 2.11 and 2.12 respectively. The $P_{O_2}\ and\ P_{CO_2}$ are the partial pressures of oxygen and carbon dioxide respectively. Similarly, $a_{C^-}, a_C, a_{O^{2-}}\ and\ a_{CO_3^{2-}}$ are the activities of $C^-, C, O^{2-} and\ CO_3^{2-}$ species respectively. Thermodynamically, carbon dissolving from coke to slag at carbon slag interface becomes favourable with increase in basicity. On the other hand, carbon depositing at iron surface becomes unfavourable with increasing basicity. Therefore, in reference [22] authors took the help of kinetics and calculated the rate of overall reaction whose profile shown in Figure 2.9. It illustrates that the carburization reaction is composed of several steps which involve:

1) Reaction at carbon-slag interface, interface "a" in Figure 2.9, reaction 2.11.
2) Diffusion of carbon (C^-) to the bulk slag.
3) Liquid phase mass transfer through bulk slag.
4) Diffusion of carbon (C^-) to slag-iron interface.
5) Reaction at slag-iron interface, interface "b" in Figure 2.9, reverse reaction of 2.11.
6) Diffusion of carbon in iron.

The same steps are applicable for reaction 2.12 as well. According to reference [22] the reactions at the carbon-slag (step 1) and the slag-metal (step 5) interfaces are sufficiently fast and easily reach equilibrium. After calculating the combined mass transfer coefficient for the rest of the steps (steps 2, 3, 4, and 6), it was found that the rate constant of the carburization reaction increases with increasing basicity. The selected composition of slags used by the authors of reference [22] is shown in Table 5.6. Also, the chemistry (normalised to 100) of slag from one of the three pellets is shown for comparison.

Slag Sample	CaO (wt.%)	SiO_2 (wt.%)	Al_2O_3 (wt.%)	B2	B3	K (mol/m^2 sec)
Simulated BF slag	40	40	20	1	0.67	2.71 x 10^{-5}
High basicity slag	50	6.6	43.4	7.57	1	8.00 x 10^{-5}
Slag for Pellet 3*	19.8	53.8	26.4	0.37	0.25	-

Table 5.6. chemical composition and calculated rate constant [22]. (* Pellet 3 from the current case and not part of reference [22]).

One can see, for high basicity slag both B2 (CaO/SiO_2) and B3 ($CaO/(SiO_2 + Al_2O_3)$) basicity is greater than the simulated slag, and the calculated rate constant k, shown in Table 5.6, for high basicity slag

is higher than simulated blast furnace slag. This was confirmed from experimental results as shown in Figure 5.20. Therefore, with an increase in basicity the degree of carburisation via slag increases. Another interesting point raised in reference [22] is that the rate of carburization through FeO-rich slag is much faster than in FeO-lean slag.

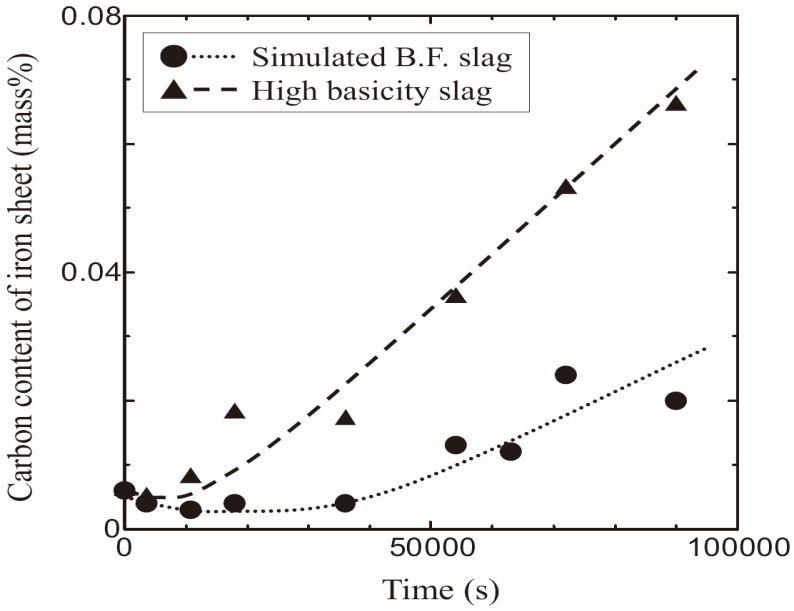

Figure 5.20. Variation of carbon content in iron with time at 1723 K [22].

5.3. Effect of Alumina on Viscosity of slag

The fundamentals of viscosity were briefly discussed in section 2.3 which lays the basis for discussion in this section. It is easy to understand the significance of viscosity for melting dripping behaviour, as the resistance to gas flow increase with an increase in viscosity which is then reflected in the area under the pressure drop curve. According to reference [6], viscosity also plays a role in melt exudation, where the slag with higher viscosity exudes out with difficulty. This can also influence the degree of carburization as was seen in the previous section that the slag exudes out and form a layer between iron shell and coke. Hence viscosity is one of the important properties influencing the melting dripping behaviour of pellets.

Alumina is an amphoteric oxide, meaning it can behave as either network former or a network modifier depending on the overall composition of the slag. The Z/r^2 ratio (ionization potential) of Al^{3+} ion is 1068 nm^{-2}, which is neither too small or too large, to put things in perspective, the ionization potential of Ca^{2+} is 200 nm^{-2} whereas that of Si^{4+} is 2500 nm^{-2} [17]. Also, the radius of Al^{3+} is 0.47 Å which is close to radius of Si^{4+} (0.34 Å), hence Al^{3+} can substitute Si^{4+} in the tetrahedral lattice. According to the literature [18], the nature of alumina depends on the ratio, Al_2O_3/MO (MO is basic oxide). When the ratio is less than 1, the Al_2O_3 behaves as an acidic oxide where the Al – O coordination would be tetrahedral just like Silica. On the other hand, when the ratio exceeds 1, the Al^{3+} ion will have an octahedral coordination like Ca^{2+} and will behave as a network modifier.

In order to understand the above, it is first necessary to note that silica and alumina are not similar on the molar basis. The basic building block of silica in the tetrahedral lattice is $[SiO_4]^{4-}$ and alumina can only fit as $[AlO_4]^{5-}$ due to its valance of 3. Therefore, due to charge neutrality alumina has to be accompanied by the cation. In the case of calcium, two alumina units would be accompanied by one

Ca^{2+}, $[AlO_4]$ Ca $[AlO_4]$, and with an alkali cation the configuration would be $[Na(AlO_4)]^{4-}$, both of which are schematically shown in Figure 5.21.

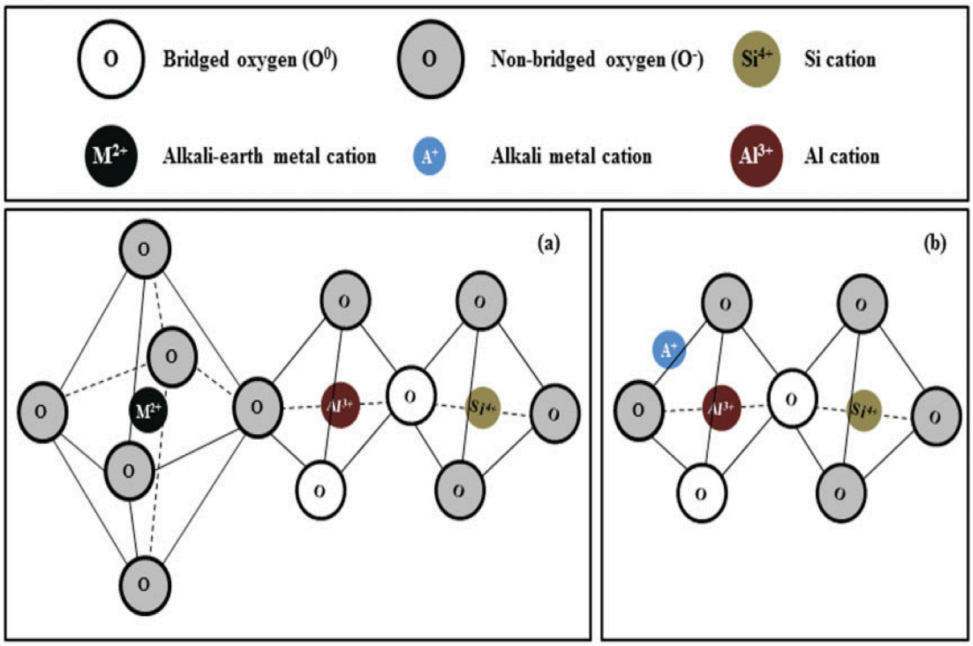

Figure 5.21. Schematic illustration of the position of Al^{3+} within the silicate structure of the (a) CaO-SiO_2-Al_2O_3 and (b) A_2O-SiO_2-Al_2O_3 (A: alkali metal) ternary slag systems. The formation of Al-O-Si bonds is more likely than the formation of Al-O-Al bonds [17].

Another interesting feature is that the oxygen in an alumina - silicate melt cannot be shared by two consecutive AlO_4^{5-} tetrahedra units. This would lead to a decrease in entropy, hence causing the free energy of the system to increase. Thus, energetically, the formation of alumina - silicate structures is preferred over highly ordered aluminate clusters.

Due to the two restrictions, namely;

1) Cation accompanying Al^{3+} for charge neutrality,

2) Al^{3+} always occupying an alternate position in silicate melt for minimisation of energy,

After a certain limit of addition, Al^{3+} would no longer sit in the tetrahedral site substituting for Si^{4+} but rather behave as a network modifier and exist in the octahedral configuration similar to that of Ca^{2+}, where the polyanionic structure would be a $[AlO_6]^{9-}$ octahedral configuration. As expected, the addition of network modifying Al_2O_3 would decrease the melt viscosity.

In literature [19], authors measured the viscosity of 5% TiO_2 bearing primary blast furnace slags using rotating cylinder method and confirmed the amphoteric behaviour of Al_2O_3, where the slag viscosity first increased with increasing Al_2O_3 content from 10 to 15 mass% and then decreased with the further increase of Al_2O_3 to 18 mass%. The highest Critical Temperature (CT) was also observed for 15% Al_2O_3, having lower values on both extremes. Interestingly from Raman Spectroscopy authors found that the reason for such behaviour is not that Al_2O_3 starts behaving as network modifier above 15%. It still behaves as an acidic oxide. The reason for the decrease in viscosity is that with an increase in Al_2O_3

the number of Al-O-Si bonds increases which are much weaker than Si-O-Si bonds. This means that the migration of structural units becomes easy as Al_2O_3 is added, hence causing viscosity to decrease.

In reference [20], using the rotating cylinder method it was observed that at fixed basicity (CaO/SiO_2) of 1.17 and 8 wt % MgO, the viscosity of the slag increases with increasing Al_2O_3 content from 12 to 18%. In reference [17], in addition to conducting their experiments, authors also reviewed the results of numerous other researchers and found that Al_2O_3 behaves as an amphoteric oxide at fixed basicity. Authors in reference [18] also studied the effect of varying Al_2O_3 on the viscosity of $CaO\text{-}Al_2O_3\text{-}SiO_2$ slags using the rotating cylinder method, at fixed basicity (CaO/SiO_2), then repeating the same for different basicities in the range 1 – 1.3. They found that with alumina varying from 0-20 mass percent, the maximum viscosity is observed at 10 wt.%, confirming the amphoteric behaviour. The effect of Al_2O_3 became more significant with an increase in basicity (B2), however, the net viscosity decreased with basicity. For CaO-10% $MgO\text{-}Al_2O_3\text{-}SiO_2$ slags it was observed that Al_2O_3 shows a similar behaviour, where viscosity increases with Al_2O_3 until 10% and then decreases. The effect of alumina became less significant due to the presence of MgO. This is because the relative fraction of the polymerized units, which are able to accommodate the $[AlO_4]$-tetrahedra, in the slags containing MgO would be less than that in the slags without MgO.

Another way of understanding the effect of Al_2O_3 is by looking into the change in the thermodynamic stability of other components due to the addition of Al_2O_3. In reference [18], it is reported that the activity coefficient of SiO_2 in the $CaO\text{-}SiO_2\text{-}Al_2O_3$ slags decreases significantly with increasing Al_2O_3 content up to 10 mass percent, and then decreases only slightly after that. While the activity coefficient of Al_2O_3 exhibits a minimum value at 10 mass percent Al_2O_3, as it increases after that. Therefore, it is suggested that the incorporation of the $[AlO_4]$-tetrahedra into the $[SiO_4]$- tetrahedral units increase the stability of the silicate poly-anions until 10 mass percent alumina. After 10 mass percent, further addition of alumina increases the fraction of $[AlO_6]$-octahedra, which is not incorporated into the silicate network, hence increasing the activity coefficient of alumina.

5.3.1. Estimation of Viscosity with Thermodynamics

Coming to the case in hand, an important feature of the primary slag is that after exudation, its FeO content decreases continuously due to direct and indirect reduction. Therefore, in order to bring the dynamic behaviour of slags into consideration, Figure 5.22 is shown. The figure has been obtained from FactSage and it shows the effect of alumina on viscosity for different FeO content. The assumption here is that only FeO reduces, which is not true as some amount SiO_2 also reduce.

Though in Figure 5.22 (a), the quantity of FeO is shown 90%, it is slightly greater and also slightly different for three pellets, the exact composition can be found in Table 5.4. From Figure 5.22, it is easy to see that the effect of alumina on viscosity becomes significant only when the FeO content of slag reduces to low values. Figure 5.22 (d) shows clearly that with an increase in alumina the Critical Temperature (CT) of the slag increases. A low critical temperature represents a wide thermostable operation region. Therefore, an increase in alumina is deleterious for blast furnace operation as it poses the danger of a sudden increase in slag viscosity causing problems like hanging and flooding. This behaviour is interesting because as mentioned in section 2.3 a high critical temperature means a high crystallization capacity of slags which occurs due to the presence of high melting point phases. Figure 5.23 confirms that with an increase in alumina in pellets the liquidus temperature of the slag increases. Additionally, the solidus temperatures of the slag can also be found in Table 5.7. The solidus temperature increases from pellets 1 to 2 and stays the same for pellets 2 and 3. As far as the critical temperature is concerned, the liquidus temperature is of interest, as the steep rise in viscosity is caused by solids precipitating out of liquid slag, which occurs below liquidus temperature.

The increase in liquidus temperature from pellet 1 to 3, can be explained by looking into the variation of phases in slag. Figure 5.24 (a) shows that with an increase in alumina the proportion of anorthite ($CaAl_2Si_2O_8$) increases while the proportion of diopside ($CaMgSi_2O_6$) decreases in the slag at solidus temperature. Anorthite (1553°C) [28] is a higher melting phase in comparison to diopside (1391°C) [29] as can be seen from anorthite-diopside binary phase diagram (Figure 5.25).

Sample	Al_2O_3, % (Pellet)	SiO_2, % (Slag)	CaO, % (Slag)	MgO, % (Slag)	Al_2O_3, % (Slag)	Solidus (°C)	Liquidus (°C)
Pellet 1	0.81	52.7	20.4	16.3	10.5	1192	1303
Pellet 2	1.37	48.8	17	17.5	16.7	1209	1322
Pellet 3	1.85	45.5	16.8	15.4	22.3	1209	1346

Table 5.7. Chemical composition of slag (FeO = 0%) and solidus and liquidus temperatures as obtained from the FactSage.

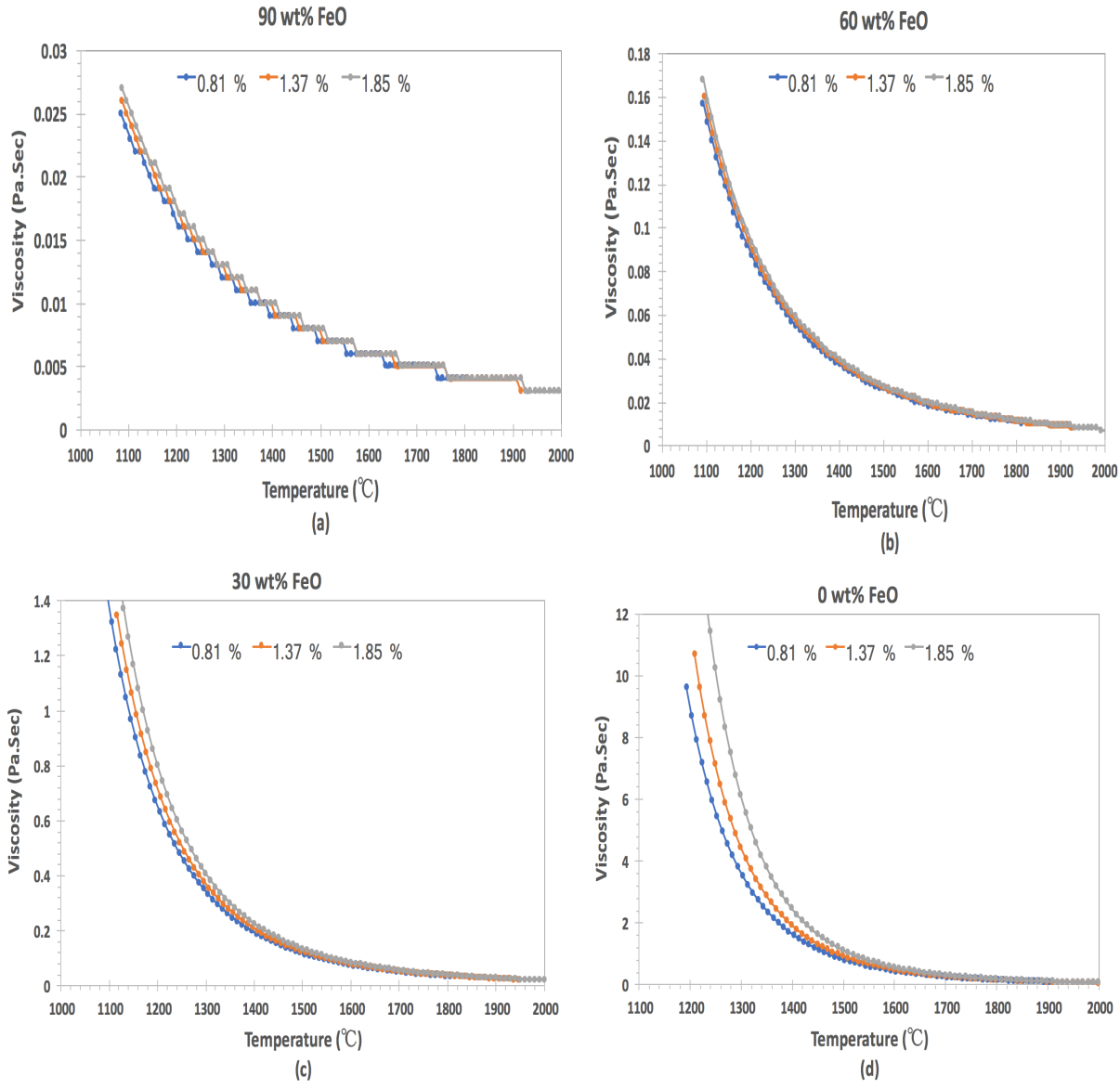

Figure 5.22. Effect of alumina on viscosity of slags, obtained from FactSage.

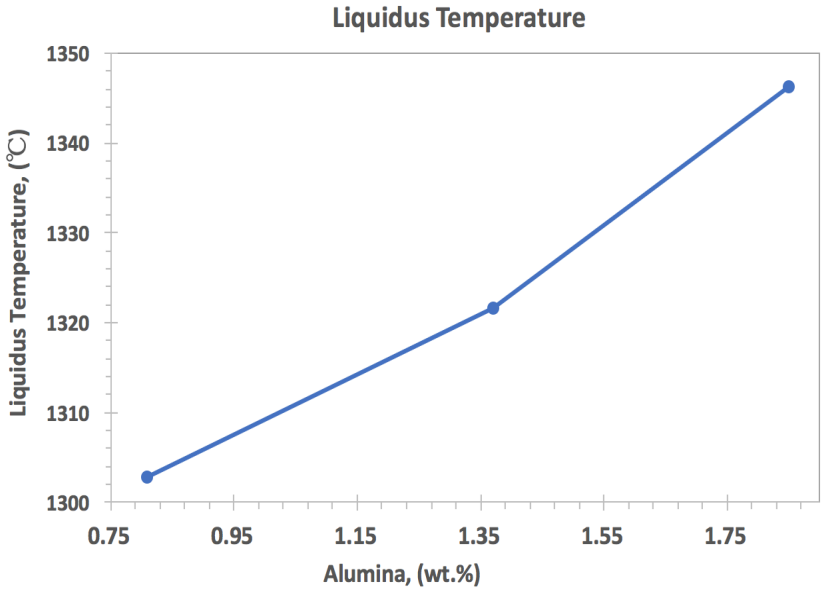

Figure 5.23. Effect of alumina on liquidus temperature of slag with 0 wt.% FeO, obtained from FactSage.

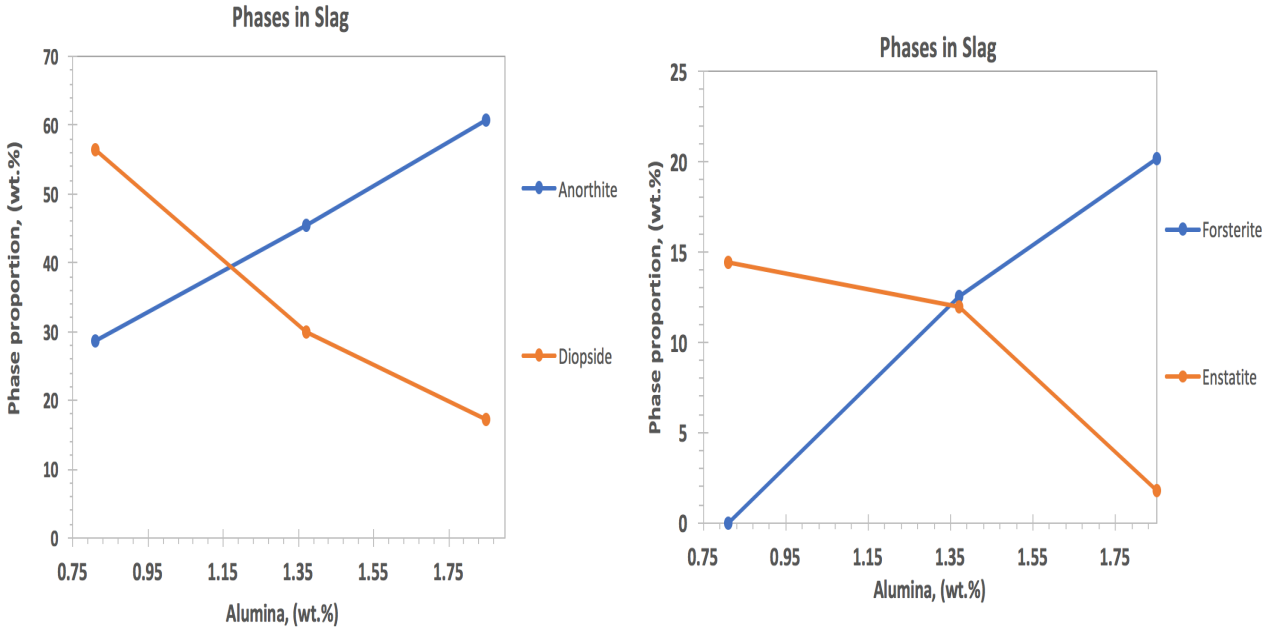

(a) (b)

Figure 5.24. Effect of alumina on phases present in slag at solidus temperatures, as obtained from FactSage.

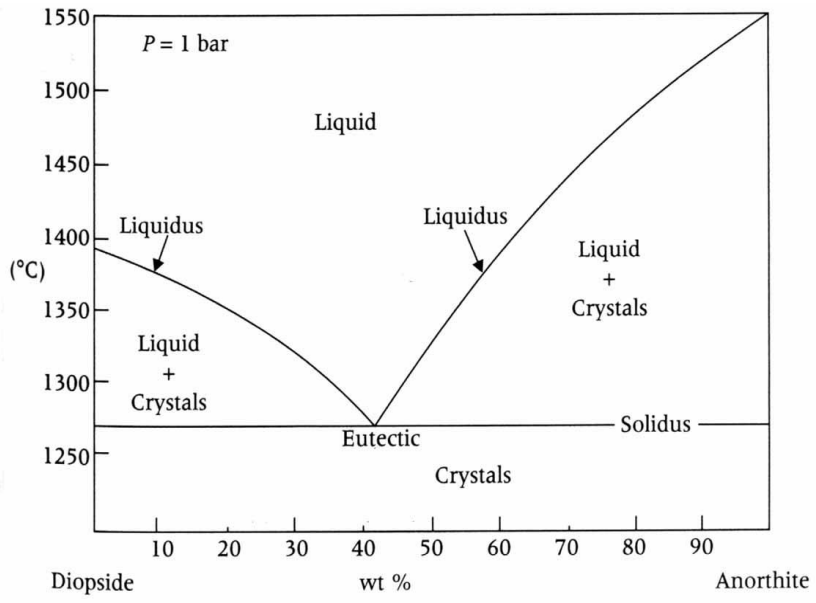

Figure 5.25. Diopside – Anorthite binary phase diagram [32].

Similarly, from Figure 5.24 (b), it can be seen that with an increase in alumina the proportion of forsterite (Mg_2SiO_4) increases and the proportion of enstatite ($MgSiO_3$) decreases. The forsterite is a very high melting phase (1890°C)[30] whereas enstatite melts at 1557°C [31]. This can be also seen from the forsterite – silica binary phase diagram (Figure 5.26), where enstatite proportion increases with an increase in silica content. This highlights an indirect effect of alumina, as it can be seen from Table 5.7, that with the decrease in alumina content from pellet 3 to pellet 1, the silica content of the slag gradually increases. This increases the proportion of enstatite and decreases forsterite.

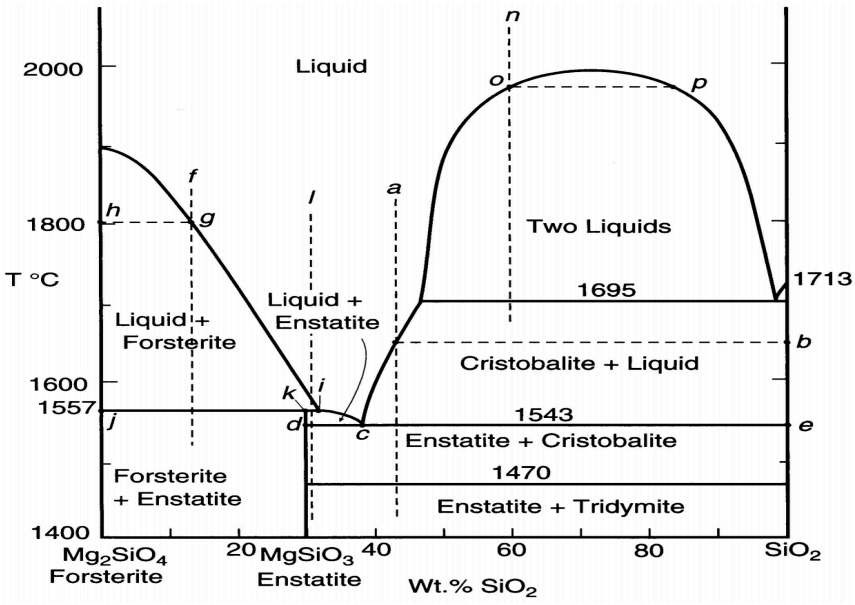

Figure 5.26. Forsterite – Silica binary phase diagram [32].

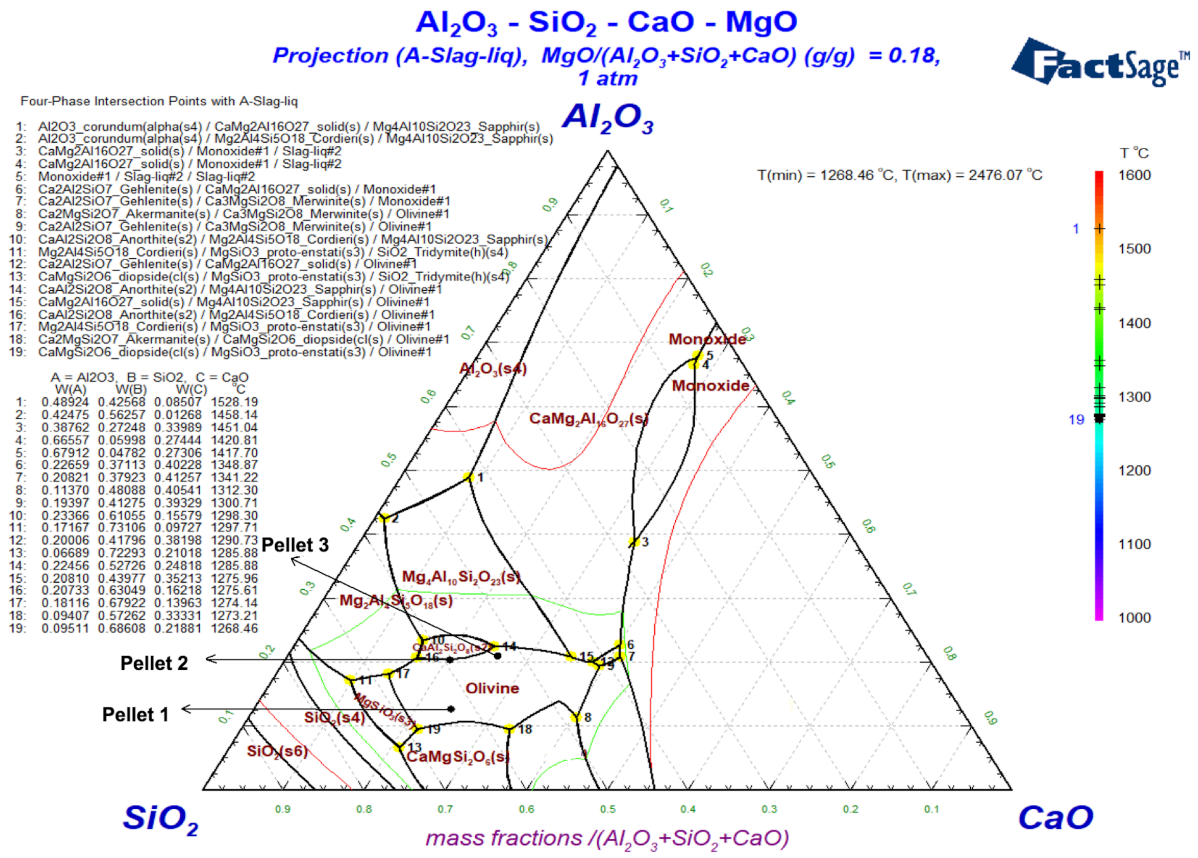

Figure 5.27. Pseudo ternary phase diagram of CaO – SiO_2 – Al_2O_3 – 15.4% MgO, obtained from FactSage.

Figure 5.27 shows the pseudo ternary phase diagram, CaO-SiO_2-Al_2O_3 with a constant MgO content of 15.4 %. The compositions of the slag of three pellets are also shown in the figure. From Table 5.7 it can be seen that the MgO content of 15.4 % represents the slag for the pellet 3, therefore points marked for pellet 1 and pellet 2 are only approximate, as their MgO content is slightly different from that of the pellet 1. Figure 5.27 shows that, with an increase in alumina and decrease in silica, the slag composition moves away from diopside and enstatite and moves towards anorthite and forsterite regions increasing their proportions. This behaviour can be summed up by the typical transformation that is generally observed in magma due to the variation of alumina [27]:

$$CaMgSi_2O_6\ (diopside) + MgSiO_3(enstatite) + Al_2O_3 = CaAl_2SiO_8(anorthite) + Mg_2SiO_4(forsterite) \quad (5.3)$$

The alumina reacts with diopside and enstatite and produces anorthite and forsterite, increasing the liquidus temperature of the slag. This is very interesting because in section 5.1.2.1 it was noted that for FeO rich primary slag with an increase in alumina the proportion of liquid phase increases. Therefore, for primary slag alumina increases the tendency for the formation of liquid, but as the FeO content of the slag decreases, alumina makes the slag more refractory by increasing its liquidus temperature.

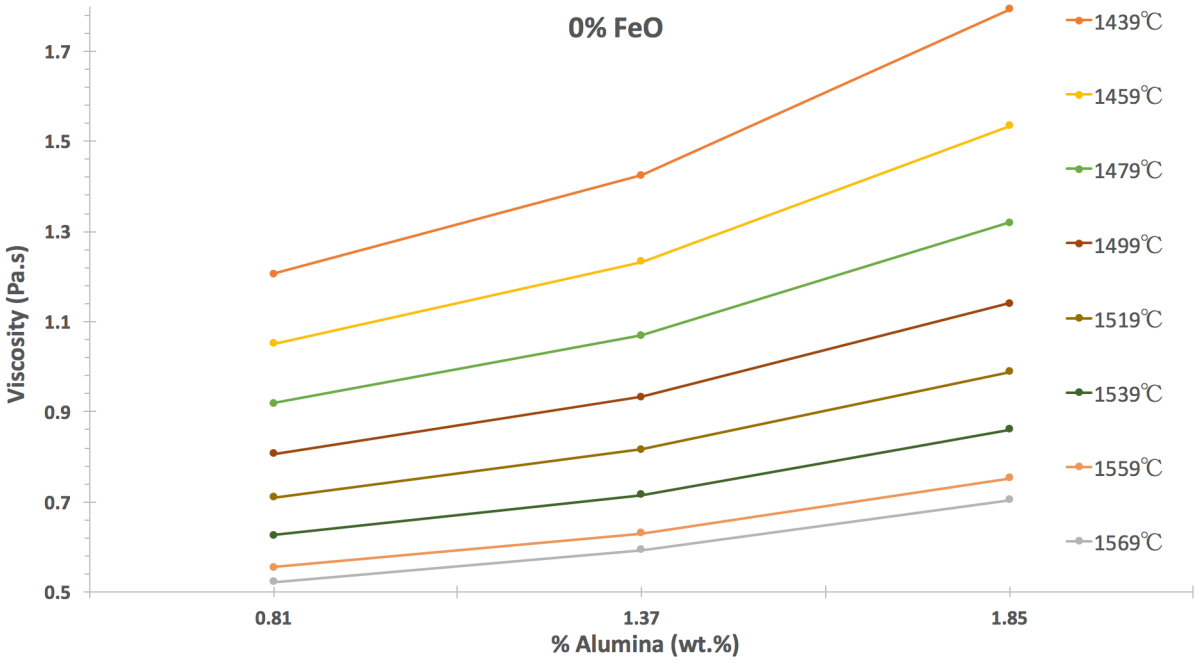

Figure 5.28. Effect of alumina on viscosity of slags.

Just like FeO, another important dynamic parameter is temperature. As the exuded slag drips, it experiences higher temperatures. Figure 5.28 shows the effect of alumina on viscosity at different temperatures. It can be seen that the effect of alumina is significant at lower temperatures. With the increase of temperature, the viscosity decreases to low values irrespective of its alumina content. Therefore, as the slag drips, on one hand due to a decrease in FeO content, the viscosity of primary slag increases, on the other hand due to an increase in temperature the viscosity of primary slag decreases. The temperature range selected for Figure 5.28 is the range in which the melting and dripping for all three pellets were observed (Figure 4.28).

As mentioned in section 2.3, the viscous flow is an activated process, hence equation 2.15 can be used to calculate the apparent activation energy of the slags. This is proportional to the slope of the plot between the natural logarithm of viscosity and reciprocal of the temperature. The plot is shown in Figure 5.29. The apparent activation energy represents the energy barrier for viscous flow, and change in activation energy indirectly suggests a change in the structure of the slag [19]. It also represents the sensitivity of viscosity to temperature [20].

The calculated values of activation energy using Figure 5.29 are shown in Table 5.8. There is a clear effect of alumina on activation energy, hence the flow of the slag becomes more viscous with an increase in alumina. From Figures 5.22, 5.28 and 5.29 it can be concluded that for the current case, the alumina behaves as a network former, an acidic oxide, as no amphoteric behaviour is seen. This is in line with the thumb rule proposed in reference [18], which is for all three samples the ratio (Al_2O_3/(CaO+MgO)) is less than 1 therefore Al_2O_3 behaves as an acidic oxide in all three systems.

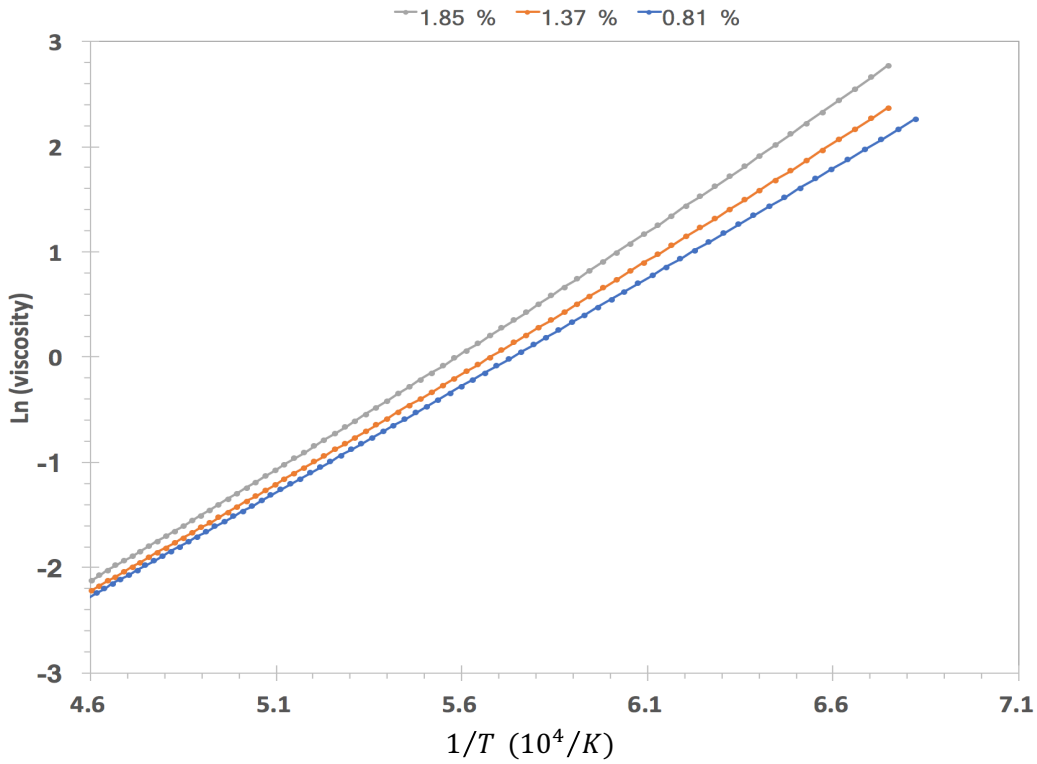

Figure 5.29. Natural logarithm of viscosity against reciprocal of temperature.

Sample	Al_2O_3 (wt% CMAS)	Activation Energy (kJ/mol)
Pellet 1	10.5	169.4
Pellet 2	16.7	175.4
Pellet 3	22.3	184.4

Table 5.8. Viscosity activation energy of slags.

In addition to Newtonian behaviour, slags can also show non-Newtonian behaviour if they drip in a semi-solid state, as has been noticed in reference [21]. For the present case, the temperatures at which the melt exudation (Tm) is observed is above the liquidus temperature of the homogenous slag for all three pellets, even when different levels of FeO is considered. But slag can still become non - Newtonian due to entrainment of dust particles externally from coke and graphite crucible. It is difficult to take into account the effect of such entrainment, hence not considered in the current case.

As visible from Figure 4.29, the resistance to gas flow (the S-value), increases with an increase in alumina content. One contributing factor to this is the increase in the viscosity of the slag with increasing alumina content of the slag. According to the reference [2], the temperature at which the dripping occurs is governed by the combined effect of liquidus temperature and viscosity. Since, alumina increases both, the dripping becomes more difficult with its increase, resulting in a higher area under the pressure drop curve.

Another point that is important to note here is that for pellet 3 melt exudations occurs at low temperature. Since viscosity is very sensitive to temperature, Figure 5.28, the dripping slag is much more viscous in the case of pellet 3 as compared to the slag of pellet 1 and pellet 2, where slag drips at higher temperatures.

The difference in viscosity can also be used to justify the unexpected behaviour for pellet 2. As with an increase in viscosity the melt exudation of the slag becomes difficult [6], hence a lower amount of slag would be present in between the iron shell and coke in the case of pellet 3. Resulting in the early melting of pellet 3 as compared to the pellet 2.

5.3.2. Effect of Basicity on Viscosity of Slag

It was discussed in section 2.3 that the CaO is a network modifier. Naturally, it should cause the viscosity of the slag to decrease. Authors in reference [19] reported that the viscosity of slags decreases with an increase in basicity. In reference [20], at 8 wt.% MgO and 12 wt.% Al_2O_3, increasing the CaO/SiO_2 ratio from 1.07 to 1.50 resulted in lower slag viscosity. Interestingly viscosity decreased quite steeply until the basicity of 1.35, after which the decrease was not at the same rate, this is because the addition of CaO does not exert the same effect when de-polymerization of the slag network structures has already occurred.

In reference [18] again the authors concluded that with an increase in basicity (CaO/SiO_2), the viscosity of slags decreases. The impact of basicity in decreasing viscosity is greater in slags with no MgO than that of slags containing MgO. This means that the modification reaction in silicate melts with a high Degree of Polymerization (DOP) is more effective than that of the systems with low DOP due to the contribution of Mg^{2+}.

5.4. Effect of Alumina on Surface Tension and Wettability of Slag

The section is divided into two parts, where section 5.4.1 explores the effect of alumina on the surface tension of slags. Section 5.4.2 carries the discussion forward by looking into the effect of alumina on the wettability of slags. Section 5.4.3 briefly discusses the effect of CaO on surface tension and wettability of slags.

5.4.1. Effect of Alumina on Surface Tension

Liu et al [23] found that, with an increase in the Al_2O_3 content of slag, keeping the basicity constant, the surface tension of the slag increases slightly as shown in Figure 5.30. In section 2.4 (equation 2.25) it was seen that the surface tension of the slag is dependent on both the composition and ionic structure. Equation 2.25 is repeated here for the ease of discussion.

$$\sigma_{net} = \sigma_i^{pure} + \frac{RT}{A_i} ln^{M_i^{Surf}}/M_i^{Bulk} \quad (2.25)$$

Where, A_i is the molar surface area of the species *i*, and σ_i^{pure} is the surface tension of the pure species *i* and M_i^p is depicted in equation 2.26.

$$M_i^p = \frac{\left(\frac{Rc_i}{Ra_i}\right).N_i^p}{\sum_i\left(\frac{Rc_i}{Ra_i}\right).N_i^p} \quad (2.26)$$

Superscripts "*Bulk*" and "*Surf*" refer to the bulk and surface respectively (p = Bulk or surface). Rc_i and Ra_i are the radius of cation and anion of a given species respectively. N_i^p is the mole fraction of given species on bulk/surface.

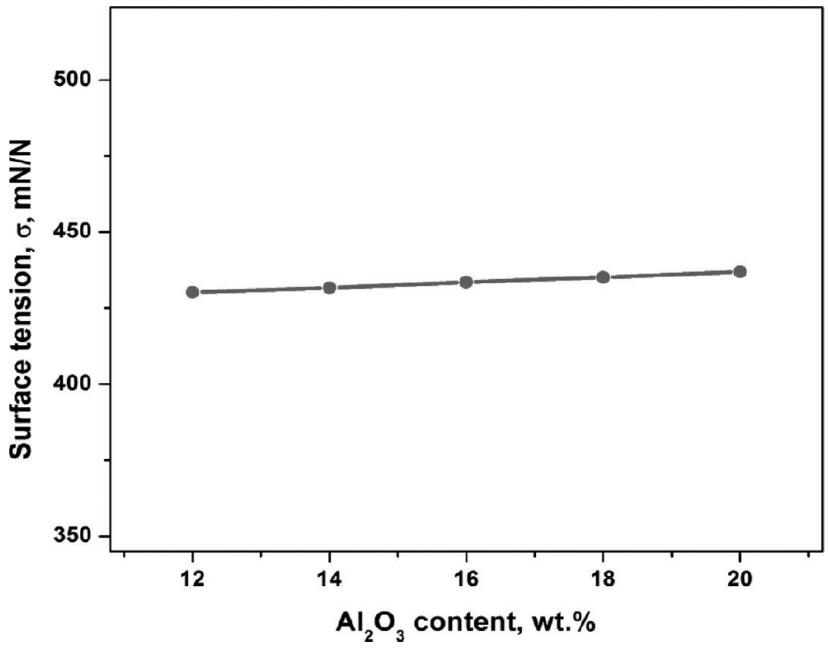

Figure 5.30. Influence of Al_2O_3 content on the surface tension of the 5-component slag (SiO_2, CaO, Al_2O_3, MgO, TiO_2) [23].

The effect of alumina on the chemical composition of the surface is discussed in section 5.4.1.1 and the effect on the ionic structure of the surface is discussed in section 5.4.1.2.

5.4.1.1. Effect of Al_2O_3 on the Chemical Composition of the Slag Surface

Liu et al [23] found that, with an increase in the Al_2O_3 content of the bulk, the moles of Al_2O_3 on the surface do not increase proportionally, as can be seen from Figure 5.31 (a) and (b). The proportion on the surface is obtained using equations 2.25 and 2.26.

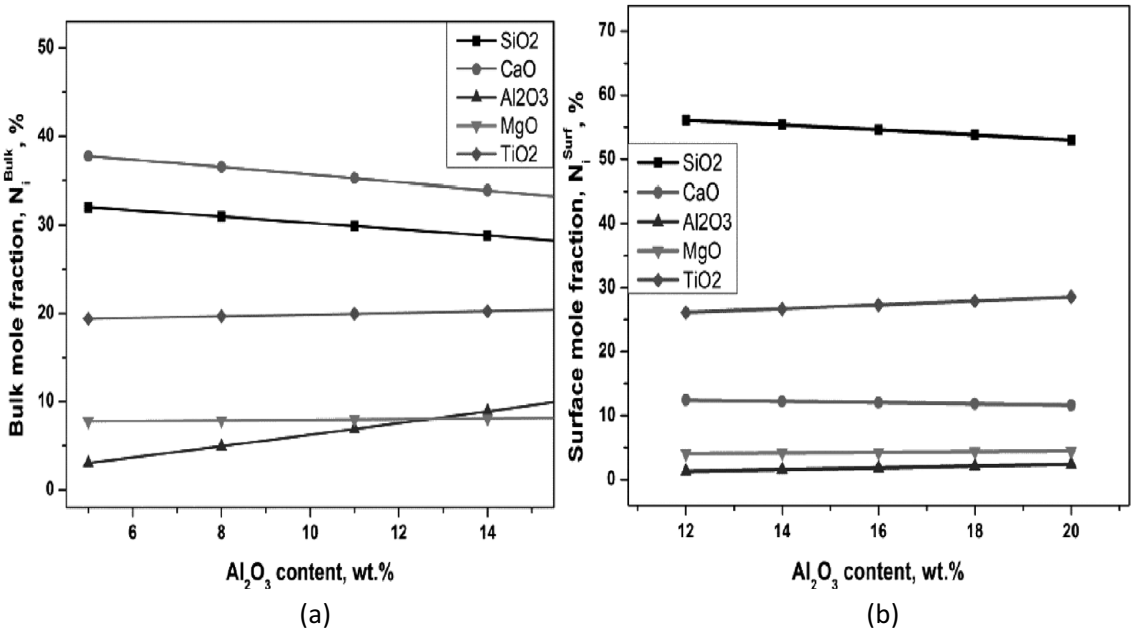

Figure 5.31. Variation of mole fractions of oxides in (a) bulk and (b) surface with the Al_2O_3 content [23]

Another important thing to note is that the content of SiO_2 is lower than the CaO in the bulk, but still SiO_2 has a higher proportion on the surface. One can understand this behaviour by comparing the surface tension of pure phases from Table 5.9. Clearly, SiO_2 has the lowest surface tension out of all the components, which explains its larger share present at the surface for minimizing the net free energy.

Coming back to Al_2O_3, the addition of Al_2O_3 in bulk, does not increase its proportion at the same level on the surface. This means SiO_2 proportion of the surface is not affected greatly by the addition of alumina in bulk hence the surface tension should not be affected substantially due to an increase in alumina.

Oxide	Temperature (K) dependence of surface tension (mN/m)
SiO_2	243.2 + 0.031T
CaO	791 – 0.0935T
Al_2O_3	1024 – 0.177T
MgO	1770 – 0.636T
TiO_2	1384.3 – 0.6254T

Table 5.9. Temperature dependence of the surface tension of pure Components [24].

5.4.1.2. Effect of Al_2O_3 on ionic structure of the Slag Surface

It is well known that Al_2O_3 acts as a network former when the ratio of alumina to basic oxide (Al_2O_3/MO) is less than 1 in the slag [18]. As seen in the previous section, the alumina content of the surface remains low, therefore alumina will act as a network former on the surface. With a slight increase in Al_2O_3 on the surface, due to an increase in Al_2O_3 of the bulk, the ratio NBO/T decreases. Where, NBO/T is the ratio of number of non-bridging oxygen per tetragonally-bonded cation. This means that more numerous and slightly less complicated units (Q^n (Si) and Q^n (Al)), with n=1, 2, will turn into large, less numerous, and more complicated units (n=3, n=4). Therefore, the total number of complicated units at the surface will reduce, and the number of free oxygen ions will increase. The O^{2-} ion has a larger dipole moment than the complicated units, therefore as their proportion increases on the surface, the surface tension increases as well. According to reference [23] this is the reason why with slight increase in the Al_2O_3, the surface tension still increases, even though the proportion of SiO_2 is not affected greatly.

According to the authors of reference [23], the reason for the relatively low effect of Al_2O_3 on surface tension (Figure 5.30) is the presence of TiO_2 in the slag. TiO_2 diminishes the impact of alumina on surface tension. It was observed that with an increase of TiO_2 in the bulk concentration, it also increases on the surface proportionally. Hence, TiO_2 addition causes a reduction in the quantity of SiO_2 on the surface. From Table 5.9 it can be seen that the coefficient of temperature is large for TiO_2. Hence at high temperatures like 1673 K, the surface tension of pure TiO_2 is only second lowest, as shown in Table 5.10. Therefore, with an increase in bulk, TiO_2 concentration on the surface increases, causing a reduction in SiO_2 on the surface, increasing the surface tension. But on the other hand, TiO_2 is also a network modifier, hence it promotes the de-polymerization of the melt on the surface. This causes more complicated units (Q^n (Si) and Q^n (Al)) (Here n=3, 4) to turn into less complicated units (here n=1, 2). Resulting in a reduction of O^{2-} ion concentration, which has a high moment, and increasing the content of less complicated units (n=1, n=2), which have a lower moment. Therefore,

TiO_2 causes a reduction in surface tension. The effect of TiO_2 on surface tension is quite substantial, which might explain the lower impact of alumina on the surface tension in slags for the case considered in reference [23].

Oxide	Temperature (K) dependence of surface tension (mN/m)
SiO2	295.06
CaO	634.57
Al_2O_3	727.88
MgO	705.97
TiO_2	338.00

Table 5.10. Surface tension of each oxide ta 1673 K [24].

The effect of alumina on the surface tension of blast furnace slags is further confirmed by the authors of reference [33]. In addition to conducting experiments, they have also analyzed the data on surface tension for blast furnace slags reported by various other authors. The effect of alumina on surface tension can be seen in Figure 5.32. An increase in surface tension with alumina for slags with different basicities and at different temperatures can be seen.

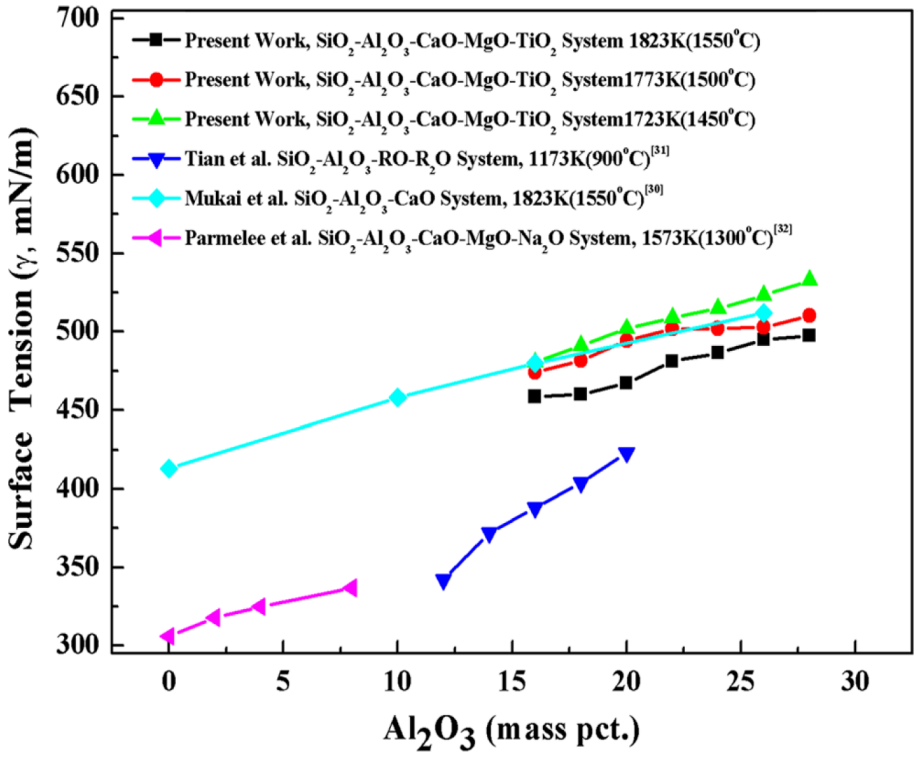

Figure 5.32. Effect of alumina on surface tension of aluminosilicate melts [33].

5.4.2. Effect of Alumina on wettability of Slag

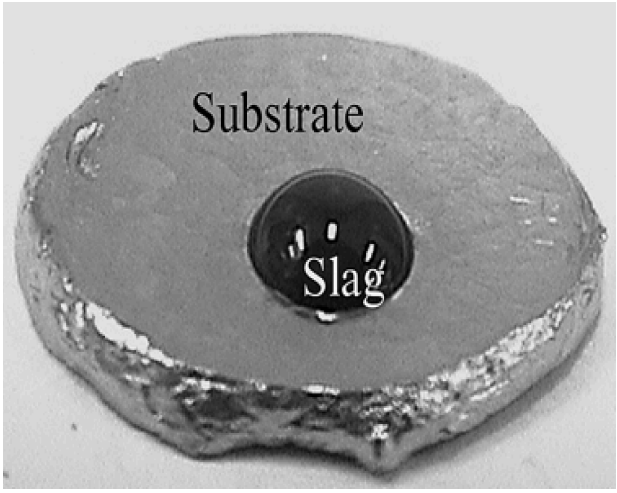

Figure 5.33. Surface appearance of Fe–CAS, (diameter of iron substrate is 15mm) [25].

Now, coming to the wettability, in reference [25] authors studied the wetting of solid iron and CaO–Al_2O_3–SiO_2 (CAS) by the sessile drop method at 1350 – 1450°C in a reducing atmosphere. Terminal contact angles after 240 min of reacting CaO–Al_2O_3–SiO_2 system with metal substrates were: 55 ±2° (1350°C), 60±2° (1390°C), 44±2° (1450°C). Though large, they are still in the first quadrant, one of the examples is shown in Figure 5.33. The values of the surface tension of slag are shown in Table 5.11. The interfacial tension as reported by authors of reference [25] are shown in Table 5.12.

Phase	Surface Tension (mN/m)	Temperature (°C)
γ Fe	2170	1360 – 1400
δ Fe	2040	1440
CAS Slag	425	1350 – 1450

Table 5.11. Surface tension of metal oxides [25].

Substrate/Temperature	1350 (°C)	1390 (°C)	1450 (°C)
Fe	1980 (γ)	1780 (δ)	1700 (δ)

Table 5.12. Interfacial Tension (mJ/ m^2) [25].

On the one hand, the surface tension of pure metal is quite high as compared to slag (Table 5.11). On the other hand, the interfacial tension is also high, resulting in high values of contact angles. If we assume that for CMAS slag the behaviour remains the same, that is contact angle stay below 90°, then with an increase in Al_2O_3 the wettability of the slag would decrease. This can be understood from the Young's equation (2.27). With an increase in alumina the surface tension of the slag (γ_{LV}) increases, and since contact angle (θ) lies in the first quadrant, the $cos\theta$ decreases, hence θ increases.

$$\gamma_{LV}.cos\theta = \gamma_{SV} - \gamma_{SL} \qquad (2.27)$$

This means with increasing Al_2O_3 the ease of slag dripping would increase as far as wettability with metallic iron is concerned. More importantly in the case of pellet 3, containing the highest alumina, the tendency for slag in the pellet to wet the iron shell would be lower than for the slag of pellets 2 and 1. Since slag acts as a barrier for carburization, it would result in a higher carburization degree for pellet 3, which might explain its lower melting temperature in comparison to pellet 2.

It is important to note that the effect of chemistry on interfacial tension is substantial, it is very much possible that a CMAS slag would result in a contact angle greater than 90 degrees, in which case with an increase in Al_2O_3 wettability would actually increase.

Coming to wettability with Coke, in reference [26] authors studied the wettability of blast furnace slags, with bosh slag composition, and coke. They found that the contact angle is very much dependent on the basicity of the slag, as can be seen from Figure 5.34.

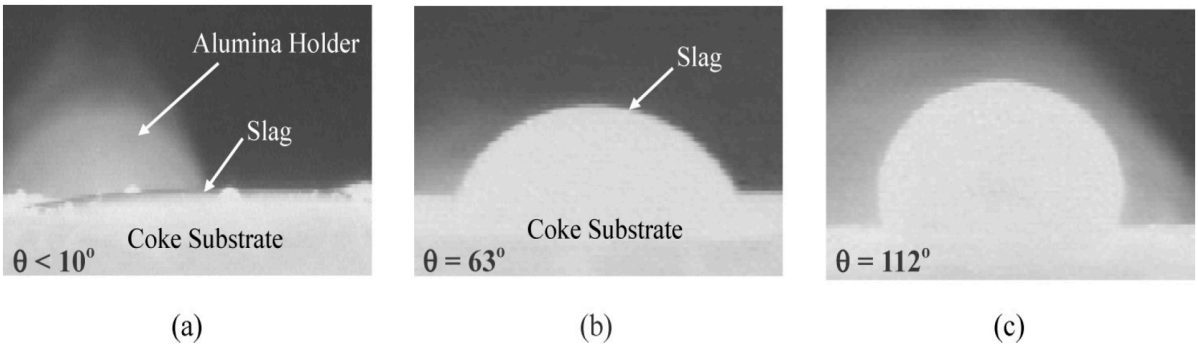

Figure 5.34. Images of sessile drop of a) slag 1, B2 = 1 b) slag 2, B2 = 1.3 c) slag 3, B2 = 1.6. On coke substrate (20 X 20 X 5 mm) after 200 min of interaction at 1500 °C [26].

Figure 5.34 shows that the contact angle can be in both, first and second quadrant. Moreover, the wettability showed dynamic behaviour. It was observed that with the reaction of slag with coke, the wettability gradually increases. But for the slag with B2=1.6, the contact angle still remained greater than 90°. Therefore, for low basicity slags with an increase in Al_2O_3 content, the wettability will decrease whereas for high basicity slags the wettability would increase.

5.4.3. Effect of Basicity on Surface Tension and Wettability of Slags

The effect of basicity can be understood on the same line of argument that was presented for TiO_2 and Al_2O_3. With an increase in CaO its proportion on the surface increases, hence it decreases the SiO_2 percentage on the surface of the slag. Since pure CaO has much greater surface tension, Tables 5.9 and 5.10, it causes an increase in surface tension of the slag even though it's a network modifier.

But coming to wettability, in reference [5] authors observed that for basic pellets the exudation was much more difficult when compared with acid pellets. According to them, it is because of the low interfacial tension between slag and metallic shell. On the other hand, in reference [2], it was observed that with an increase in basicity the adhesion to iron surface decreases, also leading to a greater carburization degree. Whereas in literature [6], authors found that basic slags have better coverage than acidic slags on the iron liner, indicating good wettability.

Either way CaO would definitely have an effect on surface tension and in turn on wettability, resulting in a difference in the melting and dripping behaviour. In reference [12], the authors noticed that degree of carburization of dripping metal increases with sinter basicity. The argument presented there

is that, with an increase in basicity reduction degree increases, due to which the low FeO high basicity slag is formed. This slag has a lower tendency to adhere to the iron surface, easing the process of dripping. Since carburization through slag is slower than direct carburization, the degree of carburization also increases.

On the other hand, as seen in Figure 5.34, the wettability with coke decreases with an increase in basicity. Hence with an increase in basicity the resistance to gas flow will decrease in the blast furnace as slag would drip with ease.

5.5. References

[1] Iljana, M., Kemppainen, A., Paananen, T., Mattila, O., Heikkinen, E. P., & Fabritius, T. (2016). Evaluating the reduction-softening behaviour of blast furnace burden with an advanced test. *ISIJ International*, *56*(10), 1705–1714.

[2] Shatokha, V., & Velychko, O. (2012). Study of softening and melting behaviour of iron ore sinter and pellets. *High Temperature Materials and Processes*, *31*(3), 215–220.

[3] Bakker, T.: "Softening in the Blast Furnace Process" PhD Thesis, Delft University of Technology, Netherlands, 1999

[4] Heaney, D. F. (2012). Handbook of metal injection molding. Cambridge, UK: Woodhead Publishing.

[5] Nogueira, P. F., & Fruehan, R. J. (2005). Blast furnace burden softening and melting phenomena: Part II. Evolution of the structure of the pellets. Metallurgical and Materials Transactions B: Process Metallurgy and Materials Processing Science, 36(5), 583–590. https://doi.org/10.1007/s11663-005-0049-5

[6] Nogueira, P. F., & Fruehan, R. J. (2006). Blast furnace burden softening and melting phenomena: Part III. Melt onset and initial microstructural transformations in pellets. *Metallurgical and Materials Transactions B: Process Metallurgy and Materials Processing Science*, *37*(4), 551–558.

[7] Lee, S. H. (2009). Reduction and Softening/Melting Behaviour of Olivine Pellet in the Experimental Blast Furnace Certificate of Originality. September.

[8] Kemppainen, A., Ohno, K. I., Iljana, M., Mattila, O., Paananen, T., Heikkinen, E. P., Maeda, T., Kunitomo, K., & Fabritius, T. (2015). Softening behaviour s of acid and olivine fluxed iron ore pellets in the cohesive zone of a blast furnace. *ISIJ International*, *55*(10), 2039–2046.

[9] Li, G. (2012). *Iron ore deposits in the Eastern Tianshan orogenic belt (China) : the magnetite-skarn-magmatism association*. Earth Sciences. Université d'Orléans.

[10] Deer, W. A., Howie, R. A., & Zussman, J. (1992). *An introduction to the rock-forming minerals.* 2nd ed. Harlow, Essex, England : New York, NY: Longman Scientific & Technical.

[11] Luo, Y., Zhu, D., Zhou, X., Shi, B., & Zhang, F. (2016). Coproduction of DRI powder and semi-coke from siderite ore and low rank coal by excessive coal-based direct reduction in rotary kiln. *ISIJ International*, *56*(1), 78–87.

[12] Dwarapudi, S., Ghosh, T. K., Shankar, A., Tathavadkar, V., Bhattacharjee, D., & Venugopal, R. (2011). Effect of pellet basicity and MgO content on the quality and microstructure of hematite pellets. *International Journal of Mineral Processing*, *99*(1–4), 43–53.

[13] Tokutake, K., & Hasegawa, N. (1990). Study and Improvement of Reduction Retardation and Melt-down Properties of Pellets. *ISIJ International*, *30*(3), 199–207.

[14] Tupkary R.H (2010), An Introduction to Modern Iron Making. Physical-thermal- chemical processes in a blast furnace, Khanna Publishers

[15] GERLACH, J. et al.: op. cit., 36, 1965, p. 543-547.

[16] Bahgat, M., Abdel Halim, K. S., El-Kelesh, H. A., & Nasr, M. I. (2009). Metallic iron whisker formation and growth during iron oxide reduction: K2O effect. *Ironmaking and Steelmaking*, *36*(5), 379–387.

[17] Sohn, I., & Min, D. J. (2012). A review of the relationship between viscosity and the structure of calcium-silicate-based slags in ironmaking. *Steel Research International*, *83*(7), 611–630.

[18] Park, J. H., Min, D. J., & Song, H. S. (2004). Amphoteric behaviour of alumina in viscous flow and structure of CaO-SiO2 (-MgO)-Al2O3 slags. *Metallurgical and Materials Transactions B: Process Metallurgy and Materials Processing Science*, *35*(2), 269–275

[19] li, Tingle & Sun, Changyu & Song, Sunny & Wang, Qi. (2019). Influences of Al_2O_3 and TiO_2 Content on Viscosity and Structure of CaO–8%MgO–Al_2O_3–SiO_2–TiO_2–5%FeO Blast Furnace Primary Slag. Metals. 9. 743.

[20] Yan, Z., Lv, X., Zhang, J., Qin, Y., & Bai, C. (2016). Influence of MgO, Al_2O_3 and CaO/SiO_2 on the viscosity of blast furnace type slag with high Al_2O_3 and 5 wt-% TiO_2. *Canadian Metallurgical Quarterly*, *55*(2), 186–194.

[21] Wu, S., Huang, W., Kou, M., Liu, X., Du, K., & Zhang, K. (2015). Influence of Al2O3 content on liquid phase proportion and fluidity of primary slag and final slag in blast furnace. Steel Research International, 86(5), 550–556.

[22] Ono, H., Tanizawa, K., & Usui, T. (2011). Rate of iron carburization by carbon in slags through carbon/slag and slag/metal reactions at 1 723 K. *ISIJ International*, *51*(8), 1274–1278.

[23] Liu, Y., Lv, X., Bai, C., & Yu, B. (2014). Surface tension of the molten blast furnace slag bearing TiO2: Measurement and evaluation. *ISIJ International*, *54*(10), 2154–2161.

[24] Hanao, M., Tanaka, T., Kawamoto, M., & Takatani, K. (2007). Evaluation of surface tension of molten slag in multi-component systems. *ISIJ International*, *47*(7), 935–939.

[25] Parry, G., & Ostrovski, O. (2009). Wetting of solid iron, nickel and platinum by liquid MnO-SiO2 and CaO-Al2O3-SiO2. *ISIJ International*, *49*(6), 788–795.

[26] Kang, T. W., Gupta, S., Saha-Chaudhury, N., & Sahajwalla, V. (2005). Wetting and interfacial reaction investigations of coke/slag systems and associated liquid permeability of blast furnaces. *ISIJ International*, *45*(11), 1526–1535.

[27] R.F. Mueller S.K. Saxena (1977), Igneoua plutons: their physical chemistry and mode of occurrence, Chemical Petrology: with applications to The Terrestrial Planets and Meteorites, Springer-Verlag New York Publications

[28] Goldsmith, J. R. (1980). Melting and breakdown reactions of anorthite at high presures and temperatures. American Mineralogist, 65(1961), 272–284.

[29] C. D. Gribble, ed. (1988). "The Silicate Minerals". Rutley's Elements of Mineralogy (27th ed.). London: Unwin Hyman Ltd. p. 378

[30] Klein, Cornelis; Hurlbut, Cornelius, Jr. (1985). Manual of Mineralogy(20th ed.). Wiley. pp. 373–375

[31] Boyd, F. R., England, J. L., & Davis, B. T. C. (1964). Effects of pressure on the melting and polymorphism of enstatite, MgSiO3 . Journal of Geophysical Research, 69(10), 2101–2109.

[32] Philpotts, A. R., & Ague, J. J. (2009). Principles of igneous and metamorphic petrology LK - (2nd ed.). Cambridge University Press.

[33] Yan, Z., Lv, X., Pang, Z., Lv, X., & Bai, C. (2018). Transition of Blast Furnace Slag from Silicate Based to Aluminate Based: Density and Surface Tension. Metallurgical and Materials Transactions B: Process Metallurgy and Materials Processing Science, 49(3), 1322–1330.

[34] Biswas, A. K. (Anil K. (1981). Principles of blast furnace ironmaking : theory and practice / Anil K. Biswas. Cootha Publishing House.

6. Conclusions & Recommendations

6.1. Conclusions

The aim of the research was to investigate the effect of alumina on reduction, softening and melting behaviour of the iron ore pellets. The lab-scale experiments were performed on commercial pellets with constant basicity and varying alumina content, using the Reduction, Softening and Melting (RSM) apparatus. The commercial pellets with alumina content of 0.81, 1.37, and 1.85 wt.% and approximately a constant basicity (B3 = (CaO+MgO)/(SiO_2)) of 0.7 were selected for the study. Based on the experimental results and thermodynamic evaluations, the following main findings and conclusions are obtained:

- The experimental results indicate that the softening start temperature (T1) lies in close proximity for all three pellets (around 1100 °C). For the analyzed chemistries (pellet 1, pellet 2, and pellet 3) the solidus temperature is similar and is close to 1100°C, as obtained from the FactSage. Therefore, the softening begins with the advent of the liquid formation in the core of the pellet.
- Experimentally it is seen that the rate of softening in stage 2, increases with an increase in alumina. This is because an increase in alumina also increases the rate at which liquid phase proportion grows in the pellet core as suggested by the FactSage calculations. The olivine phases are replaced by the anorthite phase as the alumina level rises in pellets. The anorthite phase reacts with wüstite and forms low melting slag which explains the rise in the rate of softening with alumina.
- The temperature at which the melt exudation occurs (Tm) shifts to a lower temperature region with alumina and the dripping temperature (Td) increases slightly, causing an increase in the range of melting and dripping as seen experimentally. The melting temperature (Tm) is governed by both degree of reduction and degree of carburization.
- A higher reduction degree results in a larger shell thickness, which can sustain the load to higher temperatures hence increasing the melting temperature (Tm). Since the viscous flow is an activated process, the viscosity is very sensitive to temperatures, hence pellets with lower melting temperatures also show the higher S – Values
- Alumina can cause retardation of reduction in two ways, one when pellet's microstructure is heterogeneous and other when microstructure in the core is homogenous.
- In the heterogeneous state, the interface between alumina rich particle and wüstite matrix starts melting at low temperatures, and this early melt can act as a barrier between reducing gas and the wüstite. As the microstructure homogenizes, with the increase in alumina, the proportion liquid phase increases. This liquid again acts as a barrier for reducing gases, causing reduction retardation.
- In the experiments, the reduction degree did not show a clear trend. The pellet sample with the lowest amount of alumina (0.81 % Al_2O_3) reduced the most (86 %) but the pellet sample with the highest (1.85 % Al_2O_3) was not the least (82 %). The reduction rate curve for the pellet sample 2 (1.37% Al_2O_3) exhibiting the lowest reduction degree (72%) revealed that the difference arises due to a lower reduction in the low-temperature region, 700 - 1000°C. In this temperature range, the alumina cannot influence such behaviour, as the effect of alumina on reduction rate is only seen once liquid slag starts to form, which is unlikely at such low temperatures.
- For a given reduction degree, the melting temperature (Tm) decreases with an increase in the degree of carburization of the metallic shell. Due to capillary action, slag from the core gets pulled towards the iron shell, forming a layer outside and around it. This slag layer acts as a

barrier for carburization. The extent of which depends on the wettability of slag with the iron shell.

- With an increase in alumina, the surface tension of the slag increases and the wettability of the slag with iron shell decreases. Therefore, the tendency of carburization should increase with alumina. This might help to explain the higher melting temperature (Tm) of the pellet containing 1.37 % alumina (Tm = 1458°C) as compared to the pellet containing 1.85 % Al_2O_3 (Tm = 1446 °C) even when the pellet 2 (1.37 % Al_2O_3) reduced less than the pellet 3 (1.85 % Al_2O_3). And this would also clarify the reason behind pellet 1 (0.81% Al_2O_3) showing such high melting temperature (Tm = 1491°C), as on one hand it reduces the most and on the other hand it would show the lower tendency for carburization due to the least amount of alumina present in it.
- Once the slag flows out of the pellets, after the melt exudation, it is the viscosity, that governs both the resistance to gas flow (S - Value) and the dripping temperature. With an increase in viscosity, the S-Value increases, as the tendency of slag to flow decreases also resulting in higher dripping temperatures. It has been experimentally observed that with the increase in alumina of the pellets from 0.81% to 1.85 % the S-Value increases from 13.21 k Pa.°C to 29.34 k Pa.°C.
- Alumina is an amphoteric oxide, it can act as both network modifier and network former, which depends on the overall chemistry of the slag. For the chemistries considered in this study, alumina acts as a network modifier increasing the viscosity hence resistance to gas flow (S-Value).
- The critical temperature of the slag is the temperature at which viscosity rises steeply. Hence, lower critical temperature is desirable. The reason for the increase in critical temperature with alumina is that it increases the proportion of high melting phases in the slag, namely anorthite and forsterite and decreases the proportion of low melting phases like diopside and enstatite, resulting in the increase of the liquidus temperature.
- An indirect effect of alumina is, with an increase in its proportion in pellets, the amount of alkalis also increases, as observed from the analysis of the dripped slag. Alkalis are known for decreasing the solidus temperature of slags and also causes swelling of pellets, therefore they are detrimental for softening and melting properties of pellets.
- The influence of basicity was investigated with literature; the effect on the reduction degree, in the heterogeneous state is marginal, as with CaO, the solidus temperature of the interface between anorthite and wüstite increases slightly, that too when CaO is uniformly distributed in the microstructure. In the homogenous state, however, the CaO is known for increasing the solidus temperature hence promoting the reduction. With an increase in basicity the rate of the degree of carburization via slag phase increases. Since CaO is a network modifier the viscosity decreases with increasing basicity. For the most part (except for carburization) with an increase in basicity, the negative impact of alumina should be minimized. Pellets with higher basicity, or conducting experiments with fluxed sinters, should show a lower impact of alumina on reduction softening and melting behaviour.

6.2. Recommendations

1) The effect of alumina on the reduction degree and the degree of carburization can be further confirmed with quenching experiments. This is established by comparing the iron shell thickness and its carbon content at different temperatures in the cohesive zone.
2) Since the variation of alumina in commercial pellets is small, the effect of alumina should be further clarified by customizing the pellets chemistry with a wide range of alumina content. The chemistry for alumina can be selected based on viscosity, liquids, and solidus temperatures obtained from FactSage.
3) In the present work, the effect of alumina was studied only on one constant basicity. It was theoretically revealed that basicity does have an influence and can counteract the negative effects of alumina. Therefore, it will be interesting to see the effect of alumina at different basicities.
4) The blast furnace burden consists of both sinter and pellets, therefore it is important to investigate the effect of variation of alumina in pellets with the presence of sinter of constant chemistry.
5) Repeating all the above steps for sinters, that is studying sinters separately with different alumina content, conducting quenching experiments, and mixed burden experiments with constant pellets chemistry.
6) Once the effect of alumina is clear, the purported remedy, that is the effect of MgO on reduction softening and melting behaviour of both pellets and sinters should be investigated. The chemistries can be selected based on viscosity, liquidus, and solidus temperatures of slag.

Acknowledgments

I would like to express my sincerest gratitude to my supervisor dr. Yongxiang Yang for providing his creative suggestions, technical guidance, support, encouragement and most importantly for his patience throughout this project. dr. Yongxiang Yang made sure the project does not suffer during restrictions due to COVID19 and made extra efforts in providing me access to labs where I could work safely.

I would like to thank dr. Allert Adema (TATA Steel Europe) for not only coming up with the topic of research, but also for being a guiding light throughout. dr. Allert Adema went out of his way during the difficult times of COVID19 and made sure I could receive the samples for testing. I am deeply indebted by his help.

I cannot thank enough dr. Dharm Jeet Gavel for teaching me the nuances of RSM apparatus and motivating me continuously when experiments failed. He has been nothing but kind and patient with me.

I would like to offer my special thanks to prof. Jilt Sietsma and dr. Tim Peeters (TATA Steel Europe) for giving me an opportunity to conduct my internship at Tata Steel under the guidance of dr. Allert Adema, which paved my way for this thesis.

Sander van Asperen has played a vital role in making this study possible, he made sure I worked in a safe environment and provided his expertise with microscopy. Ruud Hendrix was very kind in providing XRF and XRD results in such short notice, seeing him work with such dedication during these difficult times is an inspiration.

Finally, I would like to express my greatest gratitude towards the frontline workers of Netherlands for keeping the normalcy of our daily lives as much as possible. And putting our essential needs over their safety. Without them I wouldn't have been able to finish my thesis in time. My greatest appreciation for their on-going efforts.